

UCSF

UC San Francisco Electronic Theses and Dissertations

Title

Understanding the mechanism of bacterial cGAS immunity and its co-evolution with phage

Permalink

<https://escholarship.org/uc/item/9cc755ss>

Author

Huiting, Erin

Publication Date

2024

Peer reviewed|Thesis/dissertation

Understanding the mechanism of bacterial cGAS immunity and its co-evolution with phage

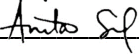
by
Erin Huiting

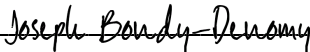
DISSERTATION
Submitted in partial satisfaction of the requirements for degree of
DOCTOR OF PHILOSOPHY

in
Biomedical Sciences

in the
GRADUATE DIVISION
of the
UNIVERSITY OF CALIFORNIA, SAN FRANCISCO

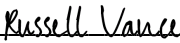
Approved:

DocuSigned by:

9BCB4DFEE8384D2... Anita Sil
Chair

DocuSigned by:

DocuSigned by:
47C... Joseph Bondy-Denomy

DocuSigned by:

James Fraser

DocuSigned by:

6923D487397C434... Russell Vance

Committee Members

Copyright 2024

by

Erin D. Huiting

Dedication and Acknowledgements

My dissertation is dedicated to all women in science – curious, ambitious, resilient women who strive to make a positive impact on the world. There are many people who have emulated these qualities and inspired me to pursue a lifetime of science. First and foremost is my sister, Dr. Leah Huiting, who truly paved the way for me early in life and continues to encourage my scientific pursuits to this day. My grandmothers, Alice Huiting and Beatrice Rothschild, and my mother, Lisa Huiting, who have shown me what it means to be strong for people beyond themselves. My father, Randy Huiting, who built his dreams from the ground up and empowers me to do the same. My mentor, Karen Sugar, whose dedication for worldwide gender equity brings a sense of purpose to my life. My incredible friends, Jessie Martin and Taylor Mooney alongside Drs. Lina León, Advait Subramanian, Fede Liccardo, and Nena Paladini, who lift my spirits and remind me to slow down and cherish life. Lastly, my partner Darnell Cuylear, who has overcome so many hurdles so gracefully and is a role model to me as he navigates his own scientific journey. Thank you all for unconditional love and support.

My dissertation is a culmination of ideas, expertise, and collaborations amongst people in and beyond my lab. My PI, Dr. Joe Bondy-Denomy, who challenges me to think bigger and bolder about science, and, about life. My faculty advisors, Drs. Anita Sil, James Fraser, Russell Vance, who always listen to me and provide thoughtful feedback. My lab mates, past and present, but especially Drs. Lina León, Yuping Li, Matt Johnson, Sukrit Silas, Januka Athukoralage, and Iana Fedorova as well as PhD students Alex Hong, Lexie Villani, and Claire Kokontis who have all taught me essential scientific skills and knowledge while also being true friends. The UCSF Biomedical Sciences and ImmunoX communities who have collectively welcomed and supported me throughout my PhD. The UCSF Graduate Division who has given me the opportunities to pursue PhD and postdoctoral research. Importantly, our steadfast collaborators, Dr. Yue Feng and his lab at the Beijing University of Chemical Technology and Dr. Lingyin Li and her lab at Stanford University, for investing their time, resources, and expertise into our projects. I am forever grateful and humbled to work alongside such incredible scientists.

Contributions

Chapter 1 contains work that has been previously published:

Huiting E and Bondy-Denomy J. Defining the expanding mechanisms of phage-mediated activation of bacterial immunity. 2023. *Current Opinions in Microbiology*. doi: 10.1016/j.mib.2023.102325.

Chapter 2 contains work that has been previously published:

Huiting E*, Cao X*, et al. Bacteriophages inhibit and evade cGAS-like immune function in bacteria. 2023. *Cell*. doi: 10.1016/j.cell.2022.12.041.

*Equal contributions

Chapter 3 contains work that has been previously published:

Cao X*, Yu X*, **Huiting E***, et al. Phage anti-CBASS protein simultaneously sequesters cyclic trinucleotide and dinucleotides. 2023. *Molecular Cell*. doi: 10.1016/j.molcel.2023.11.026.

*Equal contributions

“If you do not expect to, you will not discover the unexpected.”

– Heraclitus

Understanding the mechanism of bacterial cGAS immunity and its co-evolution with phage

Erin D. Huiting

Abstract

A fundamental strategy of eukaryotic anti-viral innate immunity involves the cGAS enzyme, which synthesizes 2',3'-cGAMP and activates a STING effector to limit viral replication. Bacteria contain cGAS-like enzymes producing a diversity of cyclic oligonucleotide signals that activate an effector protein to induce cell death upon bacteriophage (phage) infection, known as CBASS. It remains unknown whether bacteria endogenously expressing CBASS exerts anti-phage activity and how these bacteria and phage co-evolve together. Here, we identified endogenously active Type II-A CBASS in *Pseudomonas aeruginosa* that contains a cGAS-like enzyme (CdnA) producing 3',3'-cGAMP, which signals to a phospholipase (CapV) effector and limits dsDNA lytic and temperate phage replication >10,000-fold. In response, phages evolved an anti-CBASS protein (Acb2) that forms a hexamer with three cGAMP molecules to 'sponge' up signals and effectively inhibit both bacterial CapV and eukaryotic STING effector activity. Excitingly, Acb2 binds to an even broader spectrum of CBASS cyclic dinucleotides (CDNs), like 3',3'-cUU/UA/UG, and cyclic trinucleotides (CTNs), like 3',3',3'-cAAA/cAAG. One Acb2 hexamer can independently and simultaneously bind three CDNs and two CTNs, enabling phages to inhibit bacteria with Type II-A (3',3'-cGAMP-producing) and Type III-C (cA₃-producing) CBASS. These collective findings establish a new paradigm of viral proteins that sponge a remarkable breath of cyclic oligonucleotide molecules and inhibit signaling-based immunity across all domains of life. Upon deletion of Acb2, phage mutants selected under CBASS immune pressure were forced to evolve mutations in their major capsid protein to escape. While there is growing evidence of phages mutating essential structural proteins to escape CBASS, the reason for evasion remains unclear. Despite this, to counteract CBASS resistant phages, we observed that increasing CdnA enzymatic activity and 3',3'-cGAMP production vastly increases CBASS anti-phage activity and overcomes phages expressing Acb2 or mutant capsids. Surprisingly, counter to the

established dogma that CBASS induces cell death, the hyperactive and endogenously active Type II-A CBASS in *P. aeruginosa* induces cell growth and protects bacteria from phage-induced lysis. Altogether, these findings demonstrate that native bacterial hosts exert CBASS immunity and that phages can evolve and counteract this immune response through potent inhibitors that 'sponge' CBASS signaling molecules or acquisition of mutations in structural proteins.

Table of Contents

Chapter 1: Introduction.....	1
1.1. Summary.....	1
1.2. Diversity of anti-phage immune systems.....	1
1.3. Discovery and mechanisms of bacterial signaling-based immunity.....	2
1.4. Inhibition of immune systems.....	4
1.5. Activation of signaling systems.....	7
1.6. Figures.....	10
Chapter 2: Bacteriophages inhibit and evade bacterial cGAS immunity.....	13
2.1. Summary.....	13
2.1. Introduction.....	13
2.3. Results.....	15
2.3.1. Endogenous anti-phage CBASS function in <i>Pseudomonas aeruginosa</i>	15
2.3.2. PaMx41-like phages encode a CBASS antagonist.....	16
2.3.4. Acb2 has conserved function in a broadly distributed temperate phage family.....	17
2.3.5. Acb2 sequesters 3',3'-cGAMP to inhibit CBASS.....	18
2.3.6. Crystal structure of Acb2 and its complex with 3',3'-cGAMP.....	19
2.3.7. Acb2 sequesters variety of cyclic dinucleotides.....	20
2.3.8. Phages escape CBASS via mutations in the capsid gene.....	21
2.4. Discussion.....	22
2.5. Limitations of the Study.....	24
2.6. Author Contributions.....	25
2.7. Materials and Methods.....	25

2.8. Figures	41
2.9. Tables.....	54
Chapter 3: Single phage protein simultaneously sequesters cGAS- and TIR-generated signaling molecules	56
3.1. Summary	56
3.2. Introduction.....	56
3.3. Results	58
3.3.1. Acb2 sequesters diverse CDNs and is active in human cells	58
3.3.2. Acb2 sequesters CTNs with higher affinity than CDNs.....	59
3.3.3. Acb2 binds CTNs and CDNs with different binding sites	59
3.3.4. Acb2 binds to cA ₃ with a novel fold	61
3.3.5. Cyclic nucleotide binding spectra are different among Acb2 homologs	62
3.3.6. Acb2 antagonizes Type III-C CBASS immunity	63
3.4. Discussion	64
3.6. Author Contributions.....	66
3.7. Materials and Methods	66
3.8. Figures	74
3.9. Tables.....	88
Chapter 4: CBASS protects cells from phage-induced lysis in <i>Pseudomonas aeruginosa</i>	89
4.1. Summary	89
4.2. Introduction.....	89
4.3. Results	91

4.3.1. Increasing CdnA activity overcomes CBASS resistant phage	91
4.3.2. Increasing CBASS improves cell growth upon phage infection	93
4.3.3. Distinct CBASS model systems improve cell growth	95
4.3.4. Exogenous cGAMP improves CBASS-dependent cell growth.....	97
4.3.5. Phage capsid proheads are induce CBASS activity	98
4.4. Discussion	100
4.5. Author Contributions	103
4.6. Materials and Methods	103
4.7. Figures	110
References.....	120

Lists of Figures

Chapter 1

Figure 1.1: Diversity and discovery of anti-phage bacterial immune systems	10
Figure 1.2: Biochemical and bioinformatic approaches used to identify CBASS.....	11
Figure 1.3: Molecular mechanisms of bacterial signaling-based immune systems	12

Chapter 2

Figure 2.1: <i>P. aeruginosa</i> CBASS immunity protects against PaMx41 infection	41
Figure 2.2: Phage-encoded <i>acb2</i> is necessary to protect against CBASS.....	42
Figure 2.3: <i>Acb2</i> antagonizes CBASS activity by sequestering 3',3'-cGAMP	43
Figure 2.4: <i>Acb2</i> structure reveals hexamer bound to three 3',3'-cGAMP molecules	44
Figure 2.5: CBASS escape phages have mutations in the major capsid gene.....	45
Figure 2.6: Diversity of <i>P. aeruginosa</i> CBASS and phage targeting	46
Figure 2.7: <i>Acb2</i> protects phage against CBASS and reduces 3',3'-cGAMP.....	48
Figure 2.8: <i>Acb2</i> is found in a broad diversity of phages and bacteria	49
Figure 2.9: <i>Acb2</i> does not bind CBASS proteins, but does bind 3',3'/2',3'-cGAMP/cAA	50
Figure 2.10: Structures of apo and dinucleotide bound <i>Acb2</i>	51
Figure 2.11: <i>Acb2</i> binds to the predicted CdnE signals and protects against Type I-A and Type I-B CBASS	52
Figure 2.12: PaMx41 phage remains sensitive to CBASS in the presence of major capsid escape allele expression	53

Chapter 3

Figure 3.1: <i>Acb2</i> from phage PaMx33 binds cyclic trinucleotides and 3',2'-cGAMP	74
Figure 3.2: <i>Acb2</i> binds to cyclic trinucleotides with binding sites different from those of cyclic dinucleotides	75
Figure 3.3: <i>Acb2</i> binds to cyclic trinucleotides and dinucleotides simultaneously	76

Figure 3.4: The binding spectra are different among Acb2 homologs	77
Figure 3.5: Acb2 antagonizes tri- and di-nucleotide based CBASS immunity	78
Figure 3.6: The cyclic nucleotide binding spectrum of PaMx33-Acb2	79
Figure 3.7: The binding spectrum of PaMx33-Acb2 studied by ITC assays	80
Figure 3.8: Density map of bound nucleotides in the structures of this study.....	81
Figure 3.9: The binding sites of cyclic trinucleotides and dinucleotides are different	81
Figure 3.10: Acb2 binds to cA3 with a novel fold.....	82
Figure 3.11: Phylogenic analysis of unique Acb2 homologs across the genomes of prokaryotes and prokaryotic viruses	83
Figure 3.12: The binding spectrums of JBD67-Acb2 and T4-Acb2 studied by ITC assays	84
Figure 3.13: The binding spectrums of Acb2 homologs studied by native PAGE.....	85
Figure 3.14: The binding spectrum of CHI14-Acb2 studied by ITC assays	86
Figure 3.15: Mutations in Acb2 binding residues differentially impacts phage titer	87

Chapter 4

Figure 4.1: Increasing CdnA activity overcomes CBASS resistant phage.....	110
Figure 4.2: Increasing CBASS immunity improves cell growth upon phage infection	111
Figure 4.3: Heterologously expressed Type II-A and Type III-C CBASS improves anti- phage activity and cell growth.....	112
Figure 4.4: Exogenous 3',3'-cGAMP induce CBASS-dependent cell growth	113
Figure 4.5: Phage capsid prohead induces CBASS immunity.....	114
Figure 4.6: Increasing CdnA activity overcomes phage with Acb2 and MCP mutations	115
Figure 4.7: Improved cell growth is dependent on CapV effector activity	116
Figure 4.8: CBASS-dependent cell growth is tunable and can become toxic.....	117
Figure 4.9: High levels of exogenous 3',3'-cGAMP is necessary to induce CBASS- dependent cell growth	117
Figure 4.10: WT and mutant capsid proheads impact CBASS anti-phage activity	118

Figure 4.11: WT capsid proheads induce cell growth in CBASS-dependent manner..... 119

Figure 4.12: Flow cytometry gating strategy for propidium iodide expressing cells..... 119

List of Tables

Chapter 2

Table 2.1: Data collection and refinement statistics	54
Table 2.2: List of phage capsid mutations observed via Whole Genome Sequencing	55

Chapter 3

Table 3.1: Data collection and refinement statistics	88
Table 3.2: Acb2 homolog protein sequences	88

Chapter 1: Introduction

1.1. Summary

The field of bacterial immunology is exploding with hundreds of new systems identified over the last decade to target invading bacterial viruses (phages). These anti-phage systems are especially abundant and diverse in *Pseudomonas aeruginosa*, our leading model organism, to study native bacteria-phage interactions. Of the recently identified systems across bacteria, several represent the evolutionary origin of anti-viral innate immunity found in humans. Notably, cyclic GAMP-AMP synthase (cGAS) and Toll/interleukin-1 receptor (TIR) containing systems both use cyclic nucleotide signaling cascades to limit phage replication, and have been identified in anti-viral immune responses across all domains of life. A recently discovered anti-phage system that uses a pyrimidine cyclase (PycC) to generate cyclic nucleotide signals has yet to be identified in eukaryotic immunity. However, studying bacteria-phage interactions with these signaling systems uncovered new phage proteins that directly inhibit the core immune proteins or signals and have been identified in bacterial and eukaryotic viruses alike. These studies have also led to the identification of conserved phage proteins or phage-associated molecular patterns (PhAMPs) that may broadly activate many anti-phage systems. Here, we summarize our current understanding of signaling-based immune systems in bacteria and how phages inhibit or activate these systems.

1.2. Diversity of anti-phage immune systems

The co-evolution of bacteria, their viruses, and mobile genetic elements over the past billions of years has driven the emergence and diversification of immune and anti-immune systems alike. In the last three years, there has been over 250% increase in newly identified systems in bacteria (60 to 152) that protect against bacteriophages (phages)¹. The frequency of these anti-phage systems in bacterial genomes vary from one system to the next, with the well-studied Restriction-Modification (RM)² and CRISPR-Cas³ systems encoded in at least 81% and 35% of bacteria, respectively (Figure 1.1A). By comparison, the recently identified cGAS-based system (CBASS) is encoded in 13% of bacteria

(Figure 1.1A), making it the sixth most frequent bacteria immune system. There are also multiple combinations of anti-phage systems in specific bacteria, in which the Pseudomonadota phyla encodes that largest total number and diversity of anti-phage systems (Figure 1.1A). This is in part due to increased sequencing and experimental advances within few bacterial species like *Escherichia coli* (20,194 total instances), *Klebsiella pneumonia* (13,240), and *Staphylococcus aureus* (4,395)¹. However, encoding more total anti-phage systems may not translate to increased anti-phage system diversity. For instance, *Pseudomonas aeruginosa* only encodes 1,957 total instances of anti-phage systems across its genomes, but it has the richest diversity or combination of anti-phage systems compared to other highly sequenced bacterial species⁴. Moreover, *P. aeruginosa* encodes at least 85 different anti-phage systems (Figure 1.1B). Of these systems, RM is the most abundant and encoded in 57% of *P. aeruginosa* genomes while CRISPR-Cas and CBASS are two of the next most abundant systems encoded in 6% and 5% of genomes, respectively (Figure 1.1B). The recently identified TIR-based (Thoeris) and Pycsar systems are only encoded in 0.05% and 0.2% of *P. aeruginosa* genomes, respectively (Figure 1.1B). These data demonstrate the breadth and abundance of known anti-phage immune systems, especially in *P. aeruginosa*, highlighting it as an ideal model organism to study bacteria-phage interactions.

1.3. Discovery and mechanisms of bacterial signaling-based immunity

Several studies have revealed insights into the mechanistic diversity of the recently identified anti-phage immune systems, spanning nucleic acid^{5–12} or metabolite^{13–19} depletion, signaling molecule cascades^{20–22}, membrane disruption^{23–26}, and many more^{27–29}, using heterologous expression systems. These studies typically use a combination of high-throughput bioinformatic and experimental approaches (Figure 1.1C). The main bioinformatic approach involves identification of candidate genes enriched next to known anti-phage systems, commonly CRISPR-Cas and RM, in what is referred to as ‘immune islands’³⁰. In turn, it is predicted that uncharacterized gene(s) within these immune islands may also exert anti-phage activity and become candidates for *in vivo* experiments. This has led to the discovery of hundreds of new anti-phage systems, including CBASS, Thoeris, and Pycsar signaling

systems^{20,21,30}, which represent the evolutionary origin of eukaryotic immune or housekeeping proteins that are essential for cyclic nucleotide signaling cascades. In turn, these discoveries also depend on *in vitro* experimental approaches that involve solving protein structures functions³¹.

The discovery of CBASS initially relied on identifying a new *Vibrio cholerae* dinucleotide cyclase (DncV)³² and the conservation of its structural and function with human cGAS³³. Although these proteins retain <10% amino acid identity, the structural architecture and active site were strongly conserved (Figure 1.2A). It was also determined that DncV produced 3',3'-cGAMP signaling molecules while the human cGAS produced 2',3'-cGAMP that differed only by a single phosphodiester linkage³³. Afterwards, a systematic biochemical screen with over 60 DncV homologs was performed and uncovered a new family of cGAS/DncV-like nucleotidyltransferases (CD-NTase) enzymes that produce at least 12 distinct cyclic nucleotide signals and are present in ~10% of bacteria³¹. Given that the structure and function of these cGAS enzymes remained conserved over billions of years, it was thought by people in the field that its role in anti-viral immunity also remained conserved. A comparative genomic analysis revealed that the bacterial cGAS-like enzymes found gene neighborhoods or networks with other nucleotide-modifying genes, including TIR³⁴, that are involved in human innate immunity. Upon further investigation of these bacterial cGAS-like genes, it was found that ~65% are enriched in immune islands as four-gene operons that may function together in anti-phage immunity (Figure 1.2B)²¹. In turn, cGAS-like gene operons from *V. cholerae* and *E. coli* were expressed in another bacterial host that naturally lacks the system and revealed a significant reduction in phage replication that was dependent on cGAS-like enzymatic activity²¹. However, as described later, this heterologous model system may have hidden insights into bacteria-phage interactions that would otherwise be observed in a native bacterial host. That withstanding, this study provided the first evidence of bacterial cGAS-like genes functioning as an anti-phage immune system²¹. Additional genomic analyses revealed that bacterial cGAS-like genes always co-occur with an effector protein that is proposed to exert the anti-phage activity, including TIR-STING fusions, phospholipases, transmembrane proteins, or endonuclease, that are present in all major bacterial phyla and one

archaeal phylum³⁵. Collectively, these bioinformatic and experimental data culminated in defining the newfound cyclic-oligonucleotide-based anti-phage signaling system (CBASS) (Figure 1.3A).

The discovery of Thoeris and Pycsar will be touched upon more briefly given that they reflect a similar series of findings. For Thoeris, TIR domain-containing proteins had already been well-defined in both human³⁶ and plant³⁷ immunity. Human TIR proteins oligomerize and transfer signals through protein-protein interactions whereas plant TIR proteins themselves produce cyclic ADPR (cADPR) signals. In turn, the bacterial TIR protein was found to have conserved function and produce glycocyclic ADPR (gcADPR) signaling molecules²². Comprehensive bioinformatic analyses identified ~4% of bacterial TIR genes enriched in immune islands as two- and three-gene operons³⁰, both of which demonstrated anti-phage activity that was dependent on the TIR enzymatic activity (Figure 1.3C)²². For Pycsar, the originally identified adenylate cyclase had only been studied in the context of cyclic AMP (cAMP) housekeeping pathways in eukaryotes³⁸. Despite this, bioinformatic analyses revealed that ~3% of bacterial adenylate cyclase genes were enriched in immune islands as two-gene operons²⁰. Therefore, given the expanding repertoire of bacterial signaling-based immune systems, it was still possible to play a role in anti-phage. The same study identified that the cyclase uniquely produced cyclic CMP (cCMP) and cyclic UMP (cUMP) signals, which were necessary for potent anti-phage activity²⁰. These findings led to discovery the novel pyrimidine cyclase (PycC) and the pyrimidine cyclase system for anti-phage resistance (Pycsar) (Figure 1.3B).

1.4. Inhibition of immune systems

To counteract or regulate the rapidly growing diversity of anti-phage immune systems, phages, mobile genetic elements (MGEs), and even bacteria themselves have acquired inhibitors. MGEs like prophages^{39,40}, plasmids⁴¹ and conjugative elements⁴⁰ have been shown to primarily encode anti-Restriction-Modification (RM) and anti-CRISPR proteins to provide immediate protection against nucleic acid targeting systems. Bacteria have also been demonstrated to acquire anti-CRISPR proteins that tune the activity of Type III CRISPR-Cas systems⁴², which was later discovered to be co-

opted from phages and MGEs^{43,44}. By comparison, phages have been shown to encode inhibitors that antagonize a wider breath of anti-phage system mechanisms, including inhibitors that directly bind to core immune proteins^{9,14,29,45–47}, immune signaling molecules^{45,48–53}, or indirectly inhibit systems through reversal of effector function⁵⁴. Studying the natural evolution between bacteria and phage, as well as biochemical and structural screens of phage proteins, has uncovered many of these inhibitors.

To identify phage proteins that degrade CBASS and Pycsar signaling molecules, a systematic biochemical screen was performed with phage infected lysates⁴⁸. This approach was inspired by a recent biochemical screen that identified viral enzymes, known as poxins or viral phosphodiesterases, that selectively degrade eukaryotic 2',3'-cGAMP signaling molecules⁵⁵. Based on these findings, infected *E. coli* cells harboring CBASS or infected *B. subtilis* cells harboring Pycsar were screened to identify phage enzymes that selectively degrade each system's respective signaling molecules. As such, the *E. coli* phage T4 was discovered to express a protein (gp57B) that degrades cyclic dinucleotides 3',3'-cUU/cAA/cUA/cGAMP, as well as cyclic trinucleotides 3',3',3'-cAAA/cAAG, that strongly limit CBASS phospholipase (CapV) and endonuclease (Cap5) effector activity⁴⁸. This phage protein was resultantly named anti-CBASS protein 1 (Acb1). The experimentally solved structure reveal that one Acb1 protein contains a conserved catalytic fold, enabling it to bind and cleave one cyclic di- or trinucleotide⁴⁸. With the advances in predicting protein structures, a recent study revealed the discovery of the first eukaryotic virus encoding Acb1⁵⁶, highlighting that mechanistic insights on the bacterial system and its inhibitors may reveal new insights into the eukaryotic system. In addition, within the same study that identified Acb1, the *B. subtilis* phage SBSphiJ was discovered to express a protein (gp147) that effectively degrades cyclic mononucleotides (cAMP, cGMP, cCMP, cUMP) and was named anti-Pycsar protein 1 (Apyc1)⁴⁸. Apyc1 forms a homodimer and effectively binds to and cleaves one cyclic mononucleotide, and has yet to be further identified in eukaryotes.

To identify phage proteins that sequester or 'sponge' CBASS and Thoeis signaling molecules, natural phage evolution and comparative genomic analyses were used. For both systems, a comprehensive

phage sensitivity screen was performed with diverse phages against bacteria expressing each respective system^{45,49,50}. For CBASS, the *P. aeruginosa* phage PaMx41 was discovered to be uniquely inhibited, but closely related phages. PaMx41 escape phage were isolated under CBASS pressure within its native bacterial host, where it acquired a gain-of-function mutation to active its broken inhibitor (gp24). Genomic analyses revealed that the resistant phages already expressed the active gp24. Both *in vitro* and *in vivo* experiments further demonstrated that gp24 sequestered nearly all known CBASS signals, which strongly limited CBASS phospholipase (CapV) and endonuclease (Cap5) effector activity, as well as eukaryotic STING effector activity^{50,51}. This phage ‘sponge’ protein was named anti-CBASS protein 2 (Acb2) and was experimentally solved as a unique hexameric structure that could sequester three cyclic dinucleotides^{50,53} or two cyclic trinucleotides⁵¹. Acb2 will be a major focus of this dissertation.

For Thoeris, several *B. subtilis* phages from the SBSphiJ and SPO1 families were observed to have unique resistance towards the system. Genomic comparison with closely related, albeit sensitive, phages revealed that the resistant phages express what is now known as Thoeris anti-defense protein 1 (Tad1)⁴⁹ or protein 2 (Tad2)⁴⁵. Tad1 and Tad2 form hexamers or tetramers⁵², respectively, to effectively bind and sponge bacterial gcADPR, limiting the Thoeris NADase (ThsA) effector activity. That withstanding, given the structural flexibility of ‘sponge’ proteins relative to enzymatic proteins, a follow-up biochemical screen was performed with Tad1 and Tad2 proteins and revealed that they can additionally bind a broad range of both CBASS and Thoeris signals⁵². These findings, alongside the Acb2 work, establishes a new paradigm of immune inhibition where a single sponge protein can inhibit multiple anti-phage systems with two distinct binding pockets for the immune signaling molecules. Furthermore, although sponge proteins demonstrate potent and broad-spectrum inhibitory activity, the small protein size and non-enzymatic folds has made it challenging to identify any eukaryotic viral sponges.

Lastly, to inhibit anti-phage systems that all depend on NADase effector function^{14,22,57}, a large-scale genomic analysis was used across the diverse collection of *E. coli* BASEL phages⁵⁸. Upon examination of the phage genomes, a two-gene operon was observed to contain proteins involved in the NAD⁺ biosynthesis pathway and therefore may counteract NADase activity⁵⁴. *In vitro* experiments demonstrated the proteins, now ADPR-PP synthase (Adps) and Nicotinamide ADPR transferase (Namat), work together to effectively synthesize NAD⁺ and was therefore named the NAD⁺ reconstitution pathway 1 (NARP1)⁵⁴. Phylogenetic analyses additionally revealed that phages may encode a related protein to Namat, albeit distinct, now known as Nicotinamide phosphoribosyltransferase (Nampt). *In vitro* experiments showed that Nampt worked in concert with Nicotinamide mononucleotide adenylyltransferase (Nmnat) to comprise an entirely new NAD⁺ reconstitution pathway (NARP2)⁵⁴. The co-expression or knock-in of NARP2 genes conferred phage resistance to Thoeris and DSR2 anti-phage systems, highlighting that phage proteins may have broad-spectrum activity through inhibition of conserved, downstream effector function. Given the modularity of anti-phage effector proteins⁵⁹, it is likely that many more phage proteins exist to directly or indirectly inhibit CBASS, Thoeris, and Pycsar effector proteins.

1.5. Activation of signaling systems

The activation of anti-phage immune systems has remained largely understudied. However, given the conservation between bacterial and eukaryotic anti-viral immunity, mechanisms of detection or activation may also be conserved. Eukaryotic viruses are known to harbor conserved features, referred to as pathogen-associated molecular patterns (PAMPs), that directly bind to the host's cognate pattern recognition receptor and then activates an immune response⁶⁰. By contrast, viruses may produce an effector (typically a protein) that manipulates host cell structures or processes, which is detected by and activates immunity⁶¹. Although viral effectors are diverse and rapidly evolving – making them 'bad' PAMPs – the manipulated host structures or processes are widely conserved. These two strategies of immune activation are not mutually exclusive and ensures that host cells can respond to numerous, variable "patterns of pathogenesis"^{61,62}. In bacteria, there is evidence of both direct and indirect

activation mechanisms in response to phage infection akin to eukaryotic immunity. As such, we have defined these mechanisms as detection of phage-associated molecular patterns (PhAMPs) that directly activate bacterial immunity or detection of phage-associated effector activities that indirectly activate bacterial immunity. Well-studied examples of PhAMPs include phage DNA and RNA sequences, which directly activate RM² or CRISPR-Cas³ systems. Phage proteins or protein complexes have also been discovered to directly activate numerous anti-phage systems^{6,14,28,63–65}. There are also many instances of phage proteins inhibiting conserved host processes, like RecBCD-mediated DNA repair^{11,23,66}, which then activates an anti-phage system. Many of these discoveries have relied on the natural evolution of phage that escape immune pressure, revealing mutations that may be in the PhAMP or phage effector that suppresses activation and therefore enables resistance towards anti-phage systems.

Several studies have identified escape phage with mutations in essential structural proteins^{14,28,63}, including Pycsar and CBASS, but the many mechanisms of activation remain unclear. For Pycsar, *E. coli* T5 phage escaped the immune pressure through the acquisition of mutations in its major capsid protein (pb8). Monitoring bacterial cells infected with phage expressing wildtype or mutant capsid proteins revealed that the mutant phages induce a significant decrease in Pycsar-dependent cCMP production²⁰, suggesting that mutant phage can evade Pycsar activation. However, co-expression of the wildtype capsid and Pycsar system did not induce a cell death response upon phage infection, as anticipated, nor did co-IP of the wildtype capsid pull-down with the Pycsar cyclase (PycC). These data suggest that protein complex, including the phage capsid and additional phage or host components, may directly activate Pycsar and therefore the phage capsid complex serves as the PhAMP (Figure 1.3B).

For several CBASS types, phage escaped the immune pressure through mutations in their major capsid protein^{50,67}, capsid packaging proteins^{67,68}, or tail fiber proteins⁶⁷. However, co-expression of the wildtype structural proteins still induced production of their unique cyclic nucleotide signals and did

not induce a CBASS-dependent cell death response^{67,68}. Further examination of these mutant phage revealed that their infection kinetics were drastically different than the wildtype phage⁶⁷. These collective results have not demonstrated that individual phage structural proteins do not directly activate CBASS, but it is still possible that a protein complex, process, or byproduct of producing these structural proteins (e.g. using or depleting the host of essential metabolites) may activate the system (Figure 1.3A). By comparison, eukaryotic cGAS enzymes directly detect cytosolic dsDNA⁶⁹ and dsRNA^{70,71}; however, bacteria are single cells that lack the compartmentalization of nucleus and cytoplasm to separate self and non-self dsDNA. Moreover, the bacterial cGAS enzyme lacks the canonical DNA-binding zinc ribbon domain, but instead retains a long, positively-charged cleft that may bind phage-derived ligands³³. In this light, a recent report studying Type I CBASS identified a unique CBASS-activating bacteriophage RNA (cabRNA) that induced the production of cyclic nucleotides *in vitro*, but was not sufficient to activate CBASS *in vivo*⁶⁸. This evidence suggests that there may be many diverse activators of CBASS that await discovery.

For Thois, there has yet to be any naturally evolved escape phage that pinpoint the activator. There are, however, many diverse phages that are sensitive to Thois^{22,45,49} and may share conserved proteins or process that induce Thois activity. That withstanding, eukaryotic TIR proteins represent a large family of innate immune receptors that can detect a DNA, RNA, and proteins from a diversity of pathogens³⁶. However, to our knowledge, structural analyses and biochemical screens with bacterial TIR proteins have yet to be performed and may therefore provide critical insights into the Thois mechanism of activation.

1.6. Figures

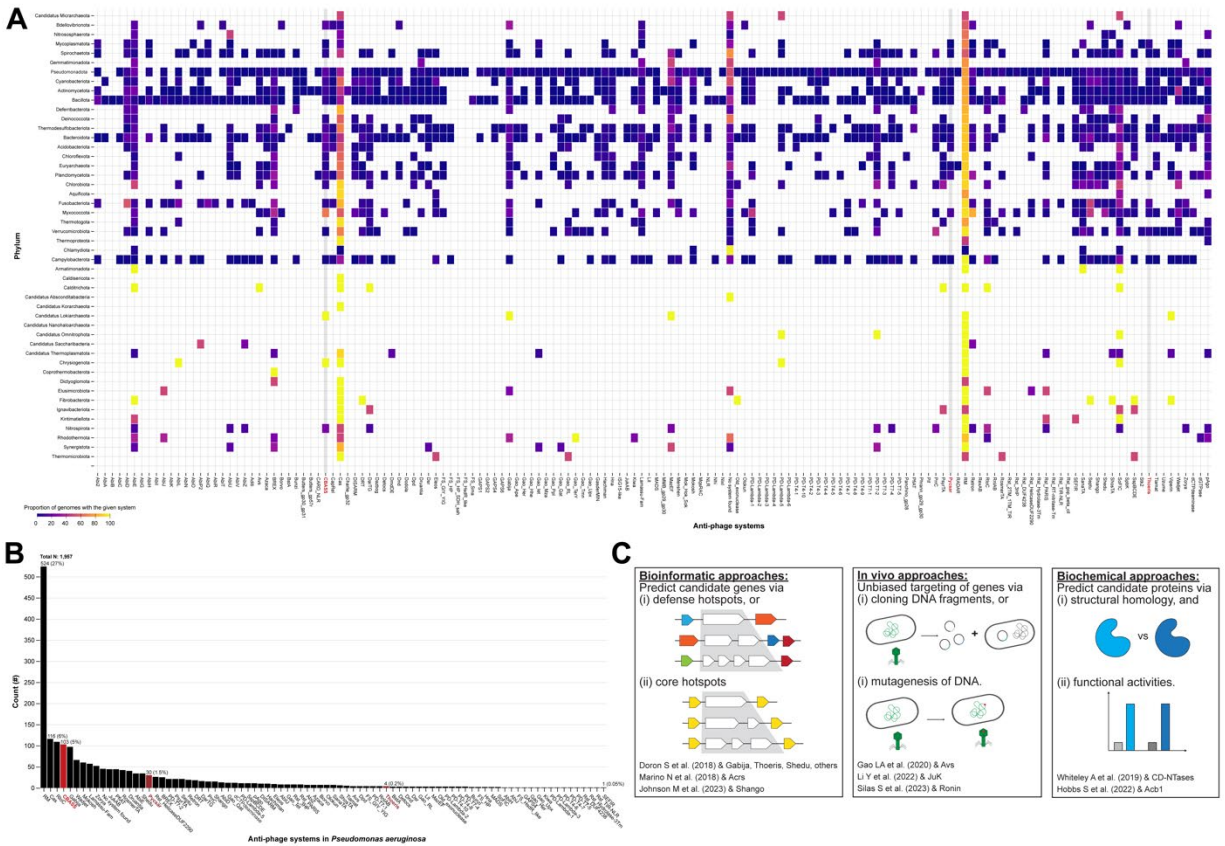


Figure 1.1: Diversity and discovery of anti-phage bacterial immune systems

(A) The frequency of different anti-phage immune systems in bacteria genomes as classified by phylum. In the heatmap, the color of each rectangle corresponds to the frequency of a system (columns) in the genomes of a phylum (rows). **(B)** The total counts of different anti-phage immune systems in *Pseudomonas aeruginosa* with the indicated count and percentage for select systems. All signaling-based systems are highlighted in red. DefenseFinder webservice^{1,72,73} was used to generate graphics in A-B. **(C)** Bioinformatic and experimental approaches to identify new anti-phage immune systems. The bioinformatic approaches involve identifying candidate genes enriched in defense/immune hotspots³⁰ or surrounded conserved, core genes^{4,40,74}. The *in vivo* experimental approaches involve cloning bacterial DNA fragments^{6,75} or random mutagenesis of bacterial DNA⁷⁶ to identify an anti-phage phenotype. The *in vitro* experimental approaches involve solving or predicting protein structures to identify homologs immune proteins and then screening for immune function^{31,48}.

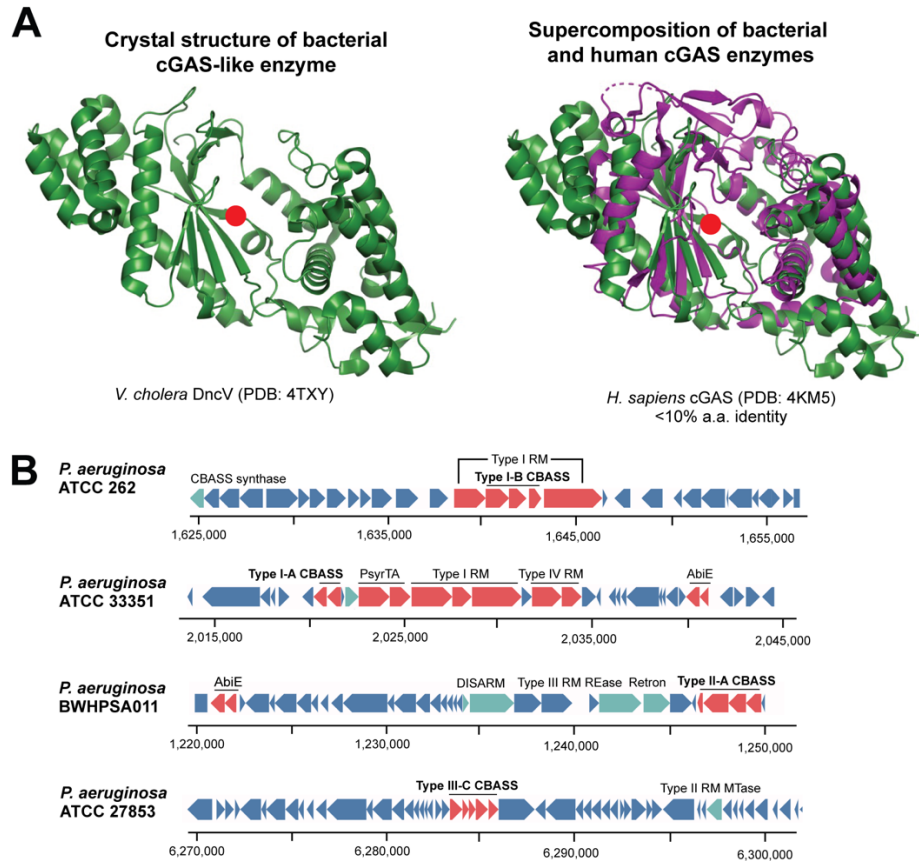


Figure 1.2: Biochemical and bioinformatic approaches used to identify CBASS

(A) Structural overlay of experimentally solved of *V. cholerae* DncV (green, PDB: 4TXY) *H. sapiens* cGAS (purple, PDB: 4KM5). Red circle represents the active site fold. Pymol “super” function was used to make the overlay and was previously shown³³. **(B)** Examples of bacterial cGAS operons that became known as CBASS (red) that are enriched next to known anti-phage systems (red). Incomplete or hypothetical anti-phage systems are also labeled (turquoise). DefenseFinder webservice^{1,72,73} was used to detect and visualize the anti-phage systems. Additional instances of diverse bacteria with cGAS operons enriched in immune islands has been previously shown²¹.

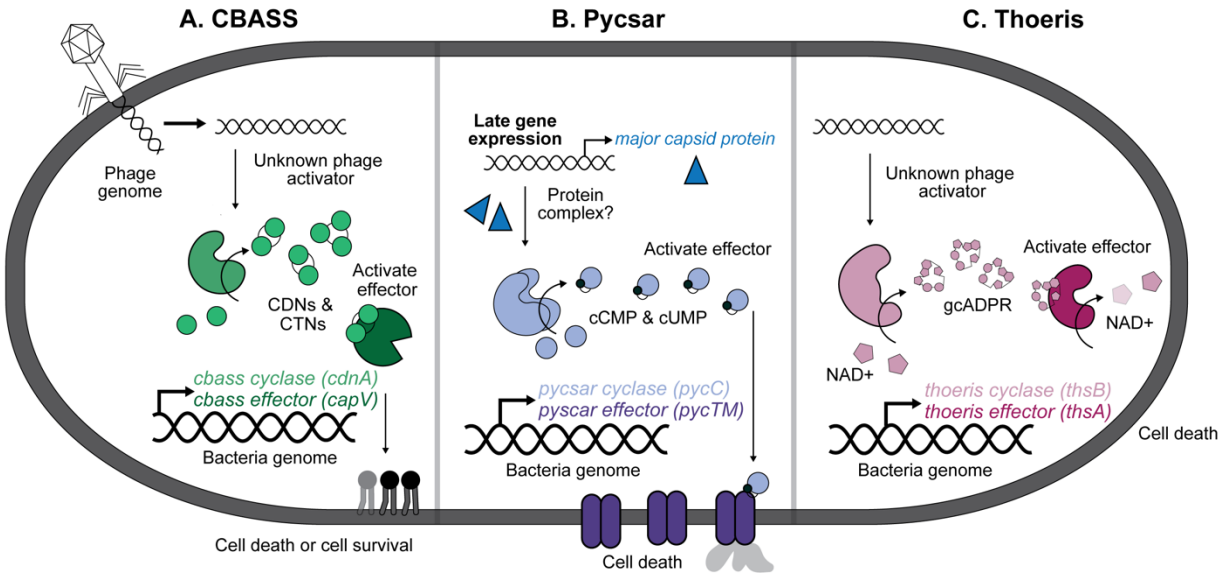


Figure 1.3: Molecular mechanisms of bacterial signaling-based immune systems

(A) Cyclic-oligonucleotide-based anti-phage signaling system (CBASS)^{21,22} produce cyclic dinucleotides (CDNs) or cyclic trinucleotides (CTNs) to activate a downstream effector that induces cell death or cell survival to stop phage infection. Note that the CBASS cyclases³¹ and effectors³⁵ can be very diverse, and may also include regulatory proteins that tune cyclase activity. (B) Pyrimidine cyclase system for anti-phage defense (Pycsar)²⁰ produce cyclic mononucleotide signals to activate a downstream transmembrane effector (PycTM) that induces cell death to stop phage infection. The phage activator for CBASS remains unknown, while the phage activator of Pycsar is proposed to be the major capsid protein in complex or indirectly binding to the Pycsar cyclase (PycC). (C) Thoeris anti-phage system produces gcADPR signals to activate a downstream effector that degrades NAD⁺ and induces cell death to stop phage infection. Note that Thoeris cyclase (ThsB) and effectors (ThsA) can be diverse²².

Chapter 2: Bacteriophages inhibit and evade bacterial cGAS immunity

2.1. Summary

A fundamental strategy of eukaryotic anti-viral immunity involves the cGAS enzyme, which synthesizes 2',3'-cGAMP and activates a STING effector to prevent viral replication. Diverse bacteria contain cGAS-like enzymes that produce cyclic oligonucleotides and induce anti-phage activity, known as CBASS. However, this activity has only been demonstrated through heterologous expression. Whether bacteria harboring CBASS antagonize and co-evolve with phages is unknown. Here, we identified an endogenous cGAS-like enzyme in *Pseudomonas aeruginosa* that generates 3',3'-cGAMP, signals to a phospholipase effector, and limits phage replication. In response, phages express an anti-CBASS protein (Acb2) that forms a hexamer with three 3',3'-cGAMP molecules and reduces phospholipase activity. Acb2 also binds to 2',3'-cGAMP and 3',3'-cUU/UA/UG, suggesting broad inhibition of cGAS-based immunity. Upon Acb2 deletion, CBASS blocks lytic phage replication and lysogenic induction, but rare phages evade CBASS through major capsid gene mutations. Together, we demonstrate endogenous CBASS anti-phage function and strategies of CBASS inhibition and evasion.

2.1. Introduction

Sensing specific macromolecules produced or possessed by viruses is a conserved strategy of anti-viral immunity across all kingdoms of life^{77,78}. In mammalian cells, viral double-stranded DNA (dsDNA) is bound by cyclic GMP-AMP synthase (cGAS) in the cytoplasm^{79,80}. The activated cGAS enzyme produces 2',3'-cyclic GMP-AMP (2',3'-cGAMP) dinucleotides that bind to the STING (stimulator of interferon genes) effector protein and induces a type I interferon response^{81,82}. Recently, thousands of cGAS-like enzymes named CD-NTases (cGAS/DncV-like nucleotidyltransferases) were identified across the entire bacterial domain and then biochemically characterized, revealing at least 8 enzymatic clades and 10 known cyclic oligonucleotides^{31,32}. These enzymes are activated during phage infection through an unknown mechanism and produce cyclic oligonucleotides, like 3',3'-cGAMP, which activate

a downstream effector^{21,24,83–85}. This strategy of bacterial immunity was coined cyclic-oligonucleotide-based anti-phage signaling system (CBASS)²¹. CD-NTases and effectors comprise the core CBASS genes (Type I CBASS), and additional ‘signature’ CD-NTase-associated proteins (Cap) have been identified in Type II and III CBASS that regulate CD-NTase activity^{35,53,83,86–88}.

Phage infection introduces nucleic acids and numerous foreign proteins into the bacterial cell. However, molecules that cause a phage to be sensitive, or resistant, to a given anti-phage immune system are largely unknown. A recent study discovered a family of phage-encoded anti-CBASS phosphodiesterase enzymes (Acb1), which cleave cyclic oligonucleotides⁴⁸ similarly to poxin enzymes encoded by eukaryotic viruses⁵⁵. Investigating the co-evolution of phages and CBASS in a host with endogenous CBASS function will inform how cGAS-based immunity functions in nature and is the main goal of this study.

Pseudomonas aeruginosa is a human opportunistic pathogen that encodes a diversity of CBASS operons and is a generalist microbe that survives in many niches. *P. aeruginosa* also has a diverse phage population and is a leading candidate for phage therapy, but our limited understanding of anti-phage immunity is a barrier for basic biology and phage therapeutic development. Here, we identified a *P. aeruginosa* strain that harbors Type II-A CBASS (3',3'-cGAMP producing CD-NTase; CdnA) with a phospholipase (CapV) effector that limits phage replication by >10,000-fold. This is a notable finding because it demonstrates that endogenous CBASS anti-phage immunity can function without overexpression. We next identified a widespread phage protein (Acb2) that forms a hexamer complex with three 3',3'-cGAMP molecules, acting as a “sponge” to reduce the available molecules to activate the phospholipase effector. In addition, Acb2 binds to multiple other cyclic dinucleotides, including 3',3'-c-di-UMP, 3',3'-cUA, and 3',3'-cUG, and is necessary for optimal phage replication in the presence of Type I or II CBASS that are predicted to encode the aforementioned cyclic dinucleotides. Phages with *acb2* deleted were unable to replicate in the lytic cycle or during exit from lysogeny in the presence of CBASS. However, mutations in the major capsid gene enabled phages to escape CBASS.

This work provides direct evidence of phage inhibition and evasion of CBASS, demonstrating a robust arms race between the two.

2.3. Results

2.3.1. Endogenous anti-phage CBASS function in *Pseudomonas aeruginosa*

Previous analyses³⁵, coupled with our own bioinformatics, revealed that 252 distinct *P. aeruginosa* strains have >300 CBASS operons (Figure 2.6A-B). These systems span Type I-III and use numerous effector proteins and cyclic oligonucleotides⁷. The diverse CBASS types in *P. aeruginosa* suggest that it is important for host fitness and that it may be well suited to study phage-CBASS interactions. To identify naturally functional CBASS immunity in *P. aeruginosa*, CBASS loci were deleted from the genome of four strains possessing representatives of the common CBASS types (Type I-A, II-A, II-C, and III-C; Figure 2.6C) using a CRISPR-Cas3 tool⁸⁹. Notably, these strains also encode numerous other anti-phage immune systems (Figure 2.1A). Therefore, due to the multitude of immune systems, we screened the CBASS mutants against a diverse panel of ~70 phages, which spanned 23 different genomic families and four different morphologies (Myoviridae, Siphoviridae, Podoviridae, and Inoviridae⁹⁰). A single *P. aeruginosa* strain (BWHPA011; Pa011) was identified with CBASS-dependent anti-phage activity (Figure 2.6D-E).

Deletion of the Pa011 Type II-A CBASS operon (Δ CBASS, Figure 2.1B) resulted in >4 orders of magnitude increase in titer of the dsDNA podophage PaMx41 (Figure 2.1C-D). Phage protection was restored when all four CBASS genes (*capV* (phospholipase effector), *cdnA* (CD-NTase), *cap2* (E1/E2 ubiquitin-ligase-like domains), and *cap3* (JAB de-ubiquitinating enzyme-like domain)) were complemented on a plasmid (Figure 2.6G). To determine which genes are necessary for CBASS anti-phage activity, chromosomal mutants known to disrupt catalytic activity^{21,53,87} were generated: *capV*^{S48A}, *cdnA*^{D87A/D89A}, *cap2*^{C450A/C453A}, and *cap3*^{E38A}. *CapV*, *cdnA*, and *cap2* mutations abolished anti-phage activity whereas the *cap3* mutation did not (Figure 2.6H). Furthermore, using an ELISA, we observed that PaMx41 infection generated low levels of 3',3'-cGAMP (~8 nM; Figure 2.7A-B)

whereas the molecule was nearly undetectable in CdnA mutant strain (~0.5 nM; 0.24 nM level of detection). These data demonstrate that Pa011 CBASS-based immunity is naturally active, significantly limits phage replication, and requires CapV, CdnA, and Cap2 enzyme activities for phage targeting.

2.3.2. PaMx41-like phages encode a CBASS antagonist

How CBASS detects and targets phage is currently unknown. Therefore, to identify phage genes required for successful CBASS activity, we isolated PaMx41 mutants that resist Pa011 CBASS-based immunity. With a frequency of 3.7×10^{-5} (Figure 2.1D), 10 independent PaMx41 CBASS “escape” phages were isolated that replicate well on Pa011 WT (Figure 2.1B). Whole genome sequencing revealed one mutation in all CBASS escape phages: a no-stop extension mutation (X37Q) in *orf24* (Figure 2.1E). X37Q lengthens gp24 from a 37 amino acid (a.a.) protein to 94 a.a. Interestingly, the naturally CBASS resistant phages, PaMx33, PaMx35, and PaMx43, share >96% nucleotide identity across the genome and naturally encode the 94 a.a. version with >98% a.a. identity.

To determine whether the short gp24 activates CBASS or the long gp24 antagonizes it, the PaMx41 gp24 variants were overexpressed in Pa011 WT and Δ CBASS cells and then plaque assays were performed. In the presence of CBASS, the long gp24 increased the titer of the PaMx41 WT phage by >4 orders of magnitude while the truncated gp24 versions had no effect (Figure 2.1F). In contrast, the PaMx41 escaper phage and PaMx33, PaMx35, and PaMx43 phages exhibited high titer on all strains (Figure 2.7C), demonstrating that the short gene is not a dominant CBASS activator. We next deleted *orf24* from all of the resistant PaMx41-like phages using a Cas13a selection tool because these phages were surprisingly resistant to all tested DNA-targeting CRISPR-Cas systems⁹¹. In Pa011 WT cells, the titer of the Δ *orf24* phages was reduced 2-4 orders of magnitude; however, expression of the long gp24 *in trans* rescued the phages (Figure 2.2A-B, 2.7D). Taken together, these results indicate that the long gp24, or Acb2 (anti-CBASS 2; PaMx33 NCBI ID: ANA48877) hereafter, inhibits Pa011 CBASS immunity and is necessary for phage replication in the presence of CBASS.

2.3.4. *Acb2* has conserved function in a broadly distributed temperate phage family

Homology searches with *Acb2* revealed that it is encoded in a striking number of tailed phages, including those infecting *Pseudomonas*, *Vibrio*, *Acinetobacter*, *Salmonella*, *Serratia*, *Erwinia*, and *Escherichia* sp. (T2 and T4 phages; gene: *vs.4*), among others (Figure 2.8A). We observed no other examples of the truncated *Acb2* variant encoded in PaMx41 WT phage. A multi-sequence alignment with diverse homologs revealed highly conserved N- and C-termini with a middle region of varied length and sequence (Figure 2.8B), but no molecular function could be predicted. Furthermore, *acb2* is commonly encoded by *P. aeruginosa* B3-like temperate phages (e.g. JBD67), which are unrelated to the PaMx41-like lytic phages. Since JBD67 phage does not replicate on the Pa011 strains, we integrated the Type II-A CBASS operon with its native promoter into the chromosome of a *P. aeruginosa* strain (POA1) that is sensitive to this phage and naturally lacks CBASS. This engineered strain (Pa^{CBASS}) was active and reduced PaMx41 WT phage titer by 3-4 orders of magnitude (Figure 2.6D, 2.6F). By contrast, JBD67 exhibited resistance to the Pa^{CBASS} strain while a related phage that naturally lacks the *acb2* gene, JBD18, was robustly inhibited (Figure 2.2C-D, 2.7E). Deletion of *acb2* from JBD67 using a helicase attenuated Cascade-Cas3 system (see Methods) sensitized it to CBASS immunity (Figure 2.2C-D, 2.7E). The titer of JBD67 Δ *acb2* and JBD18 phages were reduced by >5 orders of magnitude in the presence of CBASS. Expression of *acb2* derived from either JBD67 or PaMx41-*orf24*^{X37Q} on a plasmid fully restored the titer of the PaMx41 Δ *acb2* phage, and only partially restored the titer of the JBD67 Δ *acb2* and JBD18 phages (Figure 2.2C, 2.7E). We hypothesize that JBD67 and JBD18 more strongly activate CBASS, and consequently, *Acb2* expression *in trans* becomes partially overwhelmed. Together, these results collectively demonstrate that *acb2* retains its anti-CBASS function across distinct phage families.

Given that JBD67 is a temperate phage, we investigated whether *acb2* is active during lysogeny as a prophage and therefore inhibits a co-encoded CBASS system. Lysogens were constructed with JBD67 in the Pa^{CBASS} strain, where CBASS targets the super-infecting phage D3. JBD67 and D3 are from

hetero-immune groups, so there is no super-infection exclusion between these phages. Interestingly, the degree to which CBASS targets D3 was not impacted by the presence of *acb2* in the JBD67 prophage (Figure 2.2E, 2.7F). This suggests that *acb2* is not expressed during lysogeny and allows functional CBASS immunity despite a prophage-encoded inhibitor. However, upon exit from lysogeny, CBASS significantly blocks JBD67 Δ *acb2* prophage induction, reducing the induced titer by ~5-orders of magnitude whereas JBD67 WT prophage induction was unaffected (Figure 2.2F). These collective findings demonstrate that *acb2* is active during lysogenic induction, but not lysogenic maintenance, and importantly shows that CBASS can dramatically limit prophage induction.

2.3.5. Acb2 sequesters 3',3'-cGAMP to inhibit CBASS

To determine the mechanism of Acb2, we purified Acb2 from the naturally CBASS-resistant PaMx33 phage and each CBASS protein to test direct CBASS antagonism. First, we tested binding and found that Acb2 did not bind to purified CapV, CdnA, Cap2, nor the CdnA-Cap2 complex, which was purified as described previously⁸⁷(Figure 2.9A-D). Next, we reconstituted CapV phospholipase activity *in vitro* and confirmed that it is only activated by 3',3'-cGAMP in a concentration-dependent manner, but not by 2',3'-cGAMP, c-di-AMP, or c-di-GMP (Figure 3A). When Acb2 was preincubated with 3',3'-cGAMP, CapV activity was abrogated (Figure 2.3A), suggesting that Acb2 may directly bind to the 3',3'-cGAMP molecule. A native gel assay showed a significant shift of the purified Acb2 protein upon adding 3',3'-cGAMP (Figure 2.3B). Isothermal calorimetry (ITC) experiments further verified that Acb2 directly binds to 3',3'-cGAMP with a K_D of ~87 nM (Figure 2.3C, 2.9E). Together, these data suggest that Acb2 binding of 3',3'-cGAMP antagonizes CBASS by reducing available signaling molecules.

Recent studies have reported that eukaryotic⁵⁵ and prokaryotic^{43,48} viruses express proteins that directly degrade cyclic oligonucleotides. Therefore, to determine whether Acb2 is an enzyme that cleaves 3',3'-cGAMP molecules, we performed the CapV phospholipase activity assay using a series of Acb2 concentrations and Acb2-3',3'-cGAMP incubation times. Inhibition of CapV activity was concentration-dependent, but not time-dependent (Figure 2.3D), suggesting that Acb2 is a protein that

sponges and sequesters 3',3'-cGAMP rather than degrade it. High-performance liquid chromatography (HPLC) clearly showed that incubation of Acb2 depletes detectable 3',3'-cGAMP, and following proteolysis of Acb2, the molecule is released back into the buffer (Figure 2.3E). Filtration of the unbound 3',3'-cGAMP enabled CapV to regain its enzymatic activity, demonstrating that the molecule is still active (Figure 2.3A). Consistent with these results, overexpression of Acb2 in phage-infected Pa011 WT cells reduced detectable 3',3'-cGAMP levels, but following phenol-chloroform/chloroform nucleotide extraction, the molecule was released and levels increased ~4-fold (Figure 2.7A-B). Altogether, these results demonstrate that Acb2 antagonizes Type II-A CBASS immunity via binding and sequestering the 3',3'-cGAMP dinucleotide, which prevents phospholipase effector activation.

2.3.6. Crystal structure of Acb2 and its complex with 3',3'-cGAMP

To further understand how Acb2 interacts with 3',3'-cGAMP, we determined the crystal structures of apo Acb2 and its complex with the signaling molecule (Table 2.1). Interestingly, Acb2 folds as a homo-hexamer in its apo (Figure 2.4A) and 3',3'-cGAMP bound form (Figure 2.4B). Analytical ultracentrifugation (AUC) assay also indicated that Acb2 is a hexamer in its apo and 3',3'-cGAMP-bound forms in solution (Figure 2.10A-E). Each protomer mainly interacts with two adjacent protomers (Figure 2.10B), allowing the six protomers to interlock into a compact assembly. An Acb2 protomer consists of one short N-terminal helix and two long anti-parallel helices, with a kink in the long helix at the C-terminus (Figure 2.10C). The ligand-bound structure showed that one Acb2 hexamer binds three 3',3'-cGAMP molecules (Figure 2.4B). Each cGAMP binding pocket is formed by two Acb2 protomers that interact in a head-to-head manner, and is mainly composed of N- and C-terminal helices/loops from each protomer (Figure 2.10D). This is consistent with the Acb2 multiple sequence alignment, which revealed highly conserved N- and C-termini (Figure 2.8B). Searches using the Dali (distance-matrix alignment) server did not return entries with the same protein fold as Acb2⁹², indicating that Acb2 adopts an overall novel cyclic dinucleotide binding fold. In support of these findings, a recent

preprint⁵³ demonstrated that the Acb2 homolog from *E. coli* phage T4 (gene *vs.4*) tightly binds to 3',3'-cGAMP (K_D of ~30 nM) and adopts a hexameric structure similar to the one reported here.

Acb2 binding of a cyclic dinucleotide ligand only causes a slight movement of the loop linking $\alpha 1$ and $\alpha 2$ (named loop L12) towards the ligand (Figure 2.4D), but several other residues display rotations and movements upon ligand binding. Among them, the most dramatic movement happens in Y11 from both protomers, which rotates and forms π - π interactions with the purine bases of cGAMP, as well as hydrogen bonds with the phosphate group of cGAMP (Figure 2.4E). In addition, K26 in $\alpha 2$ of both protomers forms a salt bridge with the phosphate group of the cGAMP, possibly stabilizing the molecule together with Y11 (Figure 2.4F). Additionally, cGAMP is stabilized through hydrophobic interactions by several residues from both protomers, such as L14, M22, M81, I84 and P90 (Figure 2.4F). Consistent with these analyses, Acb2 Y11A and K26A mutants were inactive in plaque assays (Figure 4I) and the Acb2 K26A mutant expressed in the Pa011 WT strain lost its ability to sequester 3',3'-cGAMP *in vivo* (Figure 2.7A-B). Furthermore, Acb2 Y11A and K26A mutants abolished Acb2 binding of 3',3'-cGAMP *in vitro* (Figure 2.4G, 2.9I-K) and abrogated its ability to reduce CapV activity (Figure 2.4H). These data collectively show that Acb2 proteins form a complex with cyclic dinucleotides and subsequently reduces downstream CBASS activation.

2.3.7. Acb2 sequesters variety of cyclic dinucleotides

The binding mode of 3',3'-cGAMP within Acb2 implied that other cyclic dinucleotides could also be sequestered by this protein. Indeed, native gels and ITC experiments demonstrated that Acb2 also binds to 2',3'-cGAMP and c-di-AMP with high affinity (K_D of ~103 and 66 nM, respectively), but not c-di-GMP (Figure 2.3B-C, 2.9F-G). HPLC assays confirmed that Acb2 could also sequester c-di-AMP and 2',3'-cGAMP, and showed a very weak sequestering effect on c-di-GMP (Figure 2.10F-H). The Acb2-c-di-AMP structure was also solved (Table 2.1) and c-di-AMP showed a similar binding mode as 3',3'-cGAMP (Figure S5I-K). Additional native gels and ITC experiments showed that Acb2 can bind to 3',3'-c-di-UMP (cUU) and 3',3'-c-UMP-AMP (cUA) with high affinity (K_D of ~99 and 97 nM,

respectively), and binds to 3',3'-c-UMP-GMP (cUG) with lower affinity (K_D of ~524 nM) (Figure 2.11A-E). Next, we tested whether phages expressing *acb2* could inhibit CBASS subtypes *in vivo* that harbor a CdnE cyclase, which are predicted to generate cUU, cUA, and/or cUG (Personal Communication with A. Whiteley)⁷. In our strain collection, we identified that *P. aeruginosa* strains ATCC 33351 and JD332 encode Type I-A and Type I-B CBASS operons, respectively, with a CdnE cyclase (Figure 2.11F). When expressed in a *P. aeruginosa* strain (PAO1 WT) that naturally lacks CBASS, the titer of phages lacking *acb2* was reduced 1-3 orders of magnitude – most notably by JD332 Type I-B CBASS – and the isogenic phages containing *acb2* remained resistant to CBASS (Figure 2.11G). Together, these *in vitro* and *in vivo* results suggest that Acb2 can broadly inhibit CBASS types that utilize cyclic dinucleotides with uracil and adenine bases.

2.3.8. Phages escape CBASS via mutations in the capsid gene

The function and mechanism of *acb2* demonstrates that CBASS places strong evolutionary pressure on phage. Therefore, we sought to determine whether any alternative mechanisms to evade CBASS exist. We again attempted to identify mutant escape phages, but this time, we used phage lacking *acb2* (PaMx41 Δ *acb2*). Phages were first exposed directly to CBASS by plating on Pa011 WT, which yielded no escape plaques. However, the invisible phage population on the plate was collected, amplified in the Pa011 Δ CBASS strain, and ultimately escape phages were isolated under CBASS selection (Figure 2.5A). Whole genome sequencing revealed that all seven escape phages had one of four different missense point mutations in the major capsid gene (*orf11*, NCBI ID: YP_010088887.1; Figure 2.5B, Table 2.2). To confirm the causality of the capsid mutations for CBASS escape, we used plasmid-based recombination to introduce *de novo* mutations I121A, I121T, and S330P into a naive PaMx41 Δ *acb2* phage and confirmed that these mutations induced CBASS escape (Figure 2.5C-D). To test whether the major capsid is sufficient to trigger CBASS, the PaMx41 WT or mutant major capsid gene with its native promoter was cloned and expressed in Pa011 WT and Δ CBASS cells. In the presence of the WT major capsid, we did not observe any CBASS-dependent cellular toxicity, indicating that capsid monomer is not sufficient to activate CBASS. We also did not observe CBASS-

dependent targeting of resistant phage (Figure 2.12A). Likewise, expression of the mutant major capsid gene did not induce escape of CBASS sensitive phage (Figure 2.12B). We anticipate that the plasmid-encoded major capsid gene does not express well enough to sufficiently displace the phage-expressed major capsid gene in a manner that impacts the CBASS phenotype.

CBASS escape phages were also isolated from JBD67 Δ *acb2* and JBD18 phages on the Pa^{CBASS} strain (Figure 2.5A). Strikingly, whole genome sequencing revealed missense point mutations in the genes encoding their major capsid proteins [*orf32* in JBD67 (NCBI ID: YP_009625956) and *orf35* in JBD18 (NCBI ID: AFR52188); Figure 2.5B, Table 2.2]. The PaMx41 major capsid protein shares no significant amino acid identity with the JBD67 and JBD18 major capsid proteins, yet the mutations all converge on the same protein. When modeling the location of the mutations on the predicted major capsid monomer structures, we did not observe overlap between the distinct phages (Figure 2.12C). However, modeling of the predicted major capsid hexamer structures indicated that the mutations lie on the protein-protein interface within or between hexamers (Figure 2.12D-E), suggesting that a higher ordered capsid structure or process may be implicated in CBASS immunity. Interestingly, some of the observed capsid mutant genotypes (i.e. I121S/T from PaMx41, N191H from JBD67, and N275D from JBD18) are common natural alleles in the capsids of other phages, suggesting that these genotypes are fit. Follow-up studies are needed to determine the mechanistic connection between the major capsid protein and CBASS.

2.4. Discussion

The discovery and characterization of CBASS marked an exciting connection between prokaryotic and eukaryotic immunity^{31,85}. However, many questions remain in this nascent field regarding phage-host evolution, as well as CBASS regulation and activation mechanisms, that can be best addressed through utilization of endogenous CBASS model systems. We found that the *P. aeruginosa* BWHPA011 (Pa011) strain harbors a cGAS-like enzyme (CdnA) that produces 3',3'-cGAMP dinucleotides in response to PaMx41 phage infection, which activates the phospholipase (CapV)

effector. Phages related to PaMx41 (or an escape mutant derived from PaMx41) produce an anti-CBASS protein (Acb2) that is expressed as a middle gene in the phage replication cycle⁹³ and sequesters 3',3'-cGAMP. Acb2 likely accumulates prior to the production of the dinucleotide given that previous work demonstrated 3',3'-cGAMP levels increase later in the *E. coli* phage P1 replication cycle²¹. Furthermore, when studying the temperate phage JBD67 with its *acb2* gene removed, we found that CBASS limits prophage induction *and* lytic phage replication, which had not been previously noted.

The cyclic dinucleotide “sponge” protein discovered in this study, Acb2, joins an expanding repertoire of phage-encoded antagonists that directly act on signaling molecules involved in bacterial anti-phage immunity. Previous examples include the anti-CRISPR (AcrIII1) protein that cleaves c-A₄ molecules⁴³, and the anti-Pycsar (Apyc1) protein that cleaves a spectrum of cyclic nucleotides⁴⁸. In parallel, a Thoeris anti-defense (Tad1) protein was found to specifically bind to and sequester gcADPR molecules⁴⁹. Additionally, the anti-CBASS gene identified (Acb1) is another class of phage enzymes, similar to Apyc1, that harbors a phosphodiesterase fold that specifically binds and cleaves cyclic nucleotides⁴⁸. This is a common inhibitory mechanism of the eukaryotic cGAS-STING signaling system and is utilized by poxviruses⁵⁵ and a host pyrophosphatase/phosphodiesterase protein⁹⁴, which enzymatically cleaves and depletes 2',3'-cGAMP. By contrast, Acb2 binds to and sequesters bacterial 3',3'-cGAMP, c-di-AMP, 3',3'-c-di-UMP, 3',3'-cUA, 3',3'-cUG, and human 2',3'-cGAMP. The structure and mechanism of Acb2 were independently confirmed with a homolog from *E. coli* phage T4 in a recent preprint⁵³. Despite the numerous different mechanisms employed by viruses to inhibit the eukaryotic cGAS-STING signaling system⁹⁵, the cGAMP “sponge” mechanism is an entirely new inhibitory strategy.

The identification of capsid mutants that escape CBASS mirrors the recently identified major capsid mutations in *E. coli* phage T5, which enables escape from Pycsar (pyrimidine cyclase system for anti-phage resistance)²⁰. This study also noted that expression of the T5 WT major capsid protein alone

did not induce Pycsar-mediated toxicity, which we similarly observed, nor was direct binding observed between the T5 major capsid protein and any of the Pycsar proteins²⁰, suggesting a more complex or indirect activation mechanism. However, abortive immune systems can be activated through direct binding to a capsid monomer, such as the CapRel^{SJ46} Toxin-Antitoxin system²⁸ and the Lit protease⁹⁶. These mechanistically diverse systems all converge on the phage capsid protein, which is one of many phage structural proteins mutated to evade targeting of anti-phage bacterial immune systems⁶⁶. Additionally, binding to other phage structural proteins directly activate Avs (anti-viral STAND NTPases)⁶ and DSR (defense-associated sirtuins) systems¹⁴. The major capsid gene mutations identified in our study are enriched at the capsid protein interface, suggesting that a higher ordered capsid structure or process, rather than a capsid monomer, may be implicated in CBASS immunity. However, the mechanism behind the mutant phage capsid that enables CBASS evasion is unknown and remains an area of future investigation. Altogether, we present direct evidence of CBASS as an anti-phage bacterial immune system, uncover distinct paths taken by phage to inhibit or evade immunity, and expand our understanding of viral evasion strategies of cGAS-based immunity.

2.5. Limitations of the Study

Here, we report the establishment of a native CBASS model system and used it to identify phage mutants that inhibit or evade CBASS. We were unable to establish additional native CBASS model systems because we could not identify phages targeted in a CBASS-dependent manner, which is likely because *P. aeruginosa* harbors several diverse anti-phage systems and a single strain alone can encode one to 17 (known) systems^{4,72}. Furthermore, we describe a cyclic dinucleotide sponge (Acb2) as a mechanism to inhibit multiple cGAS-based immune systems. However, we have not comprehensively sampled the array of cyclic oligonucleotides that this protein family may bind to, which should be completed to further define the selectivity of the new Acb2 protein fold. An additional limitation of our study is that *in vivo* 3',3'-cGAMP measurements reveal a low intracellular concentration (<10 nM), which is likely due to lower expression of CBASS genes compared to previous studies. It is also possible that uninfected cells or asynchronous infection leads to lower 3',3'-cGAMP

levels, and given that our measurement represents an average of the entire cell population, the total 3',3'-cGAMP levels are lower. Lastly, our study identified that phage capsid mutants evade CBASS targeting. Despite this, it is unknown whether the phage capsid evades the activation of the cyclase (CdnA), regulation of the cyclase (via Cap2 or Cap3), targeting of the CapV effector, or evades another stage of CBASS that has yet to be studied.

2.6. Author Contributions

Erin Huiting (EH) conceived the project, designed, and performed all *in vivo* experiments, and wrote the manuscript. Xueli Cao (XC), Zhaorong Luo, and Na An purified the proteins. XC grew and optimized the crystals, collected the diffraction data and performed the biochemical experiments. Januka Athukoralage assisted with *in vitro* experiments. Sukrit Silas and Héloïse Carion contributed to execution and analysis of the whole genome sequencing data. Jie Ren performed the HPLC analysis. Yu Zhou performed the analysis of the binding characteristics of the ligands. James S. Fraser performed the computational modeling and analysis of the phage capsid proteins. Yue Feng designed and supervised the structural and mechanistic studies of Acb2, solved the crystal structure, analyzed the data and wrote part of the manuscript. Joseph Bondy-Denomy supervised the project, designed experiments, and wrote the manuscript.

2.7. Materials and Methods

Data and Code Availability

The accession number for the coordinate and structure factors reported in this paper is PDB: 8H2X (Acb2), 8H2J (Acb2-3',3'-cGAMP) and 8H39 (Acb2-c-di-AMP). This paper does not report original code. Any additional information required to reanalyze the data reported in this paper is available from the Lead Contact upon request.

Bacterial strains and phages

The bacterial strains and phages used in this study are listed online (doi: 10.1016/j.cell.2022.12.041). The *P. aeruginosa* strains (ATCC 33351, JD332, BWHPA011, BWH058, ATCC 27853, PAO1) and *E. coli* strains (DH5 α and SM10) were grown in Lysogeny broth (LB) medium at 37°C both with aeration at 225 r.p.m. Plating was performed on LB solid agar with 10 mM MgSO $_4$ when performing phage infections, and when indicated, gentamicin (50 μ g ml $^{-1}$ for *P. aeruginosa* and 15 μ g ml $^{-1}$ for *E. coli*) was used to maintain the pHERD30T plasmid. Gene expression was induced by the addition of L-arabinose (0.01% final for BWHPA011 bacterial genes and 0.1% for phage genes, unless otherwise specified). The *E. coli* BL21 (DE3) strain was used for recombinant protein overexpression and grown in Lysogeny broth (LB) medium. The cells were grown at 37°C until OD $_{600\text{nm}}$ reached 0.8 and then induced at 18°C for 12 h.

Identification of CBASS operons

tBLASTn was used to query the amino acid sequence of eight known CD-NTases (CdnA-H) against sequenced *Pseudomonas aeruginosa* genomes contained in the NCBI and IMG databases as well as our sequenced UCSF clinical isolates. Proteins with >25% amino acid sequence identity to a validated CD-NTase were accepted as “hits”³¹, leading to the identification of >300 CBASS operons in 252 distinct *P. aeruginosa* strains. The *P. aeruginosa* BWHPA011 (Pa011) strain contains a Type II-A CBASS operon in contig 12 (NCBI Genome ID: NZ_AXQR000000012.1) ranging from 1250439-1254679bp, with CapV (phospholipase effector, NCBI Gene ID: Q024_30602), CdnA (cyclase, Q024_30601), Cap2 (E1/E2, Q024_30600), and Cap3 (JAB, intergenic region 1250439-1250912bp).

Identification of anti-phage immune systems

DefenseFinder was used to systematically identify all known anti-phage bacterial immune system operons in *P. aeruginosa* strains^{72,97}, and the output was used to construct the table in Figure 2.1A.

Episomal gene expression

The shuttle vector that replicates in *P. aeruginosa* and *E. coli*, pHERD30T⁹⁸ was used for cloning and episomal expression of genes in *P. aeruginosa* BWHPA011 (Pa011) or PAO1 strains. This vector has an arabinose-inducible promoter and a selectable gentamicin marker. Vector was digested with SacI and PstI restriction enzymes unless stated otherwise and then purified. Inserts were amplified by PCR using bacterial overnight culture or phage lysate as the DNA template, and joined into the pHERD30T vector at the SacI-PstI restriction enzyme cut sites by Hi-Fi DNA Gibson Assembly (NEB) following the manufacturer's protocol. The resulting plasmids were transformed into *E. coli* DH5 α . All plasmid constructs were verified by sequencing using primers that annealed to sites outside the multiple cloning site. *P. aeruginosa* cells were electroporated with the pHERD30T constructs and selected on gentamicin.

Site-directed mutagenesis

Site-directed mutagenesis (SDM) of the pHERD30T constructs introduced mutations in the *acb2* gene that were not found naturally in the phages and therefore could not be amplified via PCR. Primers were designed so that the forward primer encompassed the nucleotide mutations and the reverse primer directly adjacent. Primers were subjected to a T4 PNK phosphorylation reaction and then around-the-world PCR was performed. The linearized plasmid was confirmed on a gel, subjected to DpnI digestion to remove parent wild-type plasmid, and then purified. A T4 DNA ligase reaction was performed and resulting plasmids were used for transformations and sequenced verified.

Chromosomal CBASS integration

For chromosomal insertion of the Pa011 CBASS operon, the integrating vector pUC18-mini-Tn7T-LAC⁹⁹ and the transposase expressing helper plasmid pTNS3¹⁰⁰ were used to insert the BWHPA011 CBASS operon at the Tn7 locus in *P. aeruginosa* PAO1 strain (Pa^{CBASS}), or an pUC18-mini-Tn7T-LAC empty vector (E.V.) control strain (Pa^{EV}). The vector was linearized using around-the-world PCR, treated with DpnI, and then purified. Two overlapping inserts encompassing the CBASS operon were

amplified by PCR using Pa011 overnight culture as the DNA template, and joined into the pUC18-mini-Tn7T-LAC vector at the SacI-PstI restriction enzyme cut sites by Hi-Fi DNA Gibson Assembly (NEB) following the manufacturer's protocol. The resulting plasmids were used to transform *E. coli* DH5 α . All plasmid constructs were verified by sequencing using primers that annealed to sites outside the multiple cloning site. *P. aeruginosa* PAO1 cells were electroporated with pUC18-mini-Tn7T-LAC and pTNS3 and selected for on gentamicin. Potential integrants were screened by colony PCR with primers PTn7R and PglmS-down, and then verified by sequencing using primers that anneal to sites outside the attTn7 site. Electrocompetent cell preparations, transformations, integrations, selections, plasmid curing, and FLP-recombinase-mediated marker excision with pFLP were performed as described previously⁹⁹.

Chromosomal mutants of *P. aeruginosa* BWHPA011

The allelic exchange vector that replicates in *P. aeruginosa* and *E. coli*, pMQ30¹⁰¹ was used for generating the chromosomal CBASS knockout and CBASS mutant genes in *P. aeruginosa* BWHPA011 (Pa011). Vector was digested with HindIII and BamHI restriction enzymes and purified. For the CBASS knockout strain, homology arms >500bp up- and downstream of CBASS operon were amplified by PCR using Pa011 overnight culture as the template DNA. For the CBASS gene mutant strains, homology arms >500bp up- and downstream of CBASS gene catalytic residue(s), with the appropriate mutant nucleotides, were amplified by PCR using Pa011 overnight culture as the template DNA. Previously identified catalytic residues in *Escherichia coli* TW11681 (NZ_AELD01000000)²¹ were used to aid the identification of the catalytic residues in *Pseudomonas aeruginosa* BWHPA011. Multiple Sequence Comparison by Log-Expectation (MUSCLE,⁴³ and NCBI Multiple Sequence Alignment Viewer (MSA) were subsequently used to validate conserved catalytic residues between *P. aeruginosa* BWHPA011, *Vibrio cholerae* El Tor N16961 (NC_002505.1), and *E. coli* TW11681. The inserts were joined into the pMQ30 vector at the HindIII-BamHI restriction enzyme cut sites by Hi-Fi DNA Gibson Assembly (NEB) following the manufacturer's protocol. The resulting plasmids were transformed into *E. coli* DH5 α . All plasmid constructs were verified by sequencing using primers that

annealed to sites outside the multiple cloning site. *E. coli* SM10 cells were electroporated with pMQ30 constructs and selected for on gentamicin. *E. coli* SM10 harboring the pMQ30 construct were mated with Pa011 to transfer the plasmid and enable allelic exchange. Potential mutant Pa011 strains were subjected to a phenotype cross streak screen with PaMx41-like phages and then verified by sequencing using primers that anneal to sites outside of the homology arms. Electrocompetent cell preparations, transformations, selections, and plasmid curing were performed as described previously¹⁰².

Phage growth

All phages were grown at 37°C with solid LB agar plates containing 20 ml of bottom agar containing 10 mM MgSO₄ and any necessary inducers or antibiotics. Phages were initially grown on the permissible host *P. aeruginosa* PAO1 WT, which naturally lacks CBASS. 150 µl of overnight cultures of PAO1 were infected with 10 µl of low titer phage lysate (>10⁴⁻⁷ pfu/ml) and then mixed with 3 ml of 0.7% top agar 10 mM MgSO₄ for plating on the LB solid agar. After incubating at 37°C overnight, individual phage plaques were picked from top agar and resuspended in 200 µl SM phage buffer. For high titer lysates, the purified phage was further amplified on LB solid agar plates with PAO1 WT. After incubating 37°C overnight, SM phage buffer was added until the solid agar lawn was completely covered and then incubated for 5-10 minutes at room temperature. The whole cell lysate was collected and a 1% volume of chloroform was added, and then left to shake gently on an orbital shaker at room temperature for 15 min followed by centrifugation at maximum g for 3 min to remove cell debris. The supernatant phage lysate was stored at 4°C for downstream assays.

Plaque assays

Plaque assays were conducted at 37°C with solid LB agar plates. 150 µl of overnight bacterial culture was mixed with top agar and plated. Phage lysates were diluted 10-fold then 2 µl spots were applied to the top agar after it had been poured and solidified.

Lysogen construction with JDB67 phage

Lysogens were constructed by spotting serial dilutions of JDB67 WT or JDB67 Δ *acb2* phage lysates on the engineered *P. aeruginosa* PAO1 strain that harbors BWHPSA011 CBASS in the chromosome (Pa^{CBASS}), or a mini-Tn7 E.V. control (Pa^{EV}) strain, and streaking out the bacteria (that is, putative lysogens) from the inside of the clearing resulting from a clutter of plaques onto a solid LB agar plate. Colonies were then screened using a cross streak test to confirm resistance to the phage used to lysogenize the strain. The putative lysogens were grown in liquid culture, and the presence of spontaneously produced phage in the supernatant that could plaque on the PAO1 wildtype strain confirmed lysogeny.

Isolation of CBASS phage escapers

For identifying PaMx41 WT phage escapers of CBASS, 150 μ l of overnight cultures of the *P. aeruginosa* strain BWHPSA011 (Pa011) were infected with 10 μ l of high titer phage lysate ($>10^9$ pfu/ml) and then plated on LB solid agar. After incubating at 37°C overnight, 10 individual phage plaques were picked from top agar and resuspended in 200 μ l SM phage buffer. Phage lysates were purified for three rounds using the CBASS expressing strain. Three PaMx41 WT control phages were picked, purified, and propagated in parallel by infecting the Pa011 Δ CBASS strain. To validate the phage identity, PCR and Sanger sequencing were performed on nucleotide sequences unique to PaMx41.

To identify PaMx41 Δ *acb2*, JDB67 Δ *acb2*, and JDB18 WT phage escapers of CBASS, 150 μ l of overnight cultures of the CBASS expressing strains (Pa011 WT or Pa^{CBASS}) were infected with 10 μ l of high titer phage lysate ($>10^9$ pfu/ml) and plated on LB solid agar. After incubating at 37°C overnight, no obvious plaques were observed. SM phage buffer was added to the entire lawn and whole cell lysate collected. Next, to propagate the mutant escaper phage population, 150 μ l of overnight cultures of the *P. aeruginosa* strains lacking CBASS (Pa011 Δ CBASS or Pa^{EV}) were infected with 10 μ l of the phage lysates and plated on LB solid agar. After incubating at 37°C overnight, SM phage buffer was

added to the entire lawn and whole cell lysate collected. Lastly, to isolate individual escaper plaques, 150 μ l of overnight cultures of the CBASS expressing strains (Pa011 WT or Pa^{CBASS}) were infected with 10 μ l of the previously collected phage lysate and plated on LB solid agar. After incubating at 37°C overnight, at least four individual phage plaques were picked from top agar and resuspended in 200 μ l SM phage buffer. Phage lysates were purified for three rounds using the CBASS expressing strain. At least two control or WT phages were picked, purified, and propagated in parallel by infecting the Pa011 Δ CBASS or Pa^{EV} strains. To validate the phage identity, PCR and Sanger sequencing were performed on nucleotide sequences unique to each phage.

Whole genome sequencing (WGS) and analysis

Genomic DNA from phage lysates was extracted using a modified SDS/Proteinase K method. Briefly, 200 μ L high titer phage lysate ($>10^9$ pfu/ml) was mixed with an equal volume of lysis buffer (10 mM Tris, 10 mM EDTA, 100 μ g/mL proteinase K, 100 μ g/mL RNaseA, 0.5% SDS) and incubated at 37°C for 30 min, and then 55°C for 30 min. Preps were further purified using the DNA Clean & Concentrator Kit (Zymo Research). DNA was quantified using the Qubit 4.0 Fluorometer (Life Technologies). 20-100 ng genomic DNA was used to prepare WGS libraries using the Illumina DNA Prep Kit (formerly known as Illumina Nextera Flex Kit) using a modified protocol that utilized 5x reduced quantities of tagmentation reagents per prep, except for the bead washing step with Tagment Wash Buffer (TWB), where the recommended 100 μ L of TWB was used. Subsequent on-bead PCR indexing-amplification of tagmented DNA was performed using 2x Phusion Master Mix (NEB) and custom-ordered indexing primers (IDT) matching the sequences from the Illumina Nextera Index Kit. Each 50 μ L reaction was split in two tubes, amplified for 9 and 12 cycles respectively. Libraries were further purified by agarose gel electrophoresis; DNA was excised around the ~400 bp size range and purified using the Zymoclean Gel DNA Recovery Kit (Zymo Research). Libraries were quantified by Qubit and the 9-cycle reaction was used unless the yield was too low for sequencing, in which case the 12-cycle reaction was used. Libraries were pooled in equimolar ratios and sequenced with Illumina MiSeq v3 reagents (150 cycles, Read 1; 8 cycles, Index 1; 8 cycles, Index 2). WGS data were demultiplexed

either on-instrument or using a custom demultiplexing Python script (written by Dr. Nimit Jain), and trimmed using cutadapt (v 3.4⁴⁵) to remove Nextera adapters. Trimmed reads were mapped using Bowtie 2.0 (--very-sensitive-local alignments⁴⁶) and alignments were visualized using IGV (v 2.9.4⁴⁷). Variants were detected using the SeqDiff program (<https://github.com/hansenlo/SeqDiff>).

CRISPR-Cas13a phage gene editing

Construction of template plasmids for homologous recombination and selection of engineered phages via the CRISPR-Cas13a system were performed as described previously⁹¹. Specifically, homology arms of >500bp up- and downstream of PaMx41 *acb2* were amplified by PCR using Pamx41 WT phage genomic DNA as the template. The *acrVIA1* gene was amplified from plasmid pAM383¹⁰³, a gift from Luciano Marraffini, The Rockefeller University. PCR products were purified and assembled as a recombineering substrate and then inserted into the NheI site of the pHERD30T vector. The resulting plasmids were electroporated into *P. aeruginosa* PAO1 cells. PAO1 strains carrying the recombination plasmid were grown in LB media supplemented with gentamicin. 150 µl of overnight cultures were infected with 10 µl of high titer phage lysate (>10⁹ pfu/ml; PaMx33 WT, PaMx35 WT, PaMx43 WT, PaMx41 ESC or PaMx41 WT) and then plated on LB solid agar. After incubating at 37°C overnight, SM phage buffer was added to the entire lawn and whole cell lysate collected. The resulting phage lysate containing both WT and recombinant phages were tittered on PAO1 strains with a chromosomally integrated Type VI-A CRISPR-Cas13a system, and the most efficiently targeting crRNA guide (specific to *orf11*; guide #5) was used to screen for recombinants. PAO1 strains carrying the Cas13a system and crRNA of choice were grown overnight in LB media supplemented with gentamicin. 150 µl of overnight cultures were infected with 10 µl of low titer phage lysate (10⁴⁻⁷ pfu/ml), and then plated onto LB solid agar containing 0.3% arabinose and 1 mM isopropyl β-d-1-thiogalactopyranoside (IPTG). After incubating at 37°C overnight, individual phage plaques were picked from top agar and resuspended in 200 µl SM phage buffer. Phage lysates were purified for three rounds using the Cas13a counter-selection strain (guide #5), and further propagated on a complementary Cas13a counter-selection strain (guide #4), to select against Cas13a escaper phages.

To determine whether the phages were recombinants, PCR was performed with the appropriate pairs of primers amplifying the region outside of the homology arms, an internal region of *acrVIA1*, and *acb2*.

Homologous recombination-mediated mutation of phage gene

Construction of template plasmids for homologous recombination consisted of homology arms >500bp up- and downstream of the mutation of interest encoded in PaMx41 *orf11*. The homology arms were amplified by PCR using PaMx41 Δ *acb2* escapers phage genomic DNA as the template, and PaMx41 WT phage genomic DNA as the control template. Template 1 primers were designed to symmetrically flank the PaMx41 *orf11* mutations I121S and I121T, and template 2 primers were designed to symmetrically flank mutation I327T and S330P. PCR products were purified and assembled as a recombineering substrate and then inserted into the SacI-PstI site of the pHERD30T vector. The resulting plasmids were electroporated into *P. aeruginosa* BWHPA011 (Pa011) Δ CBASS cells. Pa011 strains carrying the recombination plasmid were grown in LB media supplemented with gentamicin. 150 μ l of overnight cultures were infected with 10 μ l of high titer phage lysate ($>10^9$ pfu/ml; PaMx41 Δ *acb2*) and then plated on LB solid agar. After incubating at 37°C overnight, SM phage buffer was added to the entire lawn and whole cell lysate collected. The resulting phage lysate containing both WT and recombinant phages were screened on a lawn of Pa011 WT cells harboring an active CBASS system. Specifically, 150 μ l of overnight Pa011 WT cultures were infected with 10 μ l of low titer phage lysate (10^{4-7} pfu/ml), and then plated onto LB solid agar. After incubating at 37°C overnight, individual phage plaques were picked from top agar and resuspended in 200 μ l SM phage buffer. Phage lysates were purified for three rounds using the Pa011 WT strain. To confirm whether the phages were recombinants, PCR was performed with the appropriate pairs of primers amplifying the region outside of the homology arms and subject to Sanger Sequencing.

Helicase attenuated Cas3 removal of phage genes

Cas3 (Type I-C)-specific guides targeting JBD67 *acb2* were cloned into a pHERD30T-derived vector containing modified I-C repeats as previously described⁸⁹. The guides electroporated into *P. aeruginosa* PAO1 strains with a chromosomally integrated Type I-C helicase attenuated Cas3 system. JBD67 WT phage lysate was tittered on the PAO1 strains and the efficiently targeting crRNA guide (specific to *acb2*; guide #3) was identified. PAO1 strains carrying the Type I-C CRISPR-Cas system with a helicase attenuated Cas3 enzyme and crRNA targeting phage JBD67 *acb2* were grown overnight in LB media supplemented with gentamicin. 150 μ l of overnight cultures were infected with 10 μ l of high titer phage lysate ($>10^9$ pfu/ml; JBD67) and plated on LB agar plates containing gentamicin, 0.1% arabinose, and 1 mM isopropyl β -D-1-thiogalactopyranoside (IPTG). After incubating at 37°C overnight, SM phage buffer was added to the entire lawn and whole cell lysate collected. The resulting phage lysate containing both WT and *acb2* knockout phages were grown on a complementary Cas3 counter-selection strain (guide #4) to select against Cas3 escaper phages. 150 μ l of overnight cultures were infected with 10 μ l of low titer phage lysate (10^{4-7} pfu/ml; JBD67 WT) and then plated on LB solid agar containing 0.1% arabinose and 1 mM IPTG. After incubating at 37°C overnight, individual phage plaques were picked from top agar and replica-plated onto LB solid agar with PAO1^{EV} and PAO1^{CBASS} strains. JBD67 plaque sizes that were reduced on the PAO1^{CBASS} plate compared to the positive control (JBD18 WT phage) were identified as potential CBASS sensitive phages. Corresponding plaques on the PAO1^{EV} plate were picked and resuspended in 200 μ l SM phage buffer. To determine whether the phages harbored deletions in *acb2*, PCR was performed with the appropriate pairs of primers amplifying a ~1kb region outside of *acb2*.

Intracellular 3',3'-cGAMP measurements

Cell lysates were prepared similarly to previous methods²¹, in which *P. aeruginosa* BWHPA011 (Pa011) cells harboring a catalytically dead *capV* gene (CapV^{S48A}) were used and then transformed with a pHERD30T vector expressing *acb2* WT or K26A. Cells were taken from overnight culture, diluted 1:100 in 150ml LB medium with G50 and 0.1% arabinose (flask size 500ml), and then grown

at 37°C (190 r.p.m.) until reaching an OD_{600nm} of 0.3-0.4. From the culture, 100 ml was aliquoted and 10 mM MgSO₄ added. The cells were then infected with PaMx41Δ*acb2* to obtain an MOI of ~5 and ensure at least one or more phages were infecting each bacterial cell. After 60 minutes following infection, the culture was separated into two 50 ml samples and centrifuged at 7,500 g for 10 mins at 4°C. Following centrifugation, supernatant was removed and pellets were kept on ice until resuspended in 600 µl of phosphate buffer (50 mM sodium phosphate (pH 7.4), 300 mM NaCl, 10% (v/v) glycerol). The resuspended pellet was supplemented with 1 µl hen-lysozyme (Sigma-Aldrich), vortexed briefly, and incubated at 25°C for 10 min. The resuspended cells were then mixed with Lysing Matrix B (MP) beads and cells were disrupted mechanically using Mini-Beadbeater 16 Biospec Products (1 cycle of 2:30, 3,450 oscillations/m, at 4 °C). Cell lysates were then centrifuged at 17,500 g for 10 min at 4°C. For each condition, one 50 ml cell lysate and subsequent supernatant was (i) loaded onto a 3kDa filter (Amicon Ultra-0.5 centrifugal filter unit; Merk) and the corresponding 50 ml cell lysate and subsequent supernatant was (ii) subjected to phenol-chloroform/chloroform nucleotide extraction¹⁰⁴. For the filtration step, the unit was centrifuged at 16,000 g for 45 min at 4 °C and flow-through (containing small molecules less than 3kDa) was used as the sample for 3',3'-cGAMP measurements. For the nucleotide extraction step, 600 µl of supernatant was added to 600 µl of phenol-chloroform, vortexed for 30 sec, and then centrifuged at 17,500 g for 45 min at 4 °C. The top aqueous layer was carefully transferred into another eppendorf tube and 600 µl of chloroform was added, vortexed for 30 sec, and then centrifuged at 17,500 g for 10 min at 4 °C. The top aqueous layer was added to the 3kD filter, centrifuged at 16,000 g for 45 min at 4 °C, and flow-through collected. Each flow-through sample was run in technical triplicate on a 3',3'-cGAMP ELISA Kit (Arbor Assays) and standards were prepared in the same phosphate buffer. 3',3'-cGAMP concentrations were calculated using a sigmoidal standard curve via GraphPad Prism (v 9.4.1).

Phylogenetic analysis

Phylogenetic reconstructions were conducted similar to previous work in our lab⁷⁴. Homologs of *Acb2* were acquired through 3 iterations of psiBLASTp search the non-redundant protein database. Hits

with >70% coverage and an E value <0.0005 were included in the generation of the position specific scoring matrix (PSSM). High confidence homologs (>70% coverage, E value < 0.0005) represented in unique species of bacteria were then aligned using NCBI COBALT using default settings and a phylogeny was generated in Cobalt using the fastest minimum evolution method¹⁰⁵ employing a maximum sequence difference of 0.85 and Grishin distance to calculate the tree. The resulting phylogeny was then displayed as a phylogenetic tree using iTOL¹⁰⁶.

Computational modeling of phage capsid

Models of *P. aeruginosa* PaMx41 (orf11) and JBD18 (orf35) phage capsid proteins were generated using AlphaFold2¹⁰⁷ and aligned using the PyMol “super” function to the different chains of the *E. coli* T4 phage capsid structure (PDB: 6UZC).

Protein expression and purification

The Acb2, CapV, CdnA and Cap2 genes were synthesized by GenScript. The full-length Acb2 gene was amplified by PCR and cloned into a modified pET28a vector in which the expressed Acb2 protein contains a His-SUMO tag. The Acb2 mutants were generated by two-step PCR and were subcloned, overexpressed and purified in the same way as wildtype protein. The proteins were expressed in *E. coli* strain BL21 (DE3) and induced by 0.2 mM isopropyl- β -D-thiogalactopyranoside (IPTG) when the cell density reached an OD_{600nm} of 0.8. After growth at 18°C for 12 h, the cells were harvested, re-suspended in lysis buffer (50 mM Tris-HCl pH 8.0, 300 mM NaCl, 10 mM imidazole and 1 mM PMSF) and lysed by sonication. The cell lysate was centrifuged at 20,000 g for 50 min at 4°C to remove cell debris. The supernatant was applied onto a self-packaged Ni-affinity column (2 mL Ni-NTA, Genscript) and contaminant proteins were removed with wash buffer (50 mM Tris pH 8.0, 300 mM NaCl, 30 mM imidazole). The fusion protein was then digested with Ulp1 at 18°C for 2 h, and then the Acb2 protein was eluted with wash buffer. The eluant of Acb2 was concentrated and further purified using a Superdex-200 increase 10/300 GL (GE Healthcare) column equilibrated with a buffer containing 10

mM Tris-HCl pH 8.0, 200 mM NaCl and 5 mM DTT. The purified protein was analyzed by SDS-PAGE. The fractions containing the target protein were pooled and concentrated.

The CdnA, Cap2 and CdnA-Cap2 complex were purified as His-tagged proteins, which were eluted with elution buffer (50 mM Tris pH 8.0, 300 mM NaCl, 300 mM imidazole) after removing contaminant proteins with wash buffer. The cells expressing CapV were resuspended with lysis buffer containing 50 mM phosphate buffer pH 7.4, 300 mM NaCl, 10% glycerol (v/v). The CapV proteins bound to Ni-NTA beads were washed with a buffer containing 50 mM phosphate buffer pH 7.4, 300 mM NaCl, 10% glycerol (v/v), 30 mM imidazole and then eluted with the 50 mM phosphate buffer (pH 7.4), 300 mM NaCl, 10% glycerol (v/v), 300 mM imidazole. The eluant of CapV was concentrated and further purified using a Superdex-200 increase 10/300 GL (GE Healthcare) column equilibrated with a reaction buffer containing 50 mM phosphate buffer (pH 7.4), 300 mM NaCl, 10% glycerol (v/v). The purified protein was analyzed as described above.

Crystallization, data collection and structural determination

The Acb2 protein was concentrated to 24 mg/mL in 10 mM Tris-HCl pH 8.0, 200 mM NaCl and 5 mM DTT. Crystals were grown using the hanging-drop vapor diffusion method. Crystals of Acb2 were grown at 18°C by mixing an equal volume of the protein (24 mg/mL) with reservoir solution containing 0.2 M Sodium bromide, 0.1 M Bis-Tris propane pH 6.5, 10% Ethylene glycol and 20% v/v PEG 3350. Crystals of Acb2 in complex with 3',3'-cGAMP or c-di-AMP were grown under the same reservoir solution. Prior to crystallization, 3',3'-cGAMP or c-di-AMP were mixed with the protein at a molar ratio of 0.8:1. The crystals appeared overnight and grew to full size in about two to three days. The crystals were cryoprotected in the reservoir solution containing 20% glycerol before its transferring to liquid nitrogen. All the data were collected at the X-ray crystallography facility at Tsinghua University (XtaLAB Synergy Custom FRX and a hybrid photon counting detector HyPix-6000, Rigaku, Japan) and SSRF beamlines BL02U1 and BL19U1, integrated and scaled using the HKL2000 package¹⁰⁸. The initial model of Acb2 was obtained through modeling using AlphaFold¹⁰⁷. The structures of Acb2 and its

complex with ligands were solved through molecular replacement and refined manually using COOT¹⁰⁹. The structure was further refined with PHENIX¹¹⁰ using non-crystallographic symmetry and stereochemistry information as restraints. The final structure was obtained through several rounds of refinement. Data collection and structure refinement statistics are summarized in Table 2.1.

Isothermal titration calorimetry binding assay

The dissociation constants of binding reactions of Acb2 or Acb2 mutants with the 3',3'-cGAMP/2',3'-cGAMP/c-di-GMP/c-di-AMP/3',3'-c-di-UMP/3',3'-c-UMP-AMP/3',3'-c-UMP-GMP were determined by isothermal titration calorimetry (ITC) using a MicroCal ITC200 calorimeter. Both proteins and cyclic dinucleotides were desalted into the working buffer (20 mM HEPES pH 7.5 and 200 mM NaCl). The titration was carried out with 19 successive injections of 2 μ L cyclic dinucleotides at the 0.4 mM concentration, spaced 120 s apart, into the sample cell containing the Acb2 or Acb2 mutants with a concentration of 0.1 mM by 700 rpm at 25°C. The Origin software was used for baseline correction, integration, and curve fitting to a single site binding model.

Fluorogenic biochemical assay for CapV activity

The enzymatic reaction velocity was measured as previously described²¹. Briefly, the esterase activity of the 6 \times His-tagged CapV was probed with the fluorogenic substrate resorufin butyrate. The CapV protein was diluted in 50 mM sodium phosphate pH 7.4, 300 mM NaCl, 10% (v/v) glycerol to a final concentration of 1.77 μ M. To determine the enzymatic activity of CapV activated by 3',3'-cGAMP, increasing concentrations ranging from 0.025 to 0.8 μ M of 3',3'-cGAMP was added to DMSO solubilized resorufin butyrate (stock of 20 mM mixed with 50 mM sodium phosphate pH 7.4, 300 mM NaCl, 10% v/v glycerol reaching a final concentration of 100 μ M). Subsequently, the purified 6 \times His-tagged CapV was added to the reaction solution containing 3',3'-cGAMP to a final assay volume of 50 μ L, and fluorescence was measured in a 96-well plate (Corning 96-well half area black non-treated plate with a flat bottom). Plates were read once every 30 s for 20 min at 37°C using a EnSpire Multimode Plate Reader (PerkinElmer) with excitation and emission wavelengths of 550 and 591 nm,

respectively. To determine the function of Acb2, 32 μM Acb2 and 0.8 μM 3',3'-cGAMP were pre-incubated at 18°C, and the subsequent detection method was as described above. To examine whether the released molecule from Acb2 is able to activate CapV, 0.8 μM 3',3'-cGAMP was incubated with 32 μM Acb2 for 10 min at 18°C. Proteinase K was subsequently added to the reaction system at a final concentration of 0.065 mg/mL and the reaction was performed at 58°C for 3 h. Reaction products were transferred to Amicon Ultra-4 Centrifugal Filter Unit 3 kDa and centrifuged at 4°C, 4,000 g. Filtered products were used for CapV activity assay.

Gel filtration assay

The Acb2, CapV, CdnA, Cap2 and the CdnA-Cap2 complex purified as described above were subjected to gel filtration analysis (Superdex-200 increase 10/300 GL, GE Healthcare). The Acb2 was incubated with CapV, CdnA, Cap2 or the CdnA-Cap2 complex at a molar ratio of 5:1 overnight on ice before the gel filtration analysis in buffer containing 10 mM Tris-HCl pH 8.0, 200 mM NaCl, and 5 mM DTT. The assays were performed with a flow rate of 0.5 mL/min and an injection volume of 1 mL for each run. Samples from relevant fractions were subjected to SDS-PAGE and visualized by Coomassie blue staining.

Analytical ultracentrifugation

Proteins were extensively dialyzed against AUC buffer (10 mM Tris pH 8.0, 200 mM NaCl). Sedimentation velocity studies were performed in a Beckman XL-A analytical ultracentrifuge at 20°C and 35,000 rpm. The absorbance at 280 nm was collected every 4 min for a total of 200 scans. These values were used to fit the data to the Lamm equation in SEDFIT software using the continuous $c(s)$ distribution model. Graphs were prepared using Origin software.

Native-PAGE assay

Acb2 was pre-incubated with cyclic dinucleotides for 10 min at 18°C, where Acb2 was 14.3 μM and the concentrations of cyclic dinucleotides ranged from 1.8 to 7.2 μM (1.8, 3.6, 7.2 μM). Products of the

reaction were analyzed using 5% native polyacrylamide gels and visualized by Coomassie blue staining.

High-performance liquid chromatography (HPLC)

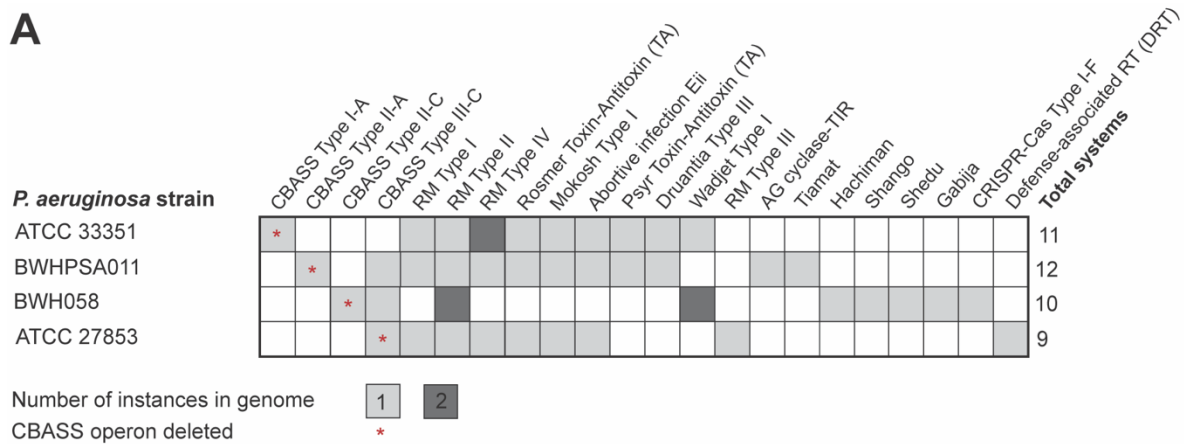
40 μ M Acb2 was pre-incubated with 4 μ M 3',3'-cGAMP for 10 min at 18°C. Proteinase K was subsequently added to the reaction system at a final concentration of 0.25 mg/mL and the reaction was performed at 58°C for 1 h. Reaction products were transferred to Amicon Ultra-15 Centrifugal Filter Unit 3 kDa and centrifuged at 4°C, 4,000 g. The products obtained by filtration were further filtered with a 0.22 μ m filter and subsequently used for HPLC experiments. The HPLC analysis was performed on an Agilent 1200 system with a ZORBAX Bonus-RP column (4.6 \times 150 mm). A mixture of acetonitrile (2%) and 0.1% trifluoroacetic acid solution in water (98%) were used as mobile phase with 0.8 mL/min. The compounds were detected at 254 nm

Quantification and Statistical analyses

Statistical details for each experiment can be found in the figure legends and outlined in the corresponding methods details section. Data are plotted with error bars representing standard deviation (s.d.).

2.8. Figures

A

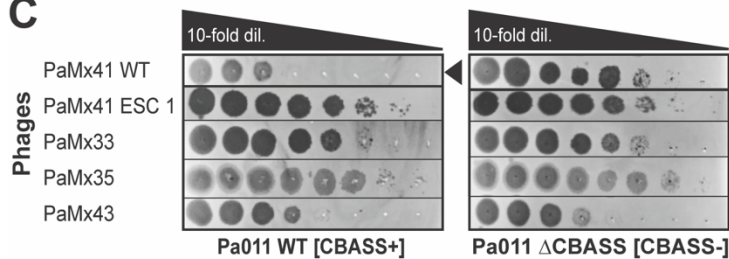


B

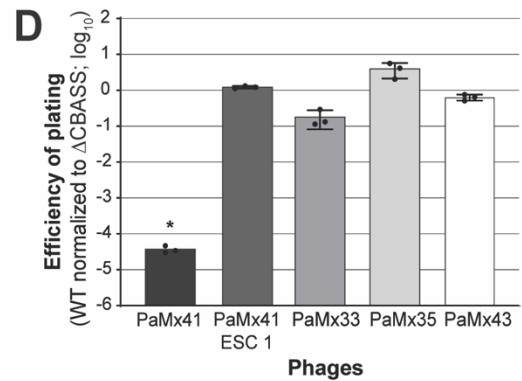
P. aeruginosa BWHPA011 (Pa011)
 Type II-A CBASS operon



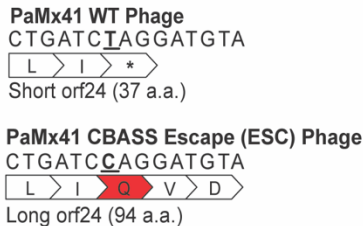
C



D



E



F

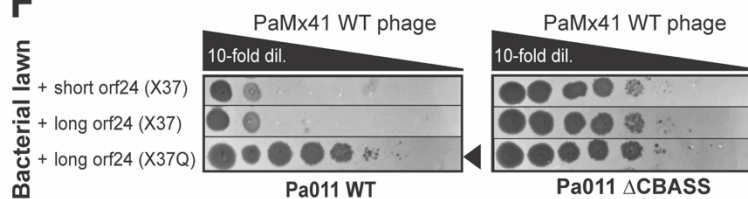


Figure 2.1: P. aeruginosa CBASS immunity protects against PaMx41 infection

(A) The presence of different anti-phage immune systems in *P. aeruginosa* strains that were used in this study. Some systems are present in the genome twice as indicated by the darker shade of gray and number (2). An asterisk (*) indicates the CBASS operon was effectively deleted from the bacterial genome. (B) Pa011 CBASS operon. (C) Plaque assays with PaMx41-like phages and an evolved PaMx41 CBASS Escaper (ESC) phage spotted in 10-fold serial dilutions on a lawn of Pa011 WT [CBASS+] or ΔCBASS [CBASS-]; clearings represent phage replication. Black arrowhead highlights the reduction in PaMx41 WT phage titer. See also Figure S1. (D) Efficiency of plating was quantified as plaque-forming units (PFU) per ml on Pa011 WT divided by PFU/ml on the ΔCBASS (n=3). Data are mean + s.d. Non-parametric ANOVA test yielded a P value of <0.0001. (E) Schematic of PaMx41 WT and CBASS escape phage genomes with the no-stop extension mutation. The bold underline indicates mutation of thymine (T) to cytosine (C), resulting in a stop codon (TAG, *) to glutamine (CAG, Q) substitution (in red). (F) Plaque assays with PaMx41 WT phage on a lawn of Pa011 WT or ΔCBASS over-expressing the indicated orf24 variants. See also Figure 2.7.

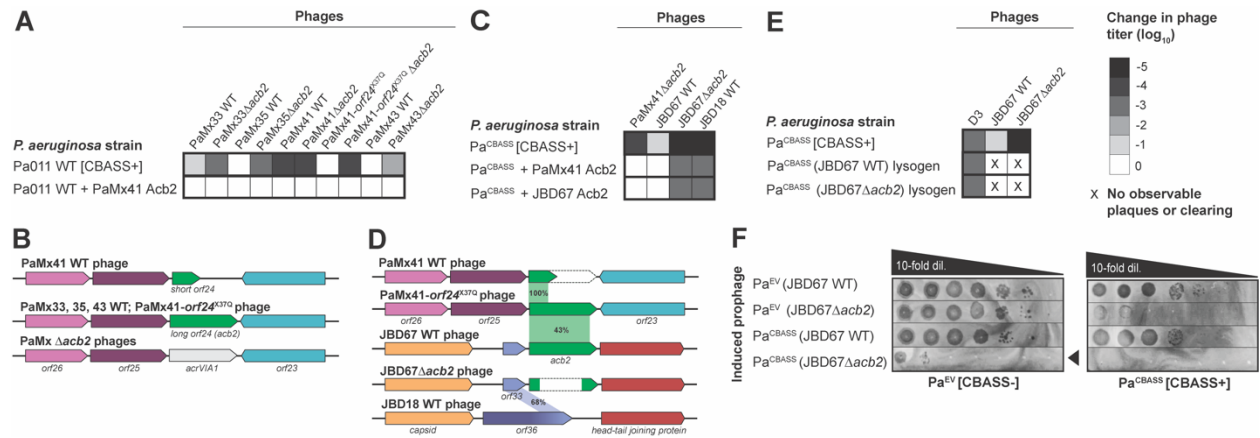


Figure 2.2: Phage-encoded *acb2* is necessary to protect against CBASS

(A, C, E) Heat maps representing the order of magnitude change in phage titer, where phage titer is quantified by comparing the number of spots (with plaques or clearing if plaques were not visible) on the CBASS+ strain divided by the CBASS- strain. Plaque assays used for these quantifications can be seen in Figure S2 (n=3). (B, D) Comparison of the *acb2* locus across phage genomes. PaMx41-like $\Delta acb2$ phages have the *acb2* gene substituted with the Type VI-A anti-CRISPR gene (*acrVIA1*) as part of the knockout procedure, and JBD67 $\Delta acb2$ phages have the *acb2* gene removed from its genome. Genes with known protein functions are indicated with names, and genes with hypothetical proteins are indicated with “orf”. *Acb2* percent amino acid identity is shown in (D). (F) Plaque assays assessing the titer induced prophages spotted on a lawn of Pa^{EV} or Pa^{CBASS}. Black arrowhead highlights reduction in JBD67 $\Delta acb2$ phage titer. See also Figure 2.7.

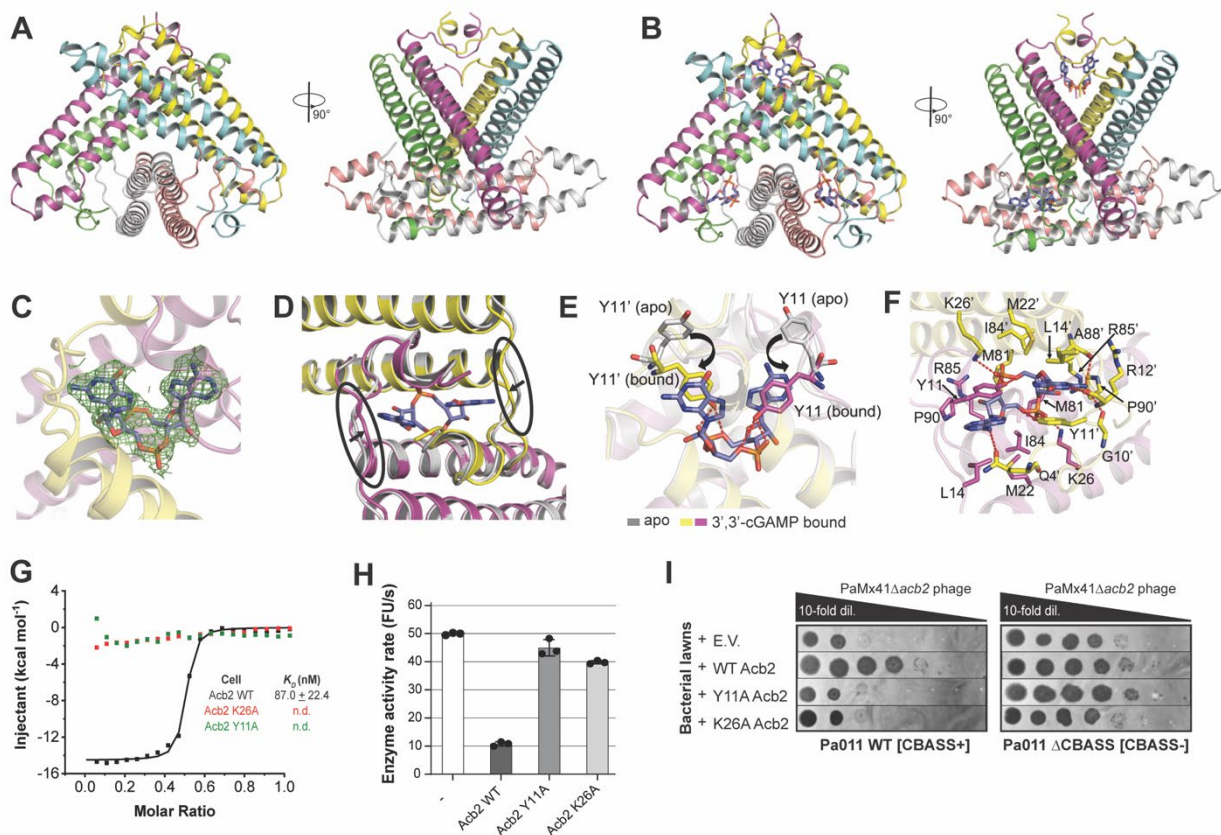


Figure 2.4: Acb2 structure reveals hexamer bound to three 3',3'-cGAMP molecules

(A) Overall structure of the Acb2 hexamer. Two views are shown. **(B)** Overall structure of the Acb2 hexamer bound to three molecules of 3',3'-cGAMP. 3',3'-cGAMP molecules are colored in slate. **(C)** 2Fo-Fc electron density of 3',3'-cGAMP in the binding pocket contoured at 1σ . **(D)** Structural comparison between an Acb2 dimer in its apo (colored in gray) and 3',3'-cGAMP-bound form (colored in yellow and light magenta). The loops which move upon 3',3'-cGAMP binding are marked with black circles. **(E)** Structural alignment between apo and 3',3'-cGAMP-bound Acb2, which are colored as in (B). Y11 from the two structures are highlighted as sticks. Red dashed lines represent polar interactions. **(F)** Binding between Acb2 or Acb2 mutants and 3',3'-cGAMP. Red dashed lines represent polar interactions. **(G)** ITC assays to test the binding of 3',3'-cGAMP to Acb2 mutants. Representative binding curves and binding affinities are shown. The K_D values are mean \pm s.d. ($n=3$). Raw data for these curves are shown in Figure S4. **(H)** CapV activity assay to test the effects of Acb2 mutations. The concentration of 3',3'-cGAMP was $0.8 \mu\text{M}$ and Acb2 or its mutants was $32 \mu\text{M}$. The 3',3'-cGAMP was pre-incubated with Acb2 or its mutants for 10 minutes. Bar graph represents average of three technical replicates. Data are mean \pm s.d. ($n=3$). **(I)** Plaque assays on a lawn of Pa011 WT or ΔCBASS overexpressing empty vector (E.V.) or the indicated PaMx41 Acb2 mutants; clearings represent phage replication.

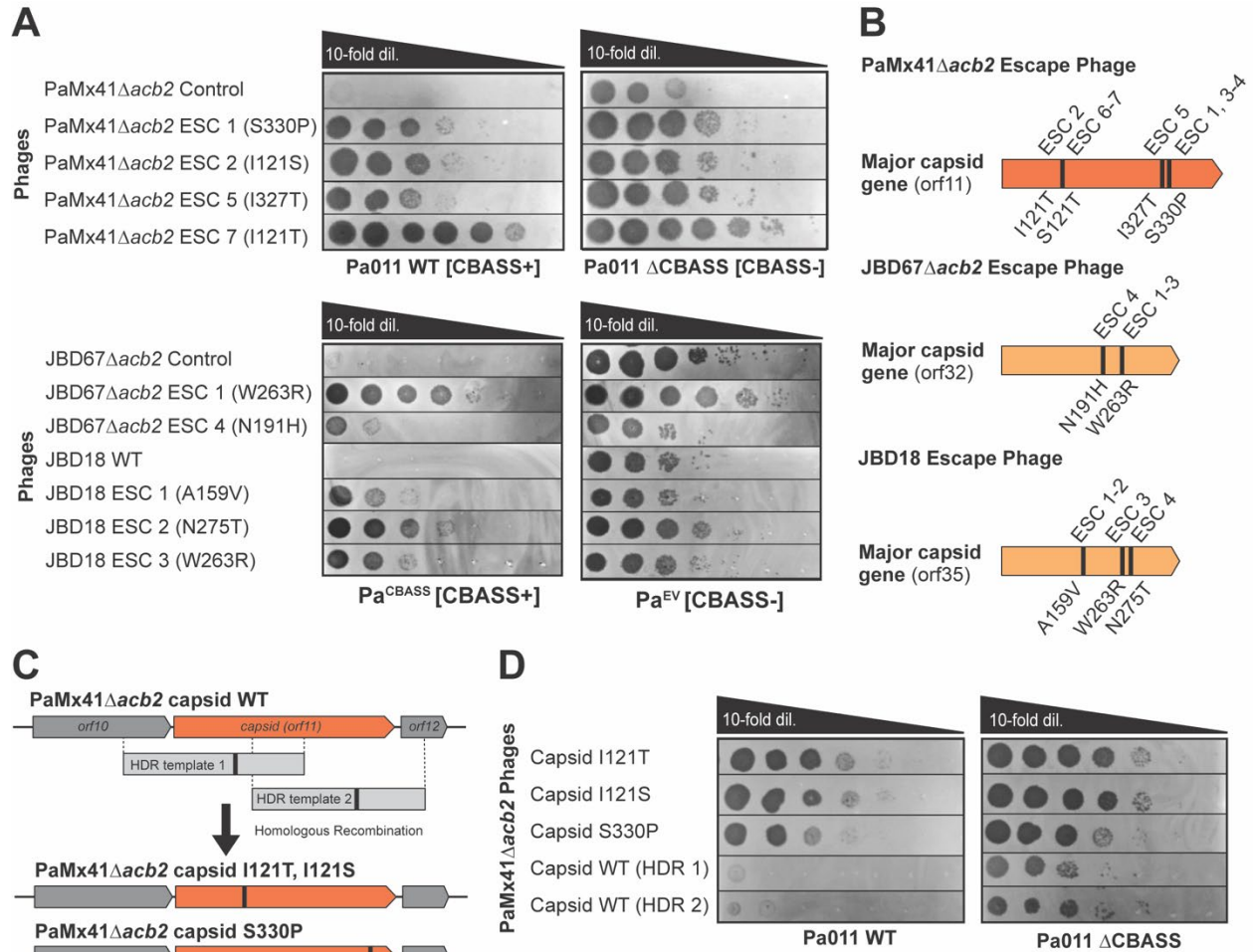


Figure 2.5: CBASS escape phages have mutations in the major capsid gene

(A) Plaque assays were performed with the indicated control/WT and escape phages spotted in 10-fold serial dilutions on lawns of bacteria expressing CBASS+ (left) or lacking CBASS- (right); clearings represent phage replication. (B) Schematic of major capsid genes with corresponding missense mutations and associated CBASS Escape (ESC) phages. (C) Schematic of in vivo homologous recombination of parental phages with homology-directed repair (HDR) template 1 (encoding I121S or I121T capsid mutations) or template 2 (S330P capsid mutation) and resultant engineered/recombinant phages. (D) Plaque assays with recombinant phages possessing major capsid mutations, or WT capsid controls, spotted on lawns of Pa011 WT or Δ CBASS.

Figure caption continued from previous page. **(C)** The presence of different CBASS types in *P. aeruginosa* strains according to their operon composition of core and signature genes. Core genes include cGAS/DncV-like nucleotidyltransferase (CD-NTase) and effector genes. Known and predicted (*) cyclic nucleotides are denoted next to the CD-NTase gene³¹. Signature genes are denoted as CD-NTase-associated proteins (Cap). **(D)** Heat map representing the order of magnitude reduction in phage titer on a CBASS-encoding (Pa011 WT Native CBASS Host or Pa^{CBASS} Heterologous CBASS Host; CBASS+) strain normalized to a strain lacking CBASS (Pa011 Δ CBASS or Pa^{EV}; CBASS-). 46 (out of 64 total) phages infected one or both strains and are represented in the heat map. **(E)** Plaque assays with indicated phages spotted in 10-fold serial dilutions on a lawn of Pa011 WT or Δ CBASS, or **(F)** on a lawn of Pa^{CBASS} or Pa^{EV}, to highlight CBASS-dependent targeting and CBASS-independent targeting (PB-1 and Ab22 phages). Plaque assays were used to quantify the order of magnitude reduction in phage titer by comparing the number of spots (with plaques, or clearing if plaques were not visible) on the CBASS+ strain divided by the CBASS- strain (n=3). **(G)** Plaque assays with the indicated phages spotted in 10-fold serial dilutions on a lawn of Pa011 WT or Δ CBASS, and Pa011 Δ CBASS over-expressing the CBASS operon or empty vector (E.V.). **(H)** Plaque assays on a lawn of Pa011 chromosomal mutants of each CBASS gene [*capV*^{S48A} (phospholipase), *cdnA*^{D87A/D89A} (cyclase), *cap2*^{C450A/C453A} (E1/E2), and *cap3*^{E38A} (JAB)]. For all plaque assays, clearings represent phage replication and black arrowheads highlight the reduction of PaMx41 WT phage titer. Related to Figure 2.1.

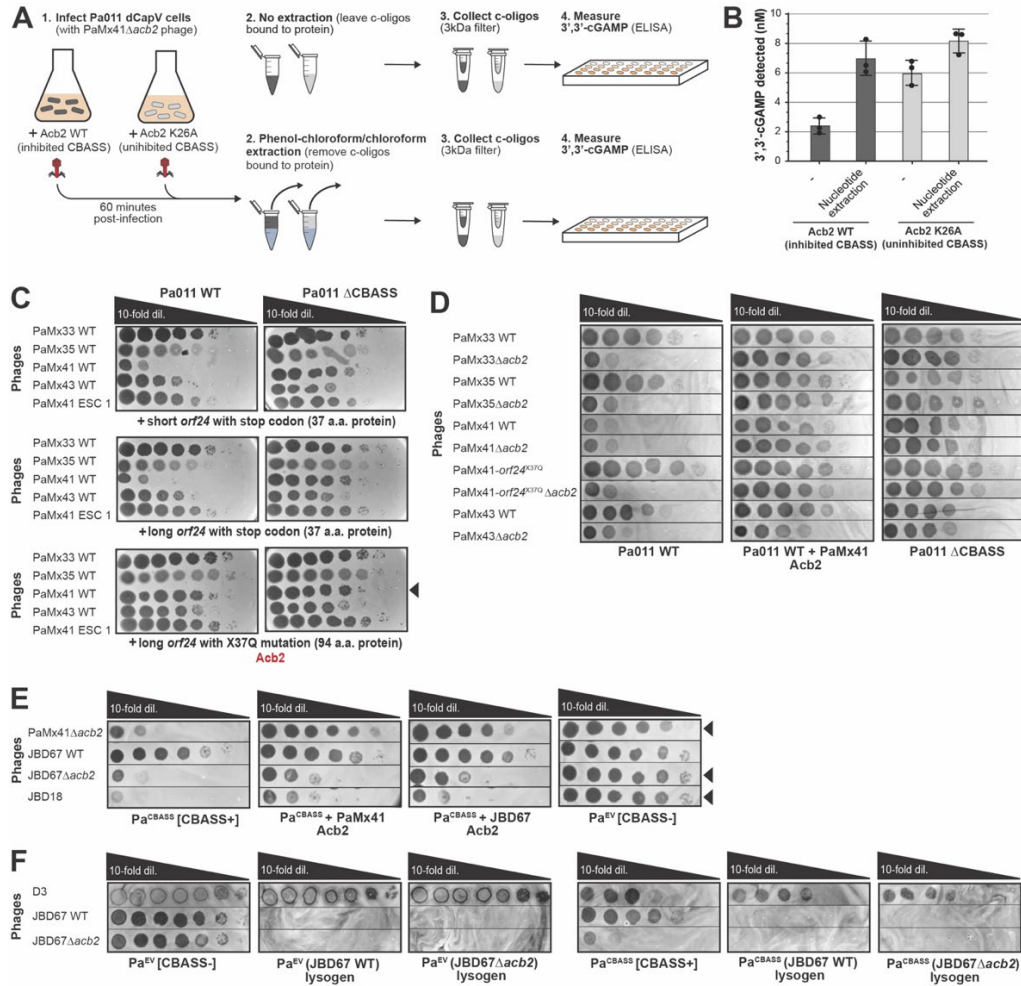
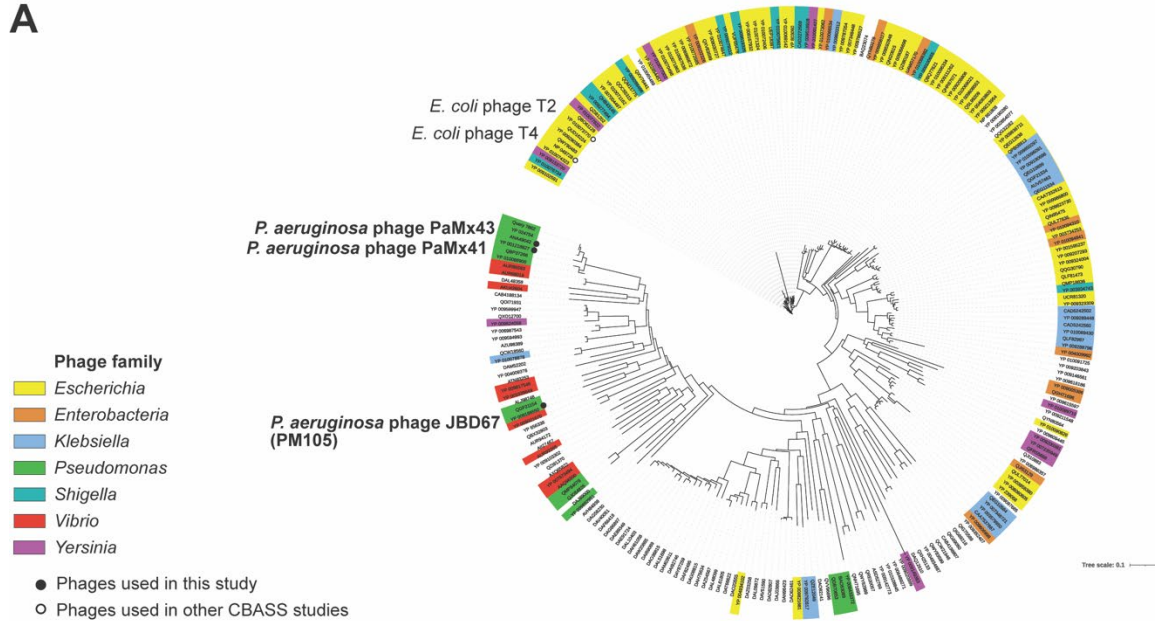


Figure 2.7: Acb2 protects phage against CBASS and reduces 3',3'-cGAMP

(A) Schematic of in vivo phage infection and cGAMP detection: (1) Pa011 cells with catalytically dead CapV^{S48A} strain overexpressing a wildtype version of an anti-CBASS gene (Acb2 WT; inhibited CBASS) or mutant version (Acb2 K26A; uninhibited or active CBASS). These cells are infected with PaMx41 phage that lacks Acb2 (PaMx41Δ*acb2*) at an MOI of ~5 for 60 minutes to provide the phage time to proceed through its replication cycle (Cruz-Plancarte et al., 2016). (2) Cell lysates are processed without (-) or with phenol-chloroform/chloroform nucleotide extraction. (3) Resultant lysates are filtered to collect cyclic oligonucleotides and then (4) 3',3'-cGAMP is specifically measured by an ELISA. (B) 3',3'-cGAMP detected in each respective condition performed in biological triplicate. Data are mean ± s.d. (C) Plaque assays were performed with PaMx33, 35, 41, and 43 WT phages, as well as an evolved PaMx41 CBASS escape (ESC) phage, spotted in 10-fold serial dilutions on a lawn of Pa011 WT [CBASS+] or ΔCBASS [CBASS-] over-expressing the indicated genes; black arrowhead highlights increase in PaMx41 WT phage titer. (D) Plaque assays were performed with the indicated phages spotted in 10-fold serial dilutions on a lawn of Pa011 WT, ΔCBASS, or WT over-expressing *acb2*. (E) Plaque assays with indicated phages on a lawn of *P. aeruginosa* cells (PAO1) with a chromosomally integrated Pa011 CBASS operon (Pa^{CBASS}), or empty vector (Pa^{EV}), and overexpressing *acb2*. Black arrowhead highlights CBASS-dependent change in phage titer. (F) Plaque assays with the indicated phages spotted in 10-fold serial dilutions on a lawn of Pa^{EV} [CBASS-], Pa^{EV} (JBD67 WT) lysogen, or Pa^{EV} (JBD67Δ*acb2*) lysogen, or Pa^{CBASS} [CBASS+], Pa^{CBASS} (JBD67 WT) lysogen, or Pa^{CBASS} (JBD67Δ*acb2*) lysogen. For all plaque assays, clearings represent phage replication. Related to Figure 2.1, 2.2, and 2.4.

A



B

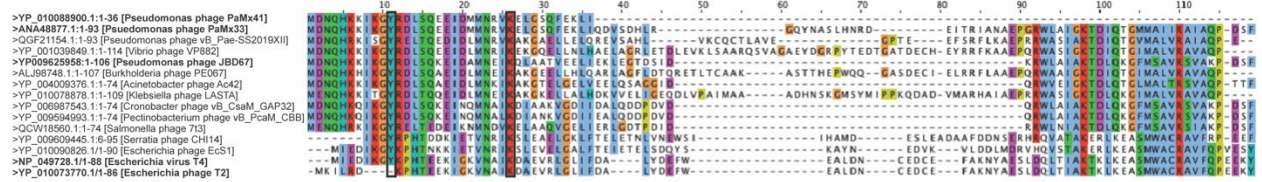


Figure 2.8: Acb2 is found in a broad diversity of phages and bacteria

(A) Phylogenetic tree of *acb2* across the genomes of 239 tailed phages (Caudovirales) following two iterations of PSI-BLAST. Phages families that are colored are the most frequently identified. Phages relevant to this study are bolded. **(B)** Multiple sequence alignment of PaMx41-*orf24*^{X37Q} Acb2, PaMx33, PaMx43, JDB67 Acb2, and other homologous proteins via MAFFT alignment in Jalview. All proteins except T2 and T4 phage homologs were acquired by standard BLASTp, while T2 and T4 were observed on a second round of a PSI-BLAST. Colors indicate an identical amino acid. Black boxes highlight residues Y11 and K26, which are necessary for Acb2 activity. Related to Figure 2.2.

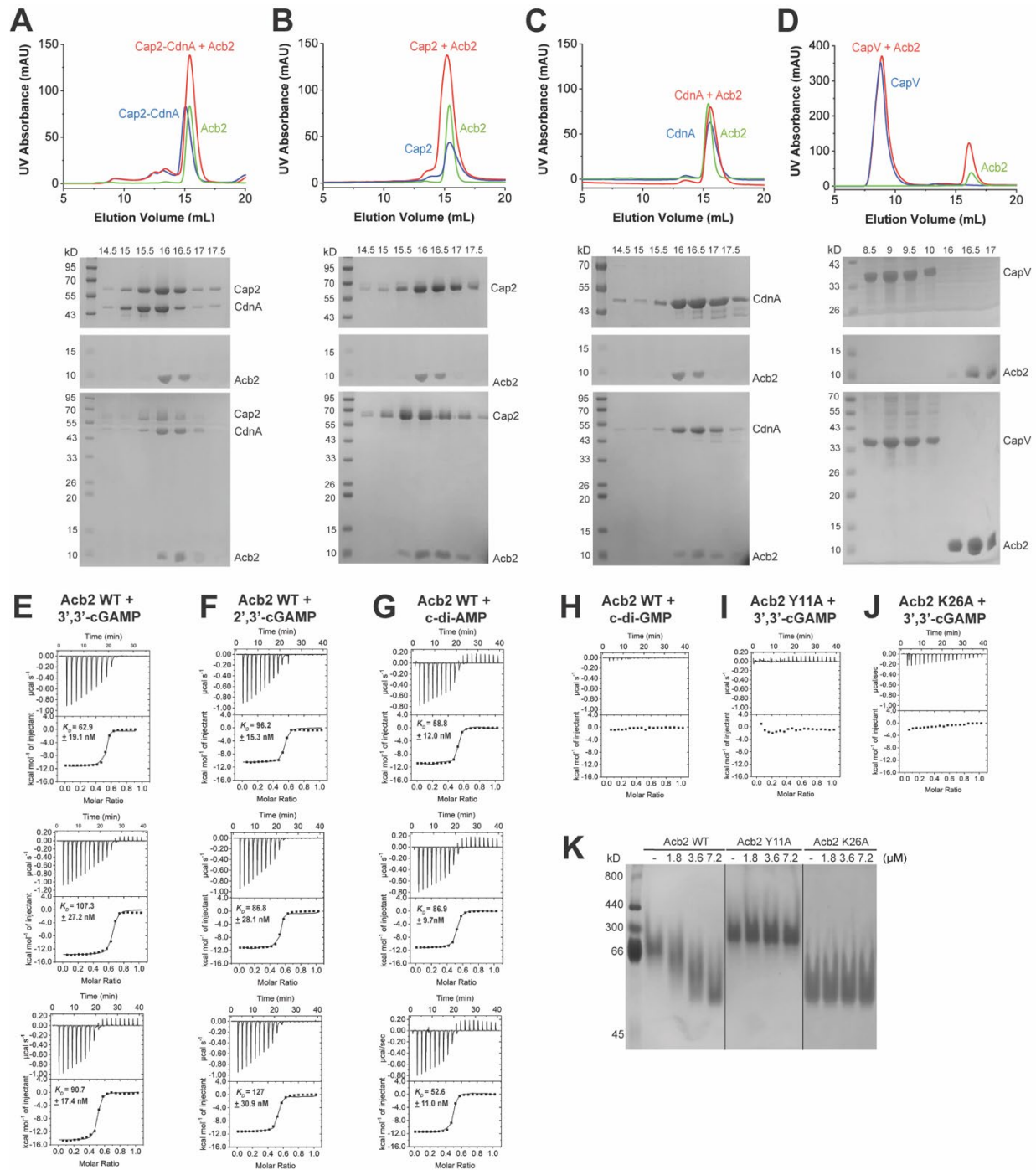


Figure 2.9: Acb2 does not bind CBASS proteins, but does bind 3',3'/2',3'-cGAMP/cAA

(A)-(D) Gel filtration profile of incubated Acb2 with Cap2-CdnA complex (A), Cap2 (B), CdnA (C) or CapV (D) (Superdex-200 increase 10/300 GL, GE Healthcare). (E) ITC assays to test binding of 3',3'-cGAMP to Acb2 WT. (F) ITC assays to test binding of 2',3'-cGAMP to Acb2. (G) ITC assays to test binding of c-di-AMP to Acb2 WT. (H) ITC assay to test binding of c-di-GMP to Acb2. (I), (J) ITC assay to test binding of 3',3'-cGAMP to Acb2 Y11A and K26A, respectively. (K) Acb2 and its mutants were incubated with 3',3'-cGAMP at indicated concentrations. Then the samples were subjected to native PAGE. Related to Figure 2.3 and 2.4.

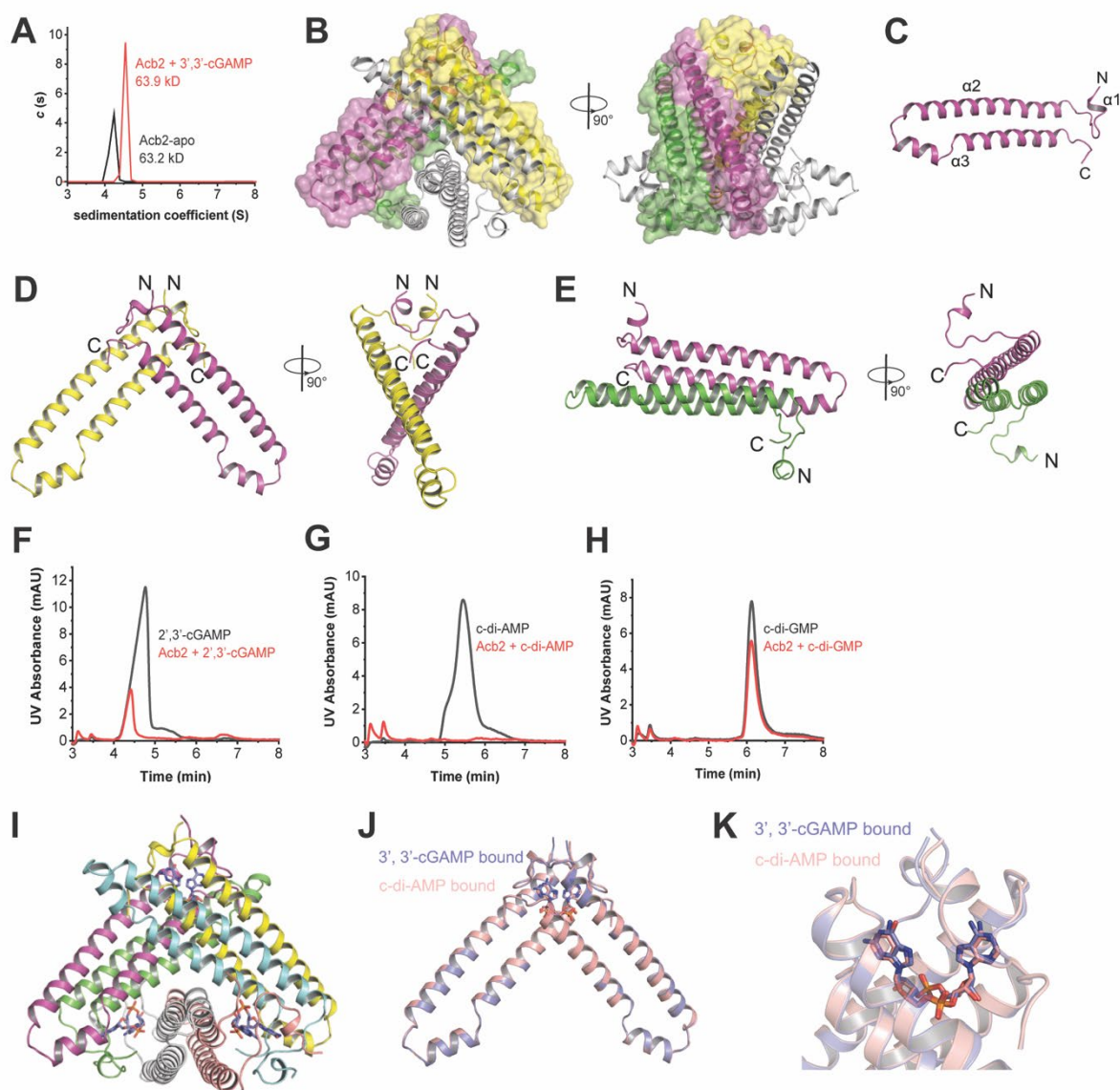


Figure 2.10: Structures of apo and dinucleotide bound Acb2

(A) Analytical Ultracentrifugation (AUC) analysis of Acb2 and its complex with 3',3'-cGAMP. (B) Structure of the Acb2 hexamer. (C) Structure of the Acb2 monomer. (D-E) Two types of dimer of protomers as shown in (B) are shown. (F)-(H), The ability of Acb2 to bind 2',3'-cGAMP/c-di-AMP/c-di-GMP was analyzed by HPLC. 2',3'-cGAMP/c-di-AMP/c-di-GMP standards were used as a control. The remaining cyclic dinucleotides after incubation with Acb2 were tested. (I) Overall structure of Acb2 bound with c-di-AMP. (J)-(K) Structural comparison between an Acb2 dimer in c-di-AMP-bound form (colored in pink) and 3',3'-cGAMP-bound form (colored in slate).

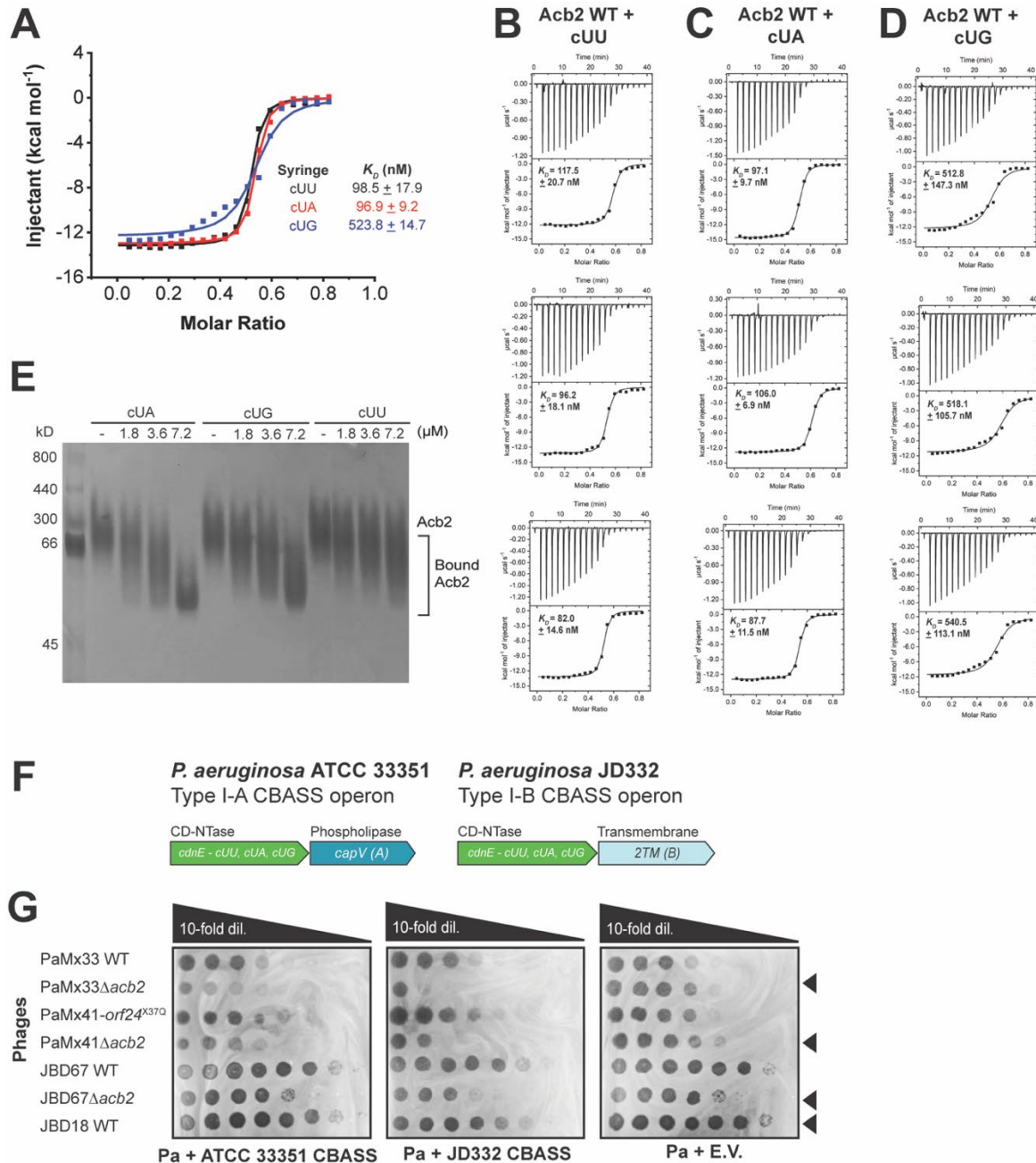


Figure 2.11: Acb2 binds to the predicted CdnE signals and protects against Type I-A and Type I-B CBASS

(A) Isothermal titration calorimetry (ITC) assays to test binding of cyclic dinucleotides to Acb2. cUU, cUA, and cUG represent 3',3'-cyclic-di-UMP, 3',3'-cyclic-UMP-AMP, and 3',3'-cyclic-UMP-GMP, respectively. Representative binding curves and binding affinities are shown. The K_D values are mean \pm s.d. ($n=3$). Raw data for these curves are shown in (B-D). (E) Native PAGE showed the binding of Acb2 to cyclic dinucleotides. (F) *P. aeruginosa* ATCC 33351 and JD332 CBASS operons with predicted cyclic dinucleotides³¹. (G) Plaque assays with the indicated phages spotted in 10-fold serial dilutions on a lawn of *P. aeruginosa* cells (PAO1), which naturally lacks CBASS, over-expressing a CBASS operon or empty vector (E.V.); clearings represent phage replication. Black arrowhead highlights change in phage titer specific to phages lacking *acb2*. Related to Figure 2.3.

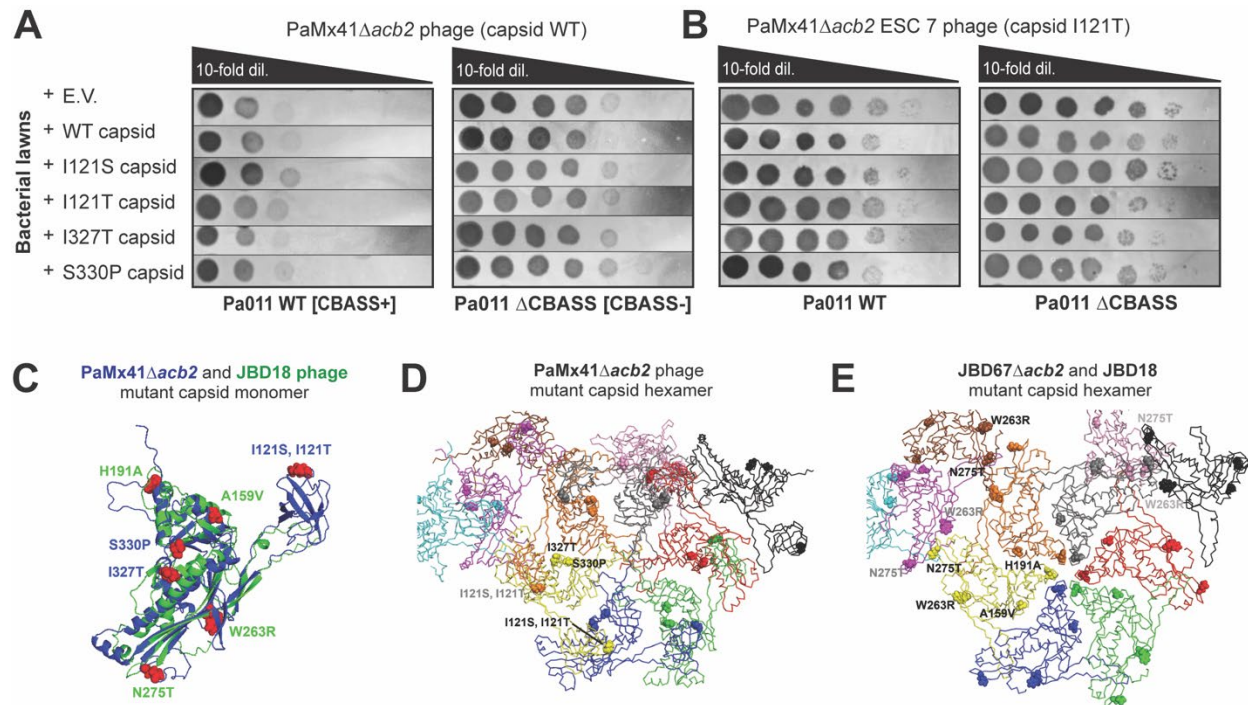


Figure 2.12: PaMx41 phage remains sensitive to CBASS in the presence of major capsid escape allele expression

(A) Plaque assays were performed with PaMx41 Δ acb2 phage, harboring a wildtype (WT) capsid, spotted in 10-fold serial dilutions on a lawn of Pa011 WT [CBASS+] or Δ CBASS [CBASS-] over-expressing the indicated genes; clearings represent phage replication. (B) Plaque assays were performed with PaMx41 Δ acb2 CBASS Escaper phage 7, harboring a mutant (I121T) capsid, spotted in 10-fold serial dilutions on a lawn of Pa011 WT or Δ CBASS. (C) AlphaFold2 prediction of the PaMx41 Δ acb2 (blue) and JBD18 (green) major capsid protein monomer structures overlaid using PyMOL (RMSD: 4.194). Red spheres represent amino acid residues that are mutated and are labeled with the corresponding a.a. change. (D) AlphaFold2 prediction of the PaMx41 Δ acb2 and (E) JBD18 capsid hexamer structures based on the experimentally solved *E. coli* T4 phage capsid structure (PDB: 6UZC). Spheres represent the a.a. residues that are mutated. Black and gray colors are indicative of mutations within a capsid monomer and highlight the inter- and intra-protein localization of the mutations. Related to Figure 2.5.

2.9. Tables

Table 2.1: Data collection and refinement statistics

	Acb2	Acb2-3',3'-cGAMP	Acb2-c-di-AMP
PDB code	8H2X	8H2J	8H39
Data collection			
Space group	P321	P321	P321
Cell dimensions			
<i>a</i> , <i>b</i> , <i>c</i> (Å)	101.9, 101.9, 101.7	103.5, 103.5, 101.6	104.1, 104.1, 102.0
(°)	90.00, 90.00, 120.00	90.00, 90.00, 120.00	90.00, 90.00, 120.00
Resolution (Å)	50-2.69 (2.79-2.69) ^b	12.87-2.40 (2.49-2.40)	67.58-2.01 (2.11-2.01)
<i>R</i> _{sym} or <i>R</i> _{merge} (%)	16.9 (66.6)	8.3 (41.6)	9.2 (122.8)
<i>I</i> / σ (<i>I</i>)	16.6 (3.0)	31.8 (5.7)	21.0 (2.8)
Completeness (%)	99.9 (100.0)	99.2 (100.0)	100.0 (100.0)
Redundancy	14.1 (10.2)	22.3 (21.9)	20.0 (20.4)
Refinement			
Resolution (Å)	33.37-2.69 (2.79-2.69)	12.87-2.40 (2.49-2.40)	67.58-2.01 (2.08-2.01)
Unique reflection	17084 (1624)	24843 (2448)	43247 (6272)
<i>R</i> _{work} / <i>R</i> _{free} ^a	0.250/0.269	0.244/0.279	0.209/0.233
No. atoms	4449	4704	4859
Protein	4302	4396	4365
Ligand/ion	62	180	208
Water	85	128	286
<i>B</i> factors	52.64	50.22	44.81
Protein	53.23	50.70	45.12
Ligand/ion	38.93	44.72	38.41
Water	32.44	41.57	44.80
R.m.s. deviations			
Bond lengths (Å)	0.010	0.005	0.004
Bond angles (°)	1.58	1.00	0.60
Ramachandran plot (%)			
Favored	97.90	97.01	98.31
Allowed	2.10	2.99	1.69
Outliers	0.00	0.00	0.00

^aFor each structure one crystal was used.

^bValues in parentheses are for highest-resolution shell.

Table 2.2: List of phage capsid mutations observed via Whole Genome Sequencing

Phage name	Nucleotide location	Nucleotide mutation*	Amino acid location	Amino acid mutation
PaMx41Δacb2 Escapers (ESC)				
ESC 1	9371	T→C	330	S→P
ESC 2	8745	T→G	121	I→S
ESC 3	9371	T→C	330	S→P
ESC 4	9371	T→C	330	S→P
ESC 5	9363	T→C	327	I→T
ESC 6	8745	T→C	121	I→T
ESC 7	8745	T→C	121	I→T
JBD67Δacb2 ESC				
ESC 1	22601	T→C	263	W→R
ESC 2	22601	T→C	263	W→R
ESC 3	22601	T→C	263	W→R
ESC 4	22385	A→T	191	N→R
JBD18 WT ESC				
ESC 1	22559	C→T	159	A→V
ESC 2	22559	C→T	159	A→V
ESC 3	22907	A→C	275	N→T
ESC 4	22870	T→C	263	W→R

*Mutations were recorded if the 100% of the reads detected the change in nucleotide relative to the reference genome.

Chapter 3: Single phage protein simultaneously sequesters cGAS- and TIR-generated signaling molecules

3.1. Summary

CBASS is a common anti-phage immune system that uses a cGAS-like enzyme to generate cyclic oligonucleotide signals and limit phage replication. In turn, phages encode anti-CBASS (Acb) proteins like Acb2, which can sequester the cyclic dinucleotide (CDN) cGAMP. Here, we identified that Acb2 sequesters many CBASS and cGAS-produced CDNs and inhibits cGAMP-mediated STING activity in human cells. Surprisingly, the Acb2 hexamer also binds with high affinity to CBASS cyclic trinucleotides (CTNs) 3',3',3'-cyclic AMP-AMP-AMP and 3',3',3'-cAAG at a distinct site from CDNs. One Acb2 hexamer can simultaneously bind two CTNs and three CDNs. Phage-encoded Acb2 provides protection from Type III-C CBASS that uses cA₃ signaling molecules *in vivo* and blocks cA₃-mediated activation of the endonuclease effector *in vitro*. Although some Acb2 homologs lack the CTN binding site, phylogenetic analysis of >2,000 Acb2 homologs encoded by diverse phages and prophages revealed that most are expected to bind both CTNs and CDNs. Altogether, Acb2 sequesters nearly all known CBASS signaling molecules through two distinct binding pockets and thereby serves as a potent, broad-spectrum inhibitor of cGAS-based immunity across all domains of life.

3.2. Introduction

Anti-viral immune pathways across all kingdoms of life sense and respond to viral infection. Cyclic GMP-AMP synthase (cGAS) is an evolutionarily conserved enzyme that performs a pivotal role in innate immunity against viruses⁷⁹. In mammalian cells, cGAS binds viral DNA and is activated to produce 2',3'-cyclic GMP-AMP (2',3'-cGAMP) dinucleotides, which activate the STING (stimulator of interferon genes) effector protein to initiate a potent interferon response^{81,82}. In bacteria, cGAS-like enzymes named cGAS/DncV-like nucleotidyltransferases (CD-NTases) have been identified and enzymatically characterized^{31,32,34}. CD-NTases have been classified into 8 enzymatic clades and at

least 12 cyclic di- and trinucleotide products have been identified^{24,31,35}. During phage infection, these enzymes are activated and produce cyclic oligonucleotides that bind to and activate a downstream effector protein. The activated effector proteins are proposed to induce premature cell death through various mechanisms, including membrane impairment^{21,24}, DNA degradation^{83,85,111}, and NAD⁺ depletion^{84,112,113} amongst others. This anti-phage strategy was named cyclic-oligonucleotide-based anti-phage signaling system (CBASS).

As a countermeasure to CBASS immunity, phages encode anti-CBASS (Acb) proteins. Acb1 degrades the cyclic nucleotide messengers to inhibit CBASS⁴⁸ and Acb2 is a cyclic dinucleotide (CDN) sponge^{50,53}. Interestingly, Acb2 also binds to a variety of other CDNs: 2',3'-cGAMP and 3',3'-cUU/UA/UG/AA with varying affinities. Structures of Acb2 from *P. aeruginosa* phage PaMx33 and from *E. coli* phage T4 in complex with 3',3'-cGAMP showed that Acb2 forms an interlocked hexamer and binds to three cyclic dinucleotides (CDNs), each with a binding pocket located in one Acb2 dimer within the hexamer^{50,53}. However, it remains unknown whether Acb2 binds to cyclic nucleotides that are utilized in Pycsar, CBASS, and Type III CRISPR-Cas signaling systems^{20,114,115}. Here, we find that Acb2 not only binds to and sequesters a broad spectrum of CDNs, but it also binds to cyclic trinucleotides (CTNs) 3'3'3'-cyclic AMP-AMP-AMP (cA₃ hereafter) and 3'3'3'-cAAG (cAAG) with an order of magnitude higher affinity. CBASS systems commonly use these CTN signals³⁵, as do some Type III CRISPR-Cas systems¹¹⁶. Structural characterization identified that one Acb2 hexamer binds two CTNs within binding pockets that are different from those binding CDNs. A co-structure of Acb2 bound to cA₃ and 3',3'-cGAMP at the same time is presented, as are mutants that independently disrupt the different binding sites. Plasmid and phage-encoded Acb2 effectively protects phage when infecting cells that independently and simultaneously express cA₃ and cGAMP CBASS systems. Together, this work identifies two distinct cyclic oligonucleotide binding sites on Acb2 and that phage sponges can serve as remarkably broad-spectrum inhibitors of CBASS and cGAS-STING signaling pathways found across all domains of life.

3.3. Results

3.3.1. Acb2 sequesters diverse CDNs and is active in human cells

To understand the selectivity of the newly identified Acb2 protein fold, we comprehensively tested an array of cyclic oligonucleotides that Acb2 may bind to. Previous work revealed that Acb2 binds to 3',3'-cGAMP, 2',3'-cGAMP and 3',3'-cUU/UA/UG/AA, but not 3',3'-cGG⁵⁰ (Figure 3.6A-B). In this current study, we first tested Acb2 binding of 3',2'-cGAMP, which was recently identified as a signaling molecule for both CBASS and cGAS-like enzymes in eukaryotes^{71,111}. A native gel assay showed a significant shift of the Acb2 protein upon adding 3',2'-cGAMP (Figure 3.6A), and isothermal calorimetry (ITC) experiments verified that Acb2 binds to 3',2'-cGAMP with a K_D of ~297.7 nM (Figures 3.1A and 3.7). Next, we solved the structure of Acb2 complexed with 3',2'-cGAMP (2.33 Å, Figure 3.1B), in which 3',2'-cGAMP binds in the same binding pocket and shows a similar binding mode as 3',3'-cGAMP and c-di-AMP (Figures 3.1C-E, 3.8A, and Table 3.1). Specifically, these CDN molecules are bound by the N-terminal domains of the two interacting Acb2 protomers, each from one Acb2 dimer (Figures 3.1D). The π - π stacking from Y11 residue and salt bridges from K26 residue of both protomers further stabilize this interaction (Figures 3.1C-D). The structure of Acb2 complexed with another cGAMP isomer, 2',3'-cGAMP, solved at 2.24 Å resolution further confirmed this mode of binding (Figures 3.1D-E, 3.8B, and Table 3.1). Interestingly, multiple CDNs are tolerated in the binding pocket. Their base groups are mainly stabilized by the π - π stacking from the Y11 residue (Figures 3.1C-D). Therefore, all the three tested base groups (adenine, guanine, and uridine) are tolerated, albeit with different affinities. For the phosphate-ribose backbone, interestingly, 3',3'-, 2',3'- and 3',2'-cGAMP linkages are all tolerated by Acb2. Detailed analysis further shows that for each linkage, its phosphate group can be stabilized by polar interactions from both K26 and Y11 (Figure 3.1D), while the other interacting Acb2 residues might vary a little. However, the cavity in Acb2 is large enough for all the three linkages (Figure 3.1E). Since 3',2'-cGAMP and 2',3'-cGAMP are ligands used in eukaryotic cGAS-STING immunity, we also tested whether Acb2 can antagonize cGAS-STING signaling pathway in human cells. The results showed that upon expression of WT Acb2, interferon (IFN) signaling mediated by 2',3'-cGAMP is significantly reduced while Y11A and K26A Acb2 mutants

were less active (Figure 3.1F). Consistent with these data, native gel assays showed that Y11A and K26A mutations abrogated 2',3'-cGAMP binding (Figure 3.6C). Taken together, our data demonstrates that Acb2 harbors a binding pocket that is well suited for many CDNs.

3.3.2. Acb2 sequesters CTNs with higher affinity than CDNs

Based on the binding pocket of Acb2, we hypothesized that Acb2 may not bind cyclic mononucleotides or oligonucleotides, such as cA₃, cA₄ or cA₆, due to potential steric clash caused by the nucleotides. Of note, cA₃ and cAAG are major products of the CD-NTase enzymes involved in CBASS whereas cA₄ is only a minor product of a single CD-NTase⁸³. cA₆ has not been identified as a product of any known CD-NTases. However, all three cyclic oligoadenylates are known products involved in Type III CRISPR-Cas anti-phage immunity¹¹⁷. A native gel assay showed that the Acb2 protein does not shift upon adding cA₄ or cA₆ molecules (Figures 3.6A-B). Furthermore, both native gel and ITC assays showed that Acb2 does not bind to cUMP, cCMP or cAMP (Figures 3.6-7 and 3.1A). However, the native gel assay revealed a significant shift of the Acb2 protein upon adding cA₃ or cAAG (Figure 3.6B). ITC experiments revealed that Acb2 binds to cA₃ and cAAG with a K_D of ~1.5 and ~2.7 nM (Figures 3.2A and 3.7), respectively, which is more than an order of magnitude stronger than Acb2 binding to 3',3'-cGAMP (K_D of ~87 nM)⁵⁰. To determine whether Acb2 sequesters or cleaves the CTN molecules, high-performance liquid chromatography (HPLC) revealed that incubating Acb2 with cA₃ depletes any detectable molecules, and following proteolysis of Acb2, cA₃ is released back into the buffer unmodified (Figure 3.2B). Collectively, these results demonstrate that Acb2 binds to and sequesters CTNs commonly used in CBASS immunity with a significantly higher affinity than CDNs.

3.3.3. Acb2 binds CTNs and CDNs with different binding sites

The binding of CTNs was unexpected because the Acb2 binding pocket appears well suited for only CDNs. To understand how Acb2 interacts with CTNs, we determined the crystal structures of Acb2 in complex with cA₃ (2.26 Å, Figure 3.8C) or cAAG (2.10 Å, Figure 3.8D) (Table 3.1). Surprisingly, the structures showed that one Acb2 hexamer binds two CTNs with two distinct binding pockets that are

far from the three pockets for the CDN binding (Figures 3.2C and 3.9A-B). An Acb2 hexamer can be viewed as a trimer of dimers, which forms a channel in the center of the hexamer (Figure 3.2D). Interestingly, each binding pocket of the CTNs is formed by three Acb2 protomers, each from one different Acb2 dimer, in a three-fold symmetry (Figure 3.9B). The two CTN molecules bind at the two ends of the channel, blocking the channel from two opposite sides (Figure 3.2E). The binding modes of CDNs and CTNs within Acb2 can be described as follows: Each of the two protomers that together bind a CDN is involved in binding to one out of the two CTNs, respectively (Figure 3.9A). Correspondingly, each of the three protomers that together bind a CTN is involved in binding to one out of the three CDNs, respectively (Figure 3.9B).

The CTN is bound mainly through its three phosphate groups, each of which is coordinated by R67 of one protomer and T74 of another protomer through hydrogen bonds (Figures 3.2F-G). Moreover, the CTN is also stabilized by hydrophobic interactions from R67, A70, and I71 from each of the three protomers (Figure 3.2G). Consistent with this analysis, the Acb2 T74A mutant displayed a significantly decreased binding affinity to cA_3 (K_D of ~291 nM), and the Acb2 R67A mutant abolished Acb2 binding of cA_3 *in vitro* (Figures 3.2A and 3.7). To confirm that the binding sites of the CTNs and CDNs in Acb2 are independent of each other, we tested the binding of 3',3'-cGAMP with the T74A or R67A Acb2 mutant proteins. A native gel assay showed similar shifts of the two Acb2 mutants as WT Acb2 upon adding 3',3'-cGAMP (Figure 3.2H), suggesting that the binding to 3',3'-cGAMP is not affected by the two mutations. In turn, we tested the binding of cA_3 with Y11A and K26A Acb2 mutants, which lose their binding to 3',3'-cGAMP⁵⁰. The native gel results showed a significant shift of Y11A and K26A mutant proteins upon adding cA_3 (Figure 3.2I). Taken together, these data collectively show that one Acb2 hexamer binds two CTNs through two pockets independent of those that bind CDNs.

Structural alignment between apo Acb2 and its complexes with CTNs showed that the binding of CTNs does not induce a conformational change of Acb2, with a root mean square deviation (RMSD) of 0.224 and 0.261 Å (C α atoms) for Acb2- cA_3 and Acb2- $cAAG$ compared to the apo Acb2, respectively (Figure

3.9C). Therefore, we co-crystallized Acb2 with both cA₃ and 3',3'-cGAMP and then solved its crystal structure at a resolution of 2.76 Å (Table 3.1). The structure clearly showed that Acb2 binds to two cA₃ and three 3',3'-cGAMP molecules simultaneously (Figures 3.3A-C). Structural alignment between Acb2-cA₃-3',3'-cGAMP and apo Acb2 also showed little conformational changes with an RMSD of 0.298 Å for C α atoms (Figure 3.9D).

3.3.4. Acb2 binds to cA₃ with a novel fold

Dali search did not return entries of experimentally determined proteins with the same fold as Acb2 nor did Foldseek searches of computationally predicted proteins¹¹⁸, suggesting that both the CDN and CTN-binding folds are novel. Foldseek also did not reveal any similar structures encoded by viruses that infect eukaryotes. Several experimentally determined proteins have been reported to bind CTNs, including the CBASS effector proteins NucC⁸⁵ and Cap4⁸³ that directly bind cA₃, as well as the human CDN sensor RECON that directly binds cAAG³¹. Compared to the cA₃ binding pocket in Acb2, those in NucC, Cap4, and RECON are significantly different. In NucC, one cA₃ molecule is bound in a three-fold symmetric allosteric pocket at the “bottom” of the protein trimer, mainly formed by an extended hairpin loop from each protomer. Additionally, each adenine base is stabilized by hydrogen bonds and π stacking interactions in NucC (Figure 3.10A, PDB code: 6Q1H). In Cap4, cA₃ is bound within its SAVED (SMODS-associated) domain, which is a fusion of two CARF (CRISPR-associated Rossmann fold) domains derived from Type III CRISPR-Cas system (Figure 3.10B, PDB code: 6WAN). RECON adopts a TIM barrel fold with eight parallel β strands surrounded by eight crossover α -helices and cAAG is bound in a deep crevice at the top of the β barrel (Figure 3.10C, PDB code: 6M7K). Moreover, the conformation of cA₃ within Acb2 is also different from those within NucC, Cap4, and RECON complex structures (Figure 3.10D). Specifically, cA₃ in both NucC and Cap4 are almost in an overall planar conformation, and two adenine bases of cAAG within RECON are nearly in the same plane as the phosphodiester ring and the third guanine base is extended out. However, each base of cA₃ forms a ~46.8 degree angle with the phosphate plane in Acb2. Together, the structure of Acb2 complexed with cA₃ reveals a novel CTN-binding fold.

3.3.5. Cyclic nucleotide binding spectra are different among Acb2 homologs

To determine the conservation of each binding site across the Acb2 family, PSI-BLAST was used to identify 2,242 total homologs. From these, clustering of the Acb2 homologs revealed 878 unique and non-redundant proteins (see Methods for details; Table 3.2). Multi-sequence alignments and phylogenetic analyses of these unique Acb2 homologs revealed that both binding sites are predicted to be intact in most homologs (78%). However, some homologs have a mutation in a residue homologous to R67 or T74 that are essential for CTN binding (19%), and very few proteins had mutated Y11 or K26 sites that are essential for CDN binding (3%; Figure 3.4A and 3.11). We therefore assessed the binding spectrum of representative Acb2 homologs to determine their cyclic oligonucleotide binding preferences. We chose Acb2 homologs from *P. aeruginosa* phage JBD67 (44.4% a.a. identity), in which both R67 and T74 residues are conserved, alongside *Serratia* phage CHI14 (23.5% a.a. identity) and *Escherichia* phage T4 (24.2% a.a. identity), in which only the R67 (*Serratia* phage) or T74 (*Escherichia* phage) residue is conserved. ITC analyses showed that JBD67-Acb2 directly binds to 3',3'-cGAMP with a K_D of ~99 nM and cA₃ with a K_D of ~3.5 nM (Figure 3.4B and 3.12A-B), both of which are comparable to those of PaMx33-Acb2. Native gel assays also suggest that JBD67-Acb2 binds to the same spectrum of cyclic nucleotides as PaMx33-Acb2 (Figure 3.13A). ITC analyses showed that T4-Acb2 directly binds to 3',3'-cGAMP with a K_D of ~84.4 nM, consistent with previous work⁸³, but does not bind to cA₃ (Figure 4C and 3.12C-D). Native gel assays also suggest that T4-Acb2 binds the same spectrum of CDNs as PaMx33-Acb2, but not to the CTNs cA₃ and cAAG (Figure 3.13B). Next, we mutated D61 of T4-Acb2 to Arginine to see whether it can endow T4-Acb2 with the binding activity of cA₃ because T4-Acb2 already has T68 residue in the place of T74 of PaMx33-Acb2 that is essential for cA₃ binding. However, based on ITC assays, we observed that the D61R mutant of T4-Acb2 was still unable to bind cA₃ (Figures 3.4C and 3.12E). Interestingly, structural alignment between T4-Acb2¹⁷ and PaMx33-Acb2 complexed with cA₃ showed that the helix lining the cA₃ binding pocket of PaMx33-Acb2 has a kink at E64, which enlarges the pocket to accommodate the base groups of cA₃ (Figure 3.4D). However, the corresponding helix of T4-Acb2 does not kink here, so the Y37, A57, L60, D61, and T64 residues of T4-Acb2 may undergo steric clashing and

prevent cA₃ binding (Figure 3.4D). More importantly, the relative angles among the three helices lining the binding pocket are also different between PaMx33-Acb2 and T4-Acb2, resulting in a smaller binding pocket in T4-Acb2 (Figure 3.4E). Together, these observations may explain the inability of T4-Acb2 binding to CTNs. Lastly, ITC analyses showed that CHI14-Acb2 directly binds to 3',3'-cGAMP with a K_D of ~62.4 nM, but also does not bind to cA₃ (Figure 3.4F). Of note, native gel assays showed almost no shift of the CHI14-Acb2 protein upon adding any cyclic oligonucleotides, including 3',3'-cGAMP (Figure 3.13C), suggesting that native gel assay is not suitable for studying the binding spectrum of CHI14-Acb2. Using ITC, CHI14-Acb2 displayed the same binding spectrum to all cyclic oligonucleotides as T4-Acb2 (Figures 3.4F-G and 3.14). The outcomes of binding experiments are summarized, along with a comparison to the enzyme Acb1 (Figure 3.4H). In summary, Acb2 homologs bind to many CTNs and CDNs used in cGAS-based immunity with certain homologs having a more limited spectrum.

3.3.6. Acb2 antagonizes Type III-C CBASS immunity

Since Acb2 displays high affinity binding to CTNs, we tested whether phage-encoded Acb2 can antagonize Type III-C CBASS immunity that uses a cA₃ signaling molecule to activate the endonuclease (NucC) effector protein. NucC is a cyclic nucleotide-activated effector in both CBASS and Type III CRISPR-Cas systems, which non-specifically degrades DNA and limits phage replication^{85,116}. First, we established an *in vitro* NucC activity assay using purified NucC from the *P. aeruginosa* strain ATCC 27853 (Pa278) and Acb2 from *P. aeruginosa* phage PaMx33 (Figure 3.5A-B). While cA₃ activates the DNA cleavage activity of NucC, WT Acb2 significantly decreased NucC activity (Figure 3.5C). Moreover, following proteolysis of WT Acb2, the released cA₃ molecule again activated NucC activity (Figure 5C; last two lanes). The R67A and T74A Acb2 mutant proteins, which lost or exhibited decreased cA₃ binding, displayed minimal inhibition of NucC activity. However, the Y11A and K26A Acb2 mutants, whose CDN binding pockets are disrupted, inhibited NucC activity similarly to WT Acb2 (Figure 3.5C). These results demonstrate that Acb2 antagonizes Type III-C CBASS immunity *in vitro* through sequestering the cA₃ molecule.

To determine whether Acb2 can inhibit this same cA_3 -based CBASS system *in vivo*, we performed phage infection assays with plasmid or phage-encoded Acb2 and the Pa278 Type III-C CBASS operon (Figure 3.5B). Phages naturally expressing *acb2* were unable to replicate on the native *P. aeruginosa* ATCC 27853 strain, so the Pa278 system was chromosomally integrated into PAO1 that is a phage sensitive strain and naturally lacks CBASS. In the presence Pa278 Type III-C CBASS, the titer of JBD67 phage lacking *acb2* (JBD67 Δ *acb2*) was reduced by 3 orders of magnitude compared to its replication in the absence of CBASS (Figure 3.5D-E). Plasmid-based expression of WT Acb2 or Y11A and K26A Acb2 (CDN binding mutants) fully rescued phage titer, while R82A and T89A (CTN binding mutants) did not (Figure 3.5D). In the presence of the Pa011 Type II-A CBASS (cGAMP producing), the titer of JBD67 Δ *acb2* phage was reduced by 5 orders of magnitude (Figure 3.5D-E), whereas JBD67 WT phage was reduced by 1-2 orders of magnitude (Figure 3.15). Plasmid-based expression of WT Acb2 or R82A and T89A Acb2 (CTN binding mutants) partially rescued phage titer, while Y11A and K26A Acb2 (CDN binding mutants) did not (Figure 3.5D). The partial targeting of JBD67 WT phage (i.e. naturally encoding Acb2) was fully reversed by plasmid-based expression of WT Acb2 or the CTN binding mutants, but not the CDN binding mutants (Figure 3.15A). We additionally introduced a K26A mutation into *acb2* within the genome of JBD67 WT phage. This rendered mutant phage completely sensitive to cells expressing the cGAMP-based system but maintained resistance against the cA_3 system (Figures 3.5E and 3.15B). These findings demonstrate Acb2 protects phage from Type III-C (cA_3 -producing) and Type II-A (3',3'-cGAMP-producing) CBASS using different interfaces, further highlighting the versatility of the Acb2 protein.

3.4. Discussion

Following phage infection, CBASS immunity functions via the activation of a cGAS-like enzyme to catalyze the synthesis of a cyclic oligonucleotide signaling molecule. To date, two phage proteins have been discovered to antagonize the CBASS immunity: Acb1 and Acb2. Acb1 uses an inhibitory mechanism common to the eukaryotic cGAS-STING signaling system⁹⁵, that is, enzymatically cleaving and depleting an array of CDNs and CTNs⁴⁸ In contrast, we, alongside another independent group,

reported that Acb2 acts as a “sponge” and sequesters 3',3'-cGAMP^{50,53}, alongside a variety of other CBASS CDN signaling molecules⁵⁰. A sponging mechanism was also reported for inhibitors of the anti-phage system Thoeris, including Tad1⁴⁹ and Tad2⁴⁵ that sequester gcADPR signaling molecules. Here, we extend the CDN binding spectrum of Acb2 to include 3',2'-cGAMP, a signaling molecule not cleaved by Acb1, but recently implicated in both CBASS and cGAS like signaling in eukaryotes^{71,116,119}. The ability of Acb2 to function in human cells against 2',3'-cGAMP reinforces the flexibility of the “sponging” mechanism (i.e. no need to bind to cGAS, STING, or host proteins), and the remarkable cross-kingdom conservation of this cyclic-oligonucleotide-based immune system. The activity of Acb2 in mammalian cells also implies the possibility that pathogenic bacteria with prophage-encoded Acb1, Acb2, or other undiscovered cGAMP interactors could use them to dampen the human immune response during intracellular infection. Similar cross-kingdom interactions have been previously reported with bacterial c-di-GMP⁸² and c-di-AMP produced by *Listeria monocytogenes*¹²⁰, serving as ligands for human STING. While we could not identify proteins with similar structures to Acb2 in eukaryotic viruses, we speculate that novel cGAMP sponges await discovery in eukaryotes and their viruses. Taken together, our work suggests that discoveries with human health implications remain to be made at the interface of cyclic oligonucleotide inhibitors and cGAS-STING immunity.

Acb2 binds to a wider spectrum of cyclic oligonucleotides compared to the enzyme Acb1, including 3',3'-cUU, 3',3'-cUG, and 3',2'-cGAMP, while also sequestering CTNs with a stronger binding affinity. In some Acb2 homologs, however, we observed that the CTN binding site is mutated and non-functional. Although it is unclear if there is a cost to the CTN binding site that would lead to its loss, in the case of phage T4, its genome encodes both Acb1 and Acb2 and therefore suggests that this phage is broadly evasive of most CBASS types. To our knowledge, Acb2 represents the first phage anti-immune protein, as well as the first protein more broadly, that can bind two types of cyclic oligonucleotides simultaneously with different binding pockets. This highlights Acb2 as a nearly universal inhibitor of CBASS, which could enhance phage therapeutics by enabling the evasion of many common CBASS types and subtypes encoded by human bacterial pathogens. Moreover, with

the recent unveiling of counter-defense ‘sponge’ mechanisms (i.e. Tad1 and Tad2 for *Thoeris*), our study sets precedent to consider other small, versatile proteins that can soak up multiple immune signaling molecules.

3.6. Author Contributions

Yue Feng (YF) and Joseph Bondy-Denomy (JBD) conceived and supervised the project and designed experiments. Xueli Cao, Dong Li, Yu Wang, and Linlin Guan purified the proteins, grew and optimized the crystals, collected the diffraction data, and performed *in vitro* activity analysis and binding assays. Yu Xiao solved the crystal structures. Erin Huiting (EH) performed all of the *in vivo* phage experiments, strain engineering, and bioinformatics. Xujun Cao performed *in vivo* human cell experiments under supervision of Lingyin Li. Jie Ren performed the HPLC analysis. YF and EH wrote the original manuscript, and JBD, YF, and EH revised the manuscript.

3.7. Materials and Methods

Data and Code Availability

The accession numbers for the coordinate and structure factors reported in this paper are PDB: 8IXZ (Acb2-3',2'-cGAMP), 8J8O (Acb2-2',3'-cGAMP), 8IY0 (Acb2-cA₃), 8IY1 (Acb2-cAAG) and 8IY2 (Acb2-3',3'-cGAMP-cA₃). This paper does not report original code. Any additional information required to reanalyze the data reported in this paper is available from the lead contact upon request.

Bacterial strains and phages

The bacterial strains and phages used in this study are listed online (doi: 10.1016/j.molcel.2023.11.026). The *P. aeruginosa* strains (BWHPSA011, ATCC 27853, PAO1) and *E. coli* strains (DH5α) were grown in Lysogeny broth (LB) medium at 37°C both with aeration at 225 r.p.m. Plating was performed on LB solid agar with 10 mM MgSO₄ when performing phage infections, and when indicated, gentamicin (50 μg ml⁻¹ for *P. aeruginosa* and 15 μg ml⁻¹ for *E. coli*) was used to maintain the pHERD30T plasmid. Gene expression was induced by the addition of L-arabinose (0.3%)

unless stated otherwise. Further, gene expression in *P. aeruginosa* was induced by the addition of 0.3 mM isopropyl- β -D-thiogalactopyranoside (IPTG) unless stated otherwise. The *E. coli* BL21 (DE3) strain was used for recombinant protein overexpression and grown in Lysogeny broth (LB) medium. The cells were grown at 37°C until OD_{600nm} reached 0.8 and then induced at 18°C for 12 h.

Protein expression and purification

The PaMx33-Acb2, JBD67-Acb2, T4-Acb2, and CHI14-Acb2 genes were synthesized by GenScript. The full-length Acb2 gene was amplified by PCR and cloned into a modified pET28a vector in which the expressed Acb2 protein contains a His₆-SUMO tag or His₆ tag. The Acb2 mutants were generated by two-step PCR and were subcloned, overexpressed and purified in the same way as wild-type protein. The proteins were expressed in *E. coli* strain BL21 (DE3) and induced by 0.2 mM isopropyl- β -D-thiogalactopyranoside (IPTG) when the cell density reached an OD_{600nm} of 0.8. After growth at 18°C for 12 h, the cells were harvested, re-suspended in lysis buffer (50 mM Tris-HCl pH 8.0, 300 mM NaCl, 10 mM imidazole and 1 mM PMSF) and lysed by sonication. The cell lysate was centrifuged at 20,000 g for 50 min at 4°C to remove cell debris. The supernatant was applied onto a self-packaged Ni-affinity column (2 mL Ni-NTA, Genscript) and contaminant proteins were removed with wash buffer (50 mM Tris pH 8.0, 300 mM NaCl, 30 mM imidazole). The fusion protein of Acb2 with His₆-SUMO tag was then digested with Ulp1 at 18°C for 2 h, and then the Acb2 protein was eluted with wash buffer. The eluant of Acb2 was concentrated and further purified using a Superdex-200 increase 10/300 GL (GE Healthcare) column equilibrated with a buffer containing 10 mM Tris-HCl pH 8.0, 500 mM NaCl and 5 mM DTT. The purified protein was analyzed by SDS-PAGE. The fractions containing the target protein were pooled and concentrated.

Crystallization, data collection and structural determination

The crystals of Acb2 were grown with reservoir solution containing 0.2 M Sodium bromide, 0.1 M Bis-Tris propane pH 6.5, 10% Ethylene glycol and 20% v/v PEG 3350 at 18°C. Prior to crystallization, cA₃, cAAG, cA₃+3',3'-cGAMP or 3',2'-cGAMP were mixed with the protein at a molar ratio of 2:1,

respectively, and the concentration of Acb2 was 24 mg/mL. The crystals appeared overnight and grew to full size in about two to three days. The crystals were cryoprotected in the reservoir solution containing 20% glycerol before its transferring to liquid nitrogen. All the data were collected at SSRF beamlines BL02U1 and BL19U1, integrated and scaled using the HKL2000 package¹⁰⁸. The initial model of Acb2 was used from PDB: 8H2X. The structures of Acb2 and its complex with cyclic oligonucleotides were solved through molecular replacement and refined manually using COOT¹⁰⁹. The structure was further refined with PHENIX¹¹⁰ using non-crystallographic symmetry and stereochemistry information as restraints. The final structure was obtained through several rounds of refinement. Data collection and structure refinement statistics are summarized in Table 3.1.

Isothermal titration calorimetry binding assay

The dissociation constants of binding reactions of Acb2 or Acb2 mutants with the cA₃/cAAG/3',2'-cGAMP/3',3'-cGAMP/2',3'-cGAMP/c-di-AMP/c-di-GMP/3',3'-cUU/3',3'-cUA/3',3'-cUG/cUMP/cCMP/cAMP/cA₆/cA₄ were determined by isothermal titration calorimetry (ITC) using a MicroCal ITC200 calorimeter. Both proteins and cyclic-oligonucleotides were desalted into the working buffer containing 20 mM HEPES pH 7.5 and 200 mM NaCl. The titration was carried out with 19 successive injections of 2 μ L cA₃/cAAG/cA₆/cA₄ at the 0.04 mM concentration, spaced 120 s apart, into the sample cell containing the Acb2 or Acb2 mutants with a concentration of 0.01 mM by 700 rpm at 25°C. Correspondingly, the 3',2'-cGAMP/3',3'-cGAMP/2',3'-cGAMP/c-di-AMP/c-di-GMP/3',3'-cUU/3',3'-cUA/3',3'-cUG/cUMP/cAMP at the 0.4 mM concentration was titrated into 0.1 mM Acb2 or Acb2 mutants at the same experimental conditions. The Origin software was used for baseline correction, integration, and curve fitting to a single site binding model.

Native-PAGE assay

Acb2 or Acb2 mutants was pre-incubated with CDNs for 10 min at 18°C, where Acb2 or Acb2 mutants was 14.3 μ M and the concentrations of CDNs ranged from 1.8 to 7.2 μ M (1.8, 3.6, 7.2 μ M). Products

of the reaction were analyzed using 5% native polyacrylamide gels and visualized by Coomassie blue staining.

High-performance liquid chromatography (HPLC)

40 μM Acb2 or Acb2 mutants was pre-incubated with 4 μM cA₃ for 10 min at 18°C. Proteinase K was subsequently added to the reaction system at a final concentration of 0.5 μM and the reaction was performed at 58°C for 1 h. Reaction products were transferred to Amicon Ultra-15 Centrifugal Filter Unit 3 kDa and centrifuged at 4°C, 4,000 g. The products obtained by filtration were further filtered with a 0.22 μm filter and subsequently used for HPLC experiments. The HPLC analysis was performed on an Agilent 1200 system with a ZORBAX Bonus-RP column (4.6 \times 150 mm). A mixture of acetonitrile (2%) and 0.1% trifluoroacetic acid solution in water (98%) were used as mobile phase with 0.8 mL/min. The compounds were detected at 254 nm.

***In vitro* NucC nuclease activity assay**

For nuclease activity assay, a pUC19 plasmid was used as substrate. Pa-NucC (10 nM) and cA₃ molecules (5 nM) were mixed with 0.5 μg DNA in a buffer containing 25 mM Tris-HCl pH 8.0, 10 mM NaCl, 10 mM MgCl₂, and 2 mM DTT (20 μL reaction volume), incubated 10 min at 37°C, then separated on a 1% agarose gel. Gels were stained with Goldview and imaged by UV illumination. To determine the function of Acb2, 50 nM Acb2 or its mutants were pre-incubated with the system at 18°C for 15 min, and the subsequent reaction and detection method was as described above. To examine whether the released molecule from Acb2 is able to activate NucC, 5 nM cA₃ was incubated with 50 nM Acb2 for 15 min at 18°C. Proteinase K was subsequently added to the reaction system at a final concentration of 1 μM and the reaction was performed at 58°C for 1 h, then the proteinase K-treated samples were heated with 100°C for 10 min to extinguish proteinase K and the subsequent detection method was as described above.

Episomal gene expression

The shuttle vector that replicates in *P. aeruginosa* and *E. coli*, pHERD30T³⁴ was used for cloning and episomal expression of *P. aeruginosa* ATCC 27853 Type III-C CBASS operon into the PAO1 WT strain. This vector has an arabinose-inducible promoter and a selectable gentamicin marker. Vector was digested with *SacI* and *PstI* restriction enzymes and then purified. Inserts were amplified by PCR using bacterial overnight culture or phage lysate as the DNA template, and joined into the pHERD30T vector at the *SacI-PstI* restriction enzyme cut sites by Hi-Fi DNA Gibson Assembly (NEB) following the manufacturer's protocol. The resulting plasmids were transformed into *E. coli* DH5 α . All plasmid constructs were verified by sequencing using primers that annealed to sites outside the multiple cloning site. *P. aeruginosa* cells were electroporated with the pHERD30T constructs and selected on gentamicin.

Chromosomal CBASS integration

For chromosomal insertion of the *P. aeruginosa* BWHP5011 Type II-A and ATCC 27853 Type III-C CBASS operons into PAO1, the integrating vector pUC18-mini-Tn7T-LAC⁹⁹ and the transposase expressing helper plasmid pTNS3⁹⁹ were used to insert the CBASS operons at the Tn7 locus in the *P. aeruginosa* PAO1 strain, or an pUC18-mini-Tn7T-LAC empty vector (E.V.) control strain (PAO1). The vector was linearized using around-the-world PCR, treated with *DpnI*, and then purified. Two overlapping inserts encompassing the CBASS operon were amplified by PCR using overnight culture as the DNA template, and joined into the pUC18-mini-Tn7T-LAC vector at the *SacI-PstI* restriction enzyme cut sites by Hi-Fi DNA Gibson Assembly (NEB) following the manufacturer's protocol. The resulting plasmids were used to transform *E. coli* DH5 α . All plasmid constructs were verified by sequencing using primers that annealed to sites outside the multiple cloning site. *P. aeruginosa* PAO1 cells were electroporated with pUC18-mini-Tn7T-LAC and pTNS3 and selected for on gentamicin. Potential integrants were screened by colony PCR with primers PTn7R and PglmS-down, and then verified by sequencing using primers that anneal to sites outside the attTn7 site. Electrocompetent cell

preparations, transformations, integrations, selections, plasmid curing, and FLP-recombinase-mediated marker excision with pFLP were performed as described previously⁹⁹.

Phage growth

All phages were grown at 37°C with solid LB agar plates containing 20 ml of bottom agar containing 10 mM MgSO₄ and any necessary inducers or antibiotics. Phages were grown on the permissible host *P. aeruginosa* PAO1, which naturally lacks CBASS, or in their native host that naturally lacks CBASS. 150 µl of overnight cultures of PAO1 were infected with 10 µl of low titer phage lysate (>10⁴⁻⁷ pfu/ml) and then mixed with 3 ml of 0.7% top agar 10 mM MgSO₄ for plating on the LB solid agar. After incubating at 37°C overnight, individual phage plaques were picked from top agar and resuspended in 200 µl SM phage buffer. For high titer lysates, the purified phage was further amplified on LB solid agar plates with PAO1 WT. After incubating 37°C overnight, 3 ml SM phage buffer was added until the solid agar lawn was completely covered and then incubated for 5-10 minutes at room temperature. The whole cell lysate was collected and a 1% volume of chloroform was added, and then left to shake gently on an orbital shaker at room temperature for 15 min followed by centrifugation at maximum g for 3 min to remove cell debris. The supernatant phage lysate was stored at 4°C for downstream assays.

Plaque assays

Plaque assays were conducted at 37°C with solid LB agar plates. 150 µL of overnight bacterial culture was mixed with top agar and plated. Phage lysates were diluted 10-fold then 2 µL spots were applied to the top agar after it had been poured and solidified.

Homologous recombination-mediated mutation of phage gene

Construction of template plasmids for homologous recombination consisted of homology arms >500bp up- and downstream of the mutation of interest encoded in JBD67 *acb2*. The homology arms were amplified by PCR using JBD67 WT phage genomic DNA as the template. Template primers were

designed to symmetrically flank the JBD67 *acb2* CDN or CTN binding sites. PCR products were purified and assembled as a recombineering substrate and then inserted into the *SacI-PstI* site of the pMQ30 vector. The resulting plasmids were electroporated into *P. aeruginosa* PAO1-JBD67 WT lysogen strain as previously described⁵⁰. PAO1 lysogen strains carrying the recombination plasmid were grown in LB media supplemented with gentamicin. 150 μ l of overnight cultures were infected with 10 μ l of high titer phage lysate ($>10^9$ pfu/ml; JBD67 WT) and then plated on LB solid agar. After incubating at 37°C overnight, SM phage buffer was added to the entire lawn and whole cell lysate collected. The resulting phage lysate containing both WT and recombinant phages and were screen by colony PCR with the appropriate pairs of primers amplifying the region outside of the homology arms and subject to Sanger Sequencing. Once confirmed, the PAO1-JBD67 lysogens were grown in liquid culture, and the presence of spontaneously produced phage in the supernatant that could plaque on the PAO1 wildtype strain confirmed lysogeny.

Interferon reporter assay in human cell line

The PaMx33-Acb2 gene was codon-optimized for human expression and synthesized by GenScript with overhangs that enabled insertion into the *XhoI-BamHI* sites of pcDNA3 via Gibson assembly. The wildtype plasmid was modified by site-directed mutagenesis using the QuikChange protocol with the indicated primers, and *Dpn1*-digested to obtain all point mutants. All recombinant plasmids were transformed into XL1-Blue competent cells (Agilent) and sequenced for verification. 293T-Dual Null cells were cultured in DMEM (Gibco) supplemented with 10% FBS (Atlanta Biologics) (v/v) and 100 U/mL penicillin-streptomycin (Gibco) and maintained in 37°C incubators with 5% CO₂. Four days prior to measurement, 293T-Dual cells were passaged and plated in 12-well tissue cultured-treated plates at 100000 cells/well. After 20 hours they were transfected with 100 ng of pcDNA3-hSTING and 100 ng of pcDNA3 empty vector or containing Acb2 using Fugene6 transfection reagent (Promega) according to its associated protocol. After 20 hours, the growth media was replaced with fresh growth media containing 50 μ M 2',3'-cGAMP or regular growth media as negative controls. The cells were further incubated for 18 h, and the media was harvested to measure luciferase activity using the

QuantiLuc system (Invivogen). The cells were directly lysed in 1 × LSB and western blot was performed on cell lysates to verify expression of STING and Acb2.

Western blot

A rabbit Acb2 polyclonal antibody was generated by a commercial vendor (GenScript) using a synthetic peptide from Acb2 (CHNRDEITRIANAEP). The polyclonal Acb2 antibody was further purified by antigen affinity (GenScript). After harvesting conditioned media, cells were directly lysed on the plate using 1× LSB. Lysates were separated on a SurePage Bis-Tris polyacrylamide gel (GenScript) and transferred to a nitrocellulose membrane using the semi-dry iBlot2 system (Invitrogen). The membrane was blocked for 1 h at room temperature (Intercept blocking buffer, Li-COR Biosciences), and incubated with primary antibodies (rabbit anti-STING (Cell Signaling Technologies), mouse anti-alpha-tubulin (Sigma-Aldrich), rabbit anti-Acb2 (GenScript)) overnight at 4°C. Following three washes in 1×TBS-0.1% tween, secondary antibody (Anti-rabbit or anti-mouse (Li-Cor Biosciences)) was added for 1 hour at room temperature, followed by three additional washes in TBS-T. Blots were imaged in IR using a Li-Cor Odyssey Blot Imager.

Phylogenetic tree analysis

Acb2 homologs were identified using PaMx33 Acb2 (NCBI ID: ANA48877.1) as a query protein to seed a position-specific iterative blast (PSI-BLAST) search of the NCBI non-redundant protein database. Three rounds of PSI-BLAST searches were performed with a max target sequence of 5,000 and E value cut-off of 0.005 for inclusion in the next search round, BLOSUM62 scoring matrix, gap costs settings existence 11 and extension 1, and using conditional compositional score matrix adjustment. Hits from the third search round of PSI-BLAST with >70% coverage and an E value of < 0.0005 were aligned using MAFFT (FFT-NS-I iterative refinement method)¹²¹. Manual analysis of the MAFFT protein alignment was performed to ensure the presence of at least one of the cyclic oligonucleotide binding site motifs (CDN site <YX(14)K and CTN site RX(6)T>) and to remove large gaps, resulting in 2,242 total sequences. MMSeq2¹²² was used to remove protein redundancies

(minimum sequence identity=0.95, minimum alignment coverage=1), which resulted in 878 representative or unique Acb2 homolog sequences. The final aligned 878 sequences were used to construct a phylogenetic tree using FastTree¹²³ and then visualized and annotated in iTOL¹⁰⁶.

3.8. Figures

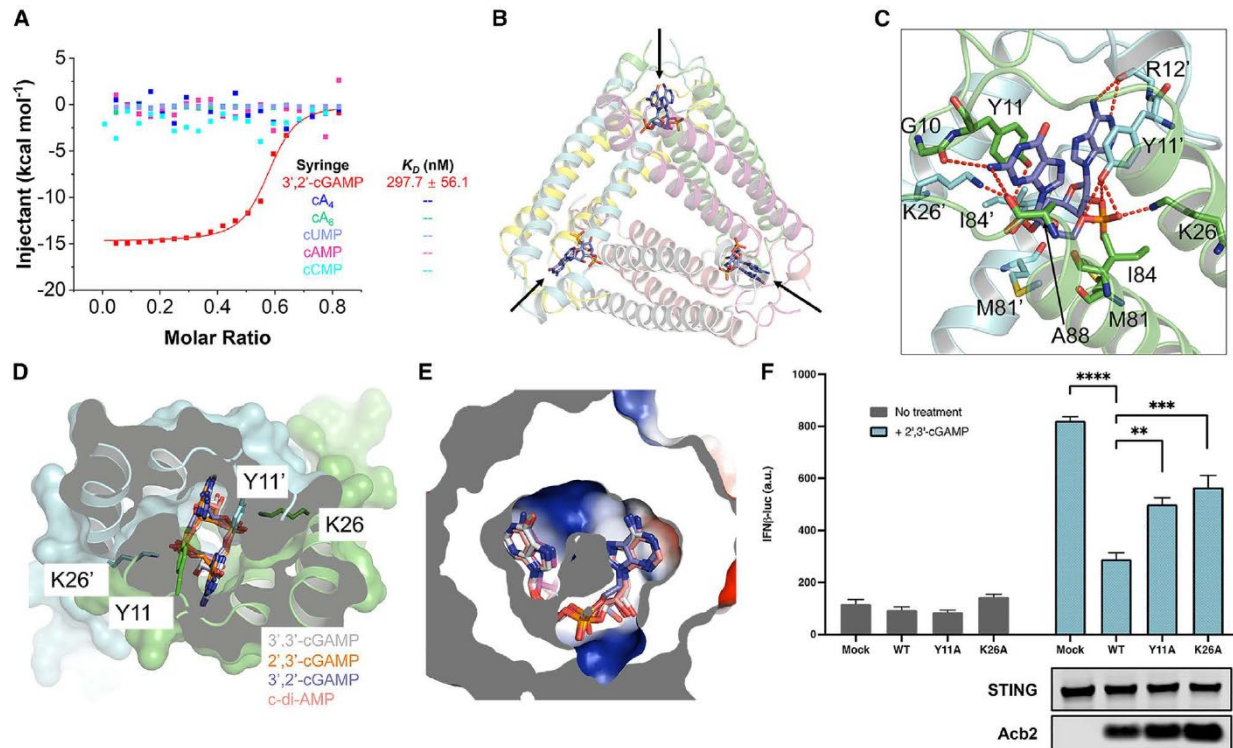


Figure 3.1: Acb2 from phage PaMx33 binds cyclic trinucleotides and 3',2'-cGAMP

(A) ITC assays to test binding of cyclic nucleotides to PaMx33-Acb2. Representative binding curves and binding affinities are shown. The K_D values are mean \pm s.d. ($n=3$). Raw data for these curves are shown in Figure 3.7. **(B)** Overall structure of Acb2 complexed with 3',2'-cGAMP, which are indicated by arrows. **(C)** Detailed binding between Acb2 and 3',2'-cGAMP. Residues involved in 3',2'-cGAMP binding are shown as sticks. Red dashed lines represent polar interactions. **(D)** Structural alignment among 3',2'-cGAMP, 2',3'-cGAMP, 3',3'-cGAMP and c-di-AMP bound Acb2. Surface representation overlaid to cartoon representation, highlighting the binding pocket of CDNs. **(E)** Electrostatic surface model showing the binding pocket of CDNs. The CDNs are colored as in D. **(F)** 293T-Dual cells were transfected with hSTING and Acb2 or its mutants, then treated with 2',3'-cGAMP. STING activation was read as luciferase signal controlled by an interferon promoter. A western blot is shown probing the expression of STING and Acb2.

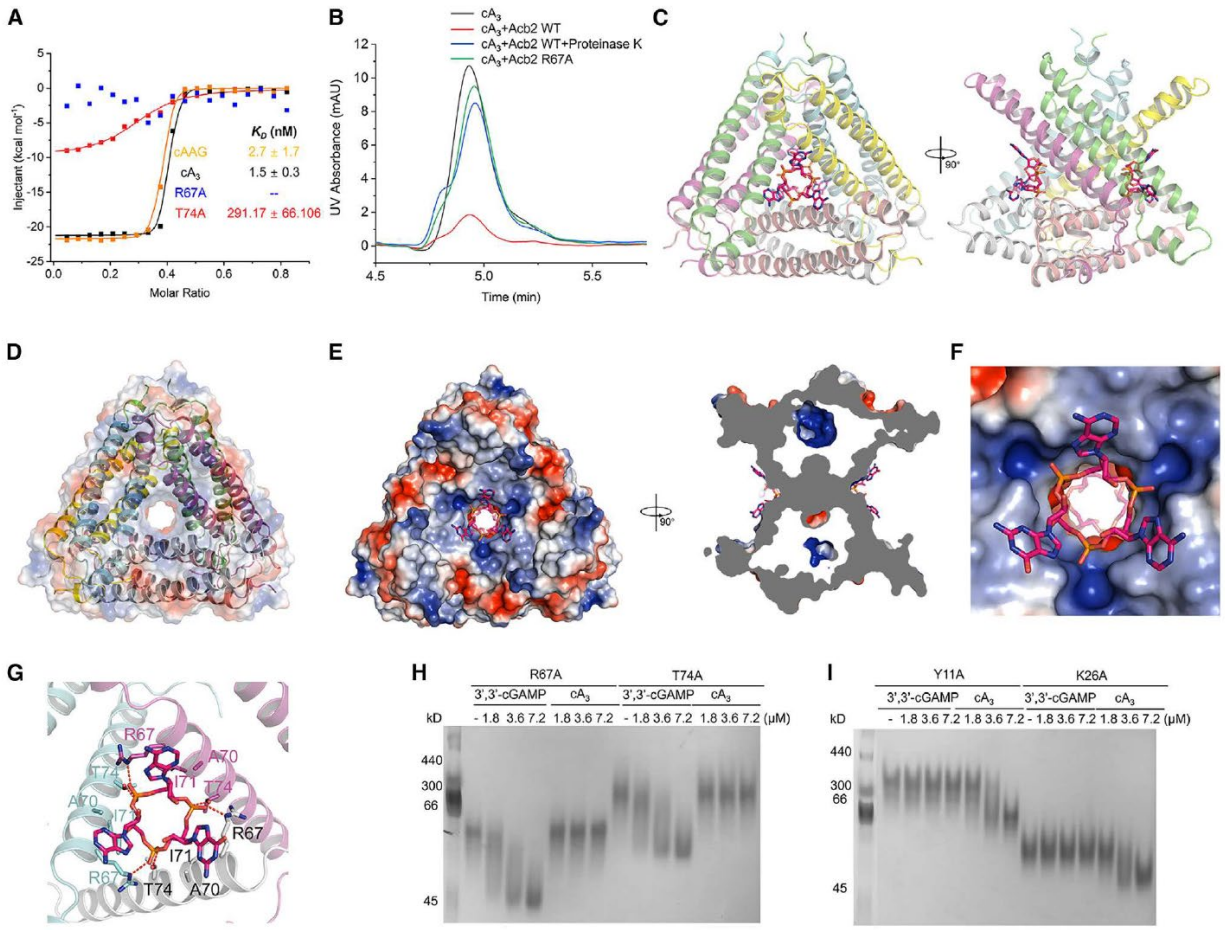


Figure 3.2: Acb2 binds to cyclic trinucleotides with binding sites different from those of cyclic dinucleotides

(A) ITC assays to test the binding of cAAG and cA₃ to PaMx33-Acb2, and binding of cA₃ to PaMx33-Acb2 mutants. Representative binding curves and binding affinities are shown. The K_D values are mean \pm s.d (n = 3). Raw data for these curves are shown in Figure 3.7. The two mutants R67A and T74A in the panel represent their binding to cA₃. (B) The ability of PaMx33-Acb2 to bind and release cA₃ when treated with proteinase K was analyzed by HPLC. cA₃ standard was used as a control. The remaining cA₃ after incubation with PaMx33-Acb2 was tested. Overall structure of Acb2 complexed with cAAG, which are shown as sticks. Two views are shown. (D) Electrostatic surface of Acb2 overlaid on the cartoon model shows the channel in the center of the Acb2 hexamer. Electrostatic surface of Acb2 bound with cAAG. Two views are shown. (F) A closer view of the binding pocket shown in the left panel of D. (G) Detailed binding between Acb2 and cAAG. Residues involved in cAAG binding are shown as sticks. Red dashed lines represent polar interactions. (H-I) Native PAGE showed the binding of PaMx33 Acb2 mutants to cyclic oligonucleotides.

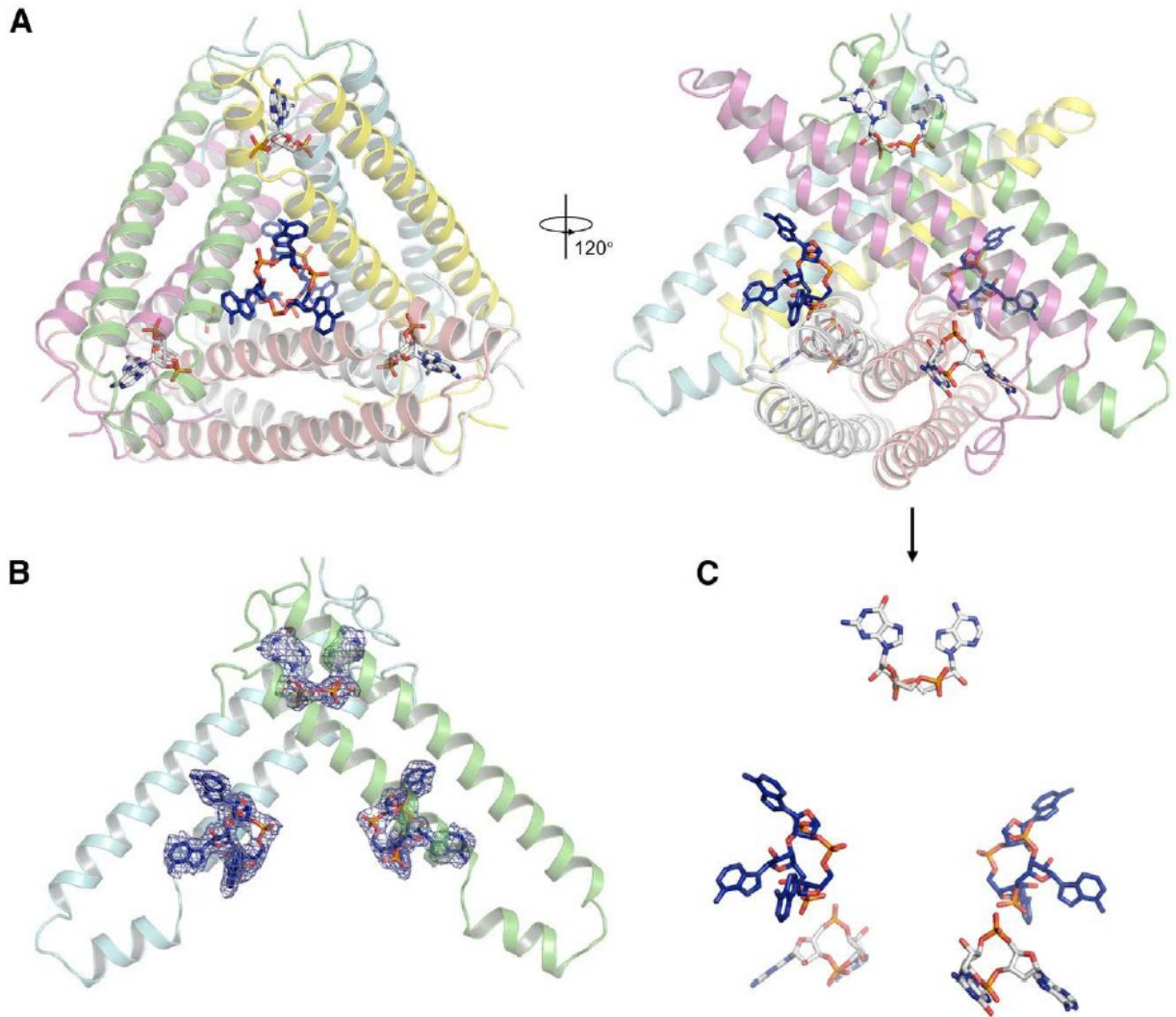


Figure 3.3: Acb2 binds to cyclic trinucleotides and dinucleotides simultaneously

(A) Overall structure of Acb2 complexed with cA₃ and 3',3'-cGAMP. cA₃ and 3',3'-cGAMP are shown as blue and light gray sticks. Two views are shown. **(B)** 2Fo-Fc electron density of cA₃ and 3',3'-cGAMP within an Acb2 dimer contoured at 1 σ . **(C)** Distribution of the small molecules within the Acb2 hexamer. The nucleotides are shown as they are in the right panel of (A).

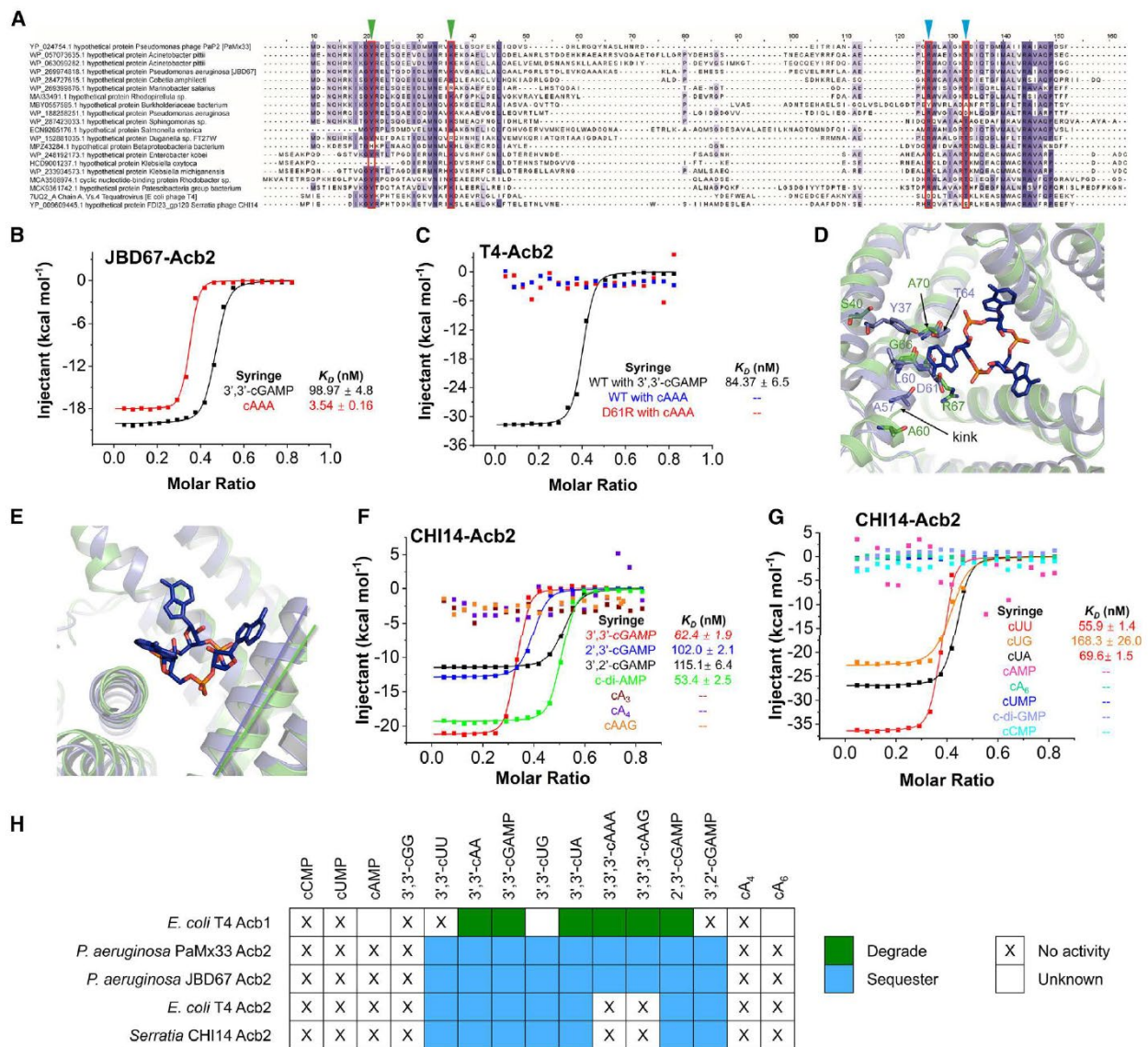


Figure 3.4: The binding spectra are different among Acb2 homologs

(A) Sequence alignment among Acb2 homologs. Residues that are >80 % conserved, >60 % conserved and >40% conserved are shaded in dark purple, light purple, and light grey, respectively. Residues involved in binding of cyclic CDNs and CTNs are marked with green and blue triangles, respectively. (B) ITC assays to test binding of cyclic oligonucleotides to JBD67-Acb2. Representative binding curves and binding affinities are shown. The K_D values are mean \pm s.d. ($n=3$). Raw data for these curves are shown in Figure 3.12. (C) ITC assays to test binding of cyclic oligonucleotides to T4-Acb2. Representative binding curves and binding affinities are shown. The K_D values are mean \pm s.d. ($n=3$). Raw data for these curves are shown in Figure 3.12. (D) Structural alignment between PaMx33-Acb2 and T4-Acb2 at one monomer. Residues with potential steric clash with cA_3 in T4-Acb2 and the corresponding residues in PaMx33-Acb2 are shown in sticks. (E) The same alignment shown in (D), highlighting the different relative angles formed by the three helices lining the binding pocket of cA_3 . (F-G) ITC assays to test binding of cyclic nucleotides to CHI14-Acb2. Representative binding curves and binding affinities are shown. The K_D values are mean \pm s.d. ($n=3$). Raw data for these curves are shown in Figure 3.14. (H) Summary of the binding results of Acb2 homologs and Acb1⁴⁸.

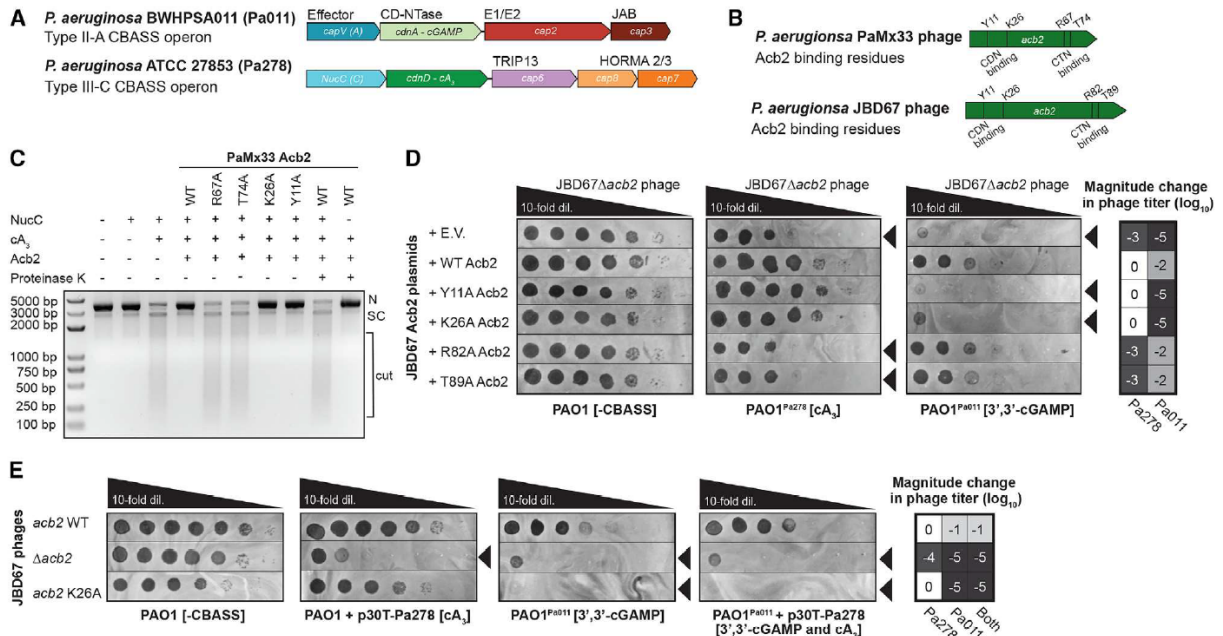


Figure 3.5: *Acb2* antagonizes tri- and di-nucleotide based CBASS immunity

(A) *Pseudomonas aeruginosa* BWHP5A011 (Pa011) Type II-A CBASS and ATCC 27853 (Pa278) Type III-C CBASS operons. (B) *Pseudomonas aeruginosa* PaMx33 and JBD67 phages *acb2* gene annotated with residues essential for CDN (3',3'-cGAMP) binding and CTN (cA₃) binding. (C) Effect of PaMx33 *Acb2* or its mutants on cA₃-activated NucC effector protein function. After treatment with proteinase K, the released cA₃ also showed the ability to activate the nuclease activity of NucC. The concentration of NucC, cA₃, *Acb2* and proteinase K is 10 nM, 5 nM, 50 nM and 1 μM, respectively. N denotes nicked plasmid, SC denotes closed-circular supercoiled plasmid, and cut denotes fully digested DNA. (D) Plaque assays with JBD67Δ*acb2* phage spotted in 10-fold serial dilutions on PAO1 strains harboring an empty vector (E.V.) plasmid or JBD67 *Acb2* variants. The PAO1 strains either contain no CBASS operon (-CBASS), a chromosomally integrated Pa011 CBASS operon (PAO1^{Pa011}), or a chromosomally integrated Pa278 CBASS operon (PAO1^{Pa278}). These plaque assays were used to quantify the order of magnitude change in phage titer by comparing the number of spots (with plaques, or clearings if plaques were not visible) on the PAO1^{Pa011} or PAO1^{Pa278} CBASS-expressing strains divided by the PAO1 (-CBASS) strain (n=3). Basal expression of the Pa011 CBASS operon and 0.3mM IPTG-inducible expression of the Pa278 CBASS operon is sufficient for phage targeting. Black arrowheads highlight significant CBASS-dependent reductions in phage titer. (E) Plaque assays with JBD67 phages spotted in 10-fold serial dilutions on PAO1 strains with and without CBASS. Pa278 CBASS was expressed from the pHERD30T (p30T) plasmid, while Pa011 CBASS was expressed from the chromosome. These plaque assays were used to quantify the order of magnitude change in phage titer (n=3). Basal expression (i.e. no arabinose added) of the Pa278 CBASS operon is sufficient for phage targeting. Black arrowheads highlight significant CBASS-dependent reductions in phage titer.

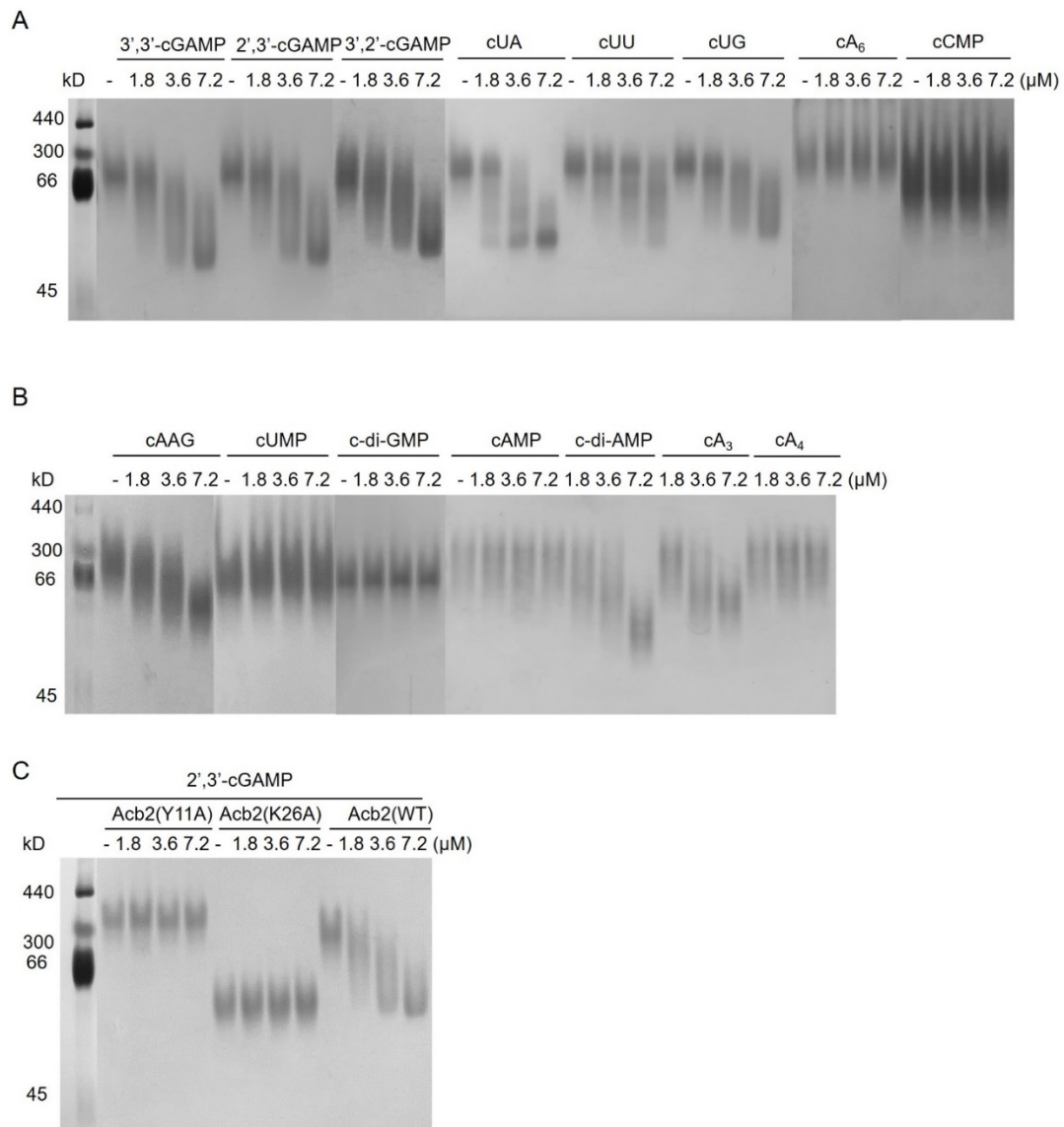


Figure 3.6: The cyclic nucleotide binding spectrum of PaMx33-Acb2
(A-C) Native PAGE assay showed the binding of PaMx33-Acb2 and its mutants to cyclic nucleotides. Related to Figures 3.1 and 3.2.

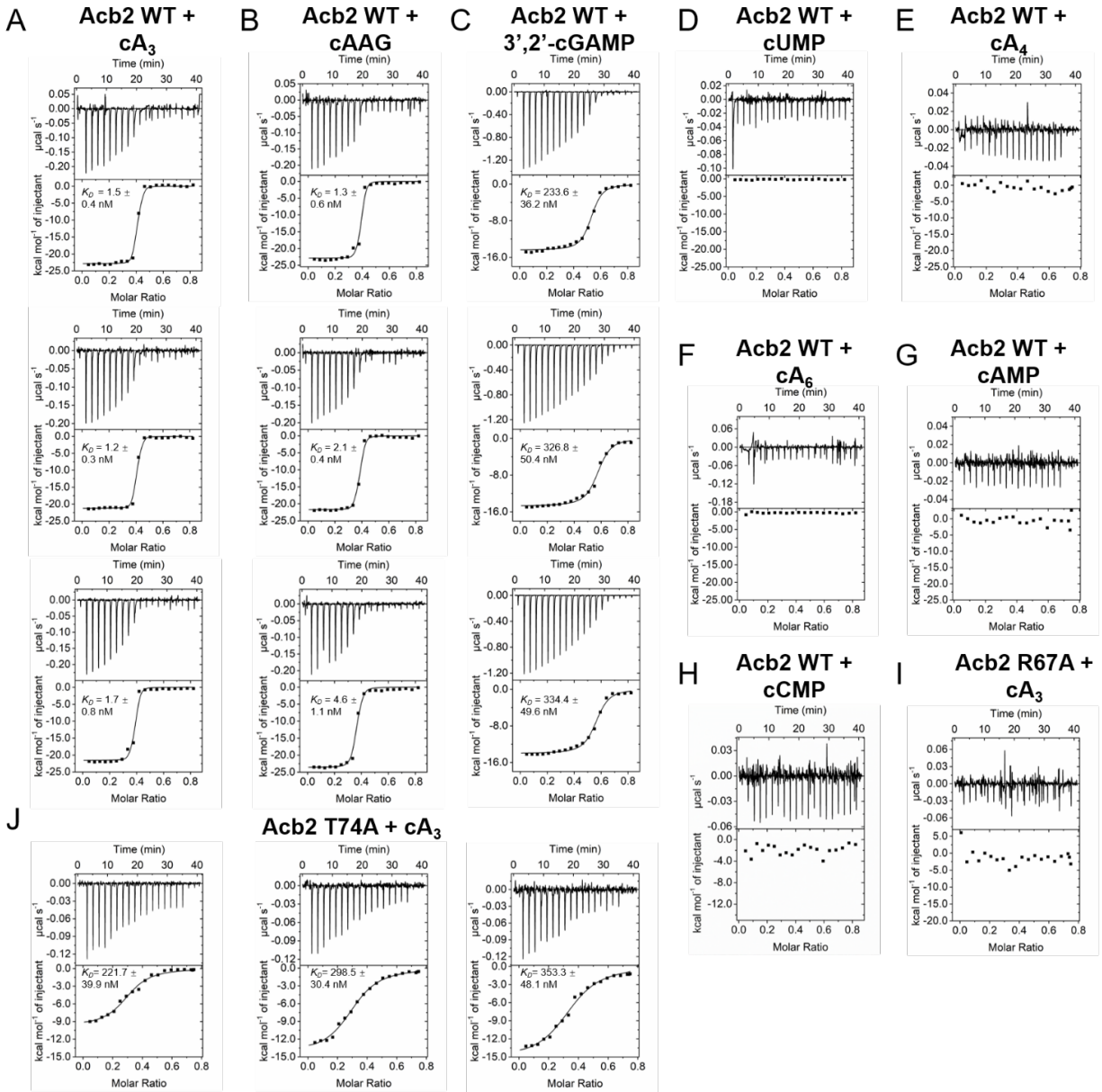


Figure 3.7: The binding spectrum of PaMx33-Acb2 studied by ITC assays

(A-H) ITC assays to test binding of PaMx33-Acb2 to cyclic nucleotides. (I-J) ITC assays to test binding of cA₃ to PaMx33-Acb2 T74A and PaMx33-Acb2 R67A. Related to Figures 3.1 and 3.2.

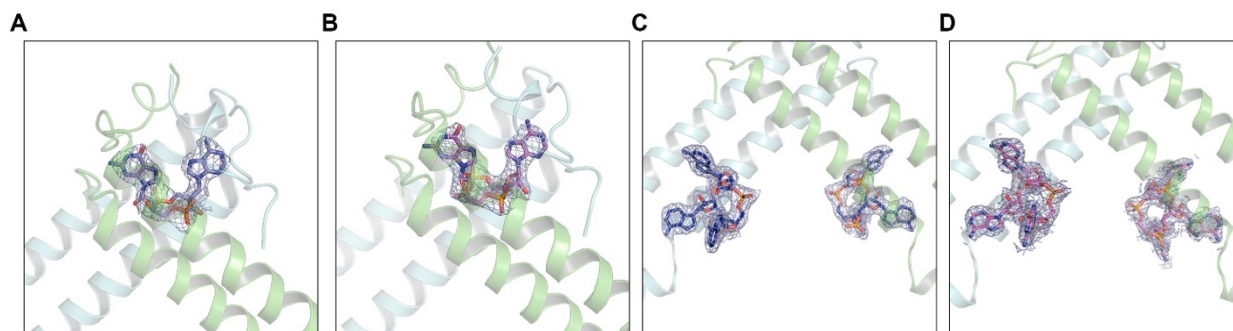


Figure 3.8: Density map of bound nucleotides in the structures of this study
 2Fo-Fc electron density of 3',2'-cGAMP, 2',3'-cGAMP, cA₃ and cAAG within the structures of Acb2-3',2'-cGAMP, Acb2-2',3'-cGAMP, Acb2-cA₃ and Acb2-cAAG contoured at 1 σ , respectively. Related to Figures 3.1 and 3.2.

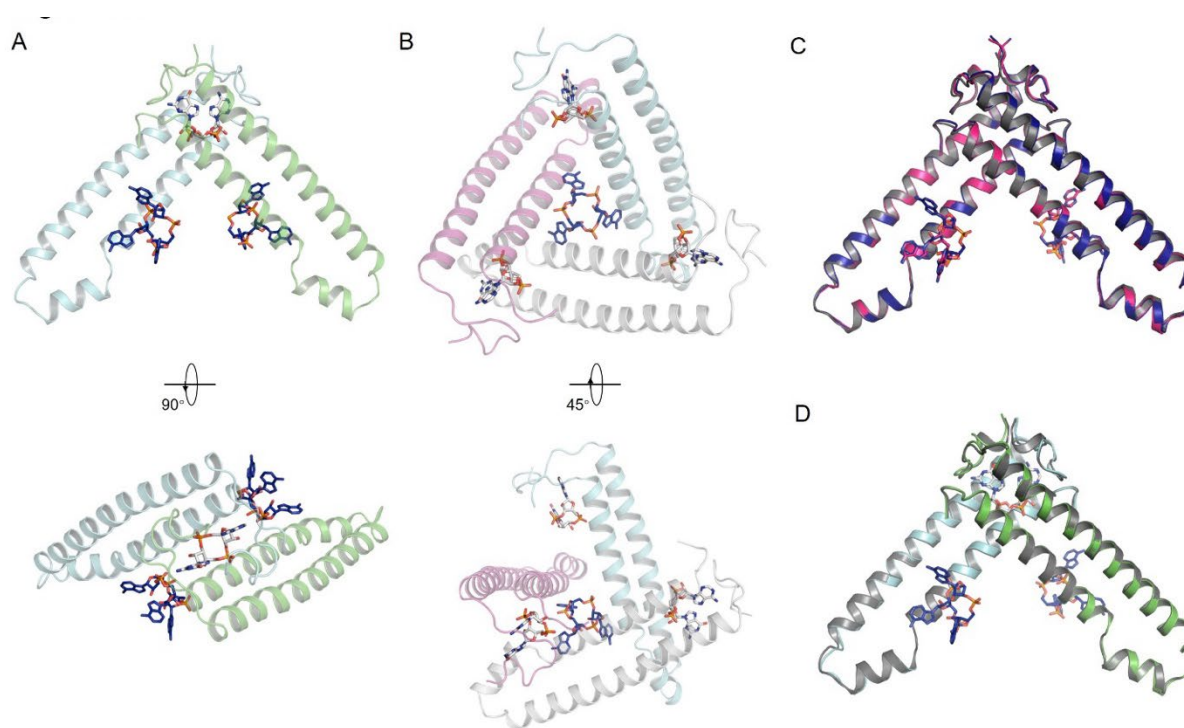


Figure 3.9: The binding sites of cyclic trinucleotides and dinucleotides are different
(A) An Acb2 dimer and the bound 3',3'-cGAMP within the Acb2-3',3'-cGAMP structure is shown. The Acb2-cA₃ structure is aligned to the structure and only the two cA₃ molecules are shown. **(B)** An Acb2 trimer and the bound cA₃ within the Acb2-cA₃ structure is shown. The Acb2-3',3'-cGAMP structure is aligned to the structure and only the three 3',3'-cGAMP molecules are shown. **(C)** Structural superimposition among Acb2-cA₃ (colored deep blue), Acb2-cAAG (colored hot pink) and apo Acb2 (colored grey) structures. Only an Acb2 dimer and the cyclic trinucleotides it is binding are shown. **(D)** Structural superimposition between Acb2-cA₃-3',3'-cGAMP and apo Acb2 structures. Only an Acb2 dimer and the cyclic nucleotides it is binding are shown. Related to Figure 3.2.

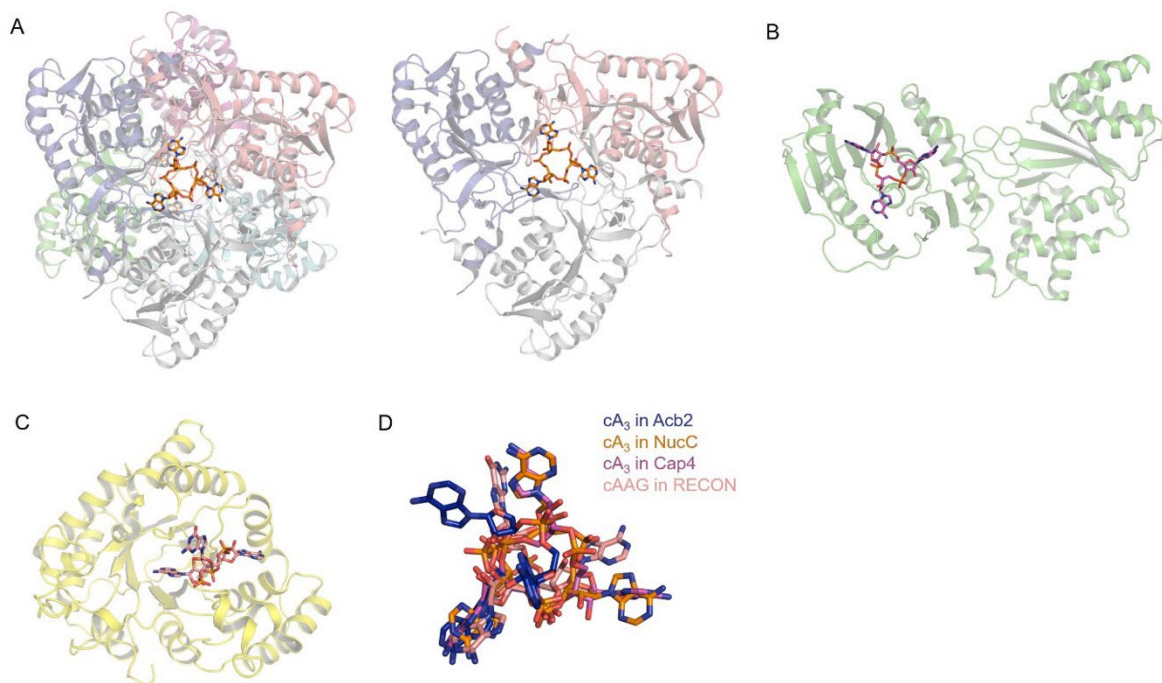


Figure 3.10: Acb2 binds to cA3 with a novel fold

(A) The binding of cA₃ in NucC from *Escherichia coli* (PDB code: 6P1H). A NucC hexamer bound with two cA₃ molecules and a NucC trimer bound with one cA₃ molecule are shown in the left and right, respectively. (B) The binding of cA₃ in Cap4 from *Acinetobacter baumannii* (PDB code: 6WAN). (C) The binding of cAAG in RECON from *Mus musculus* (PDB code: 6M7K). (D) cA₃ and cAAG molecules in the structures of Acb2-cA₃, NucC-cA₃, Cap-cA₃ and RECON-cAAG are aligned together and highlighted. Related to Figure 3.3.

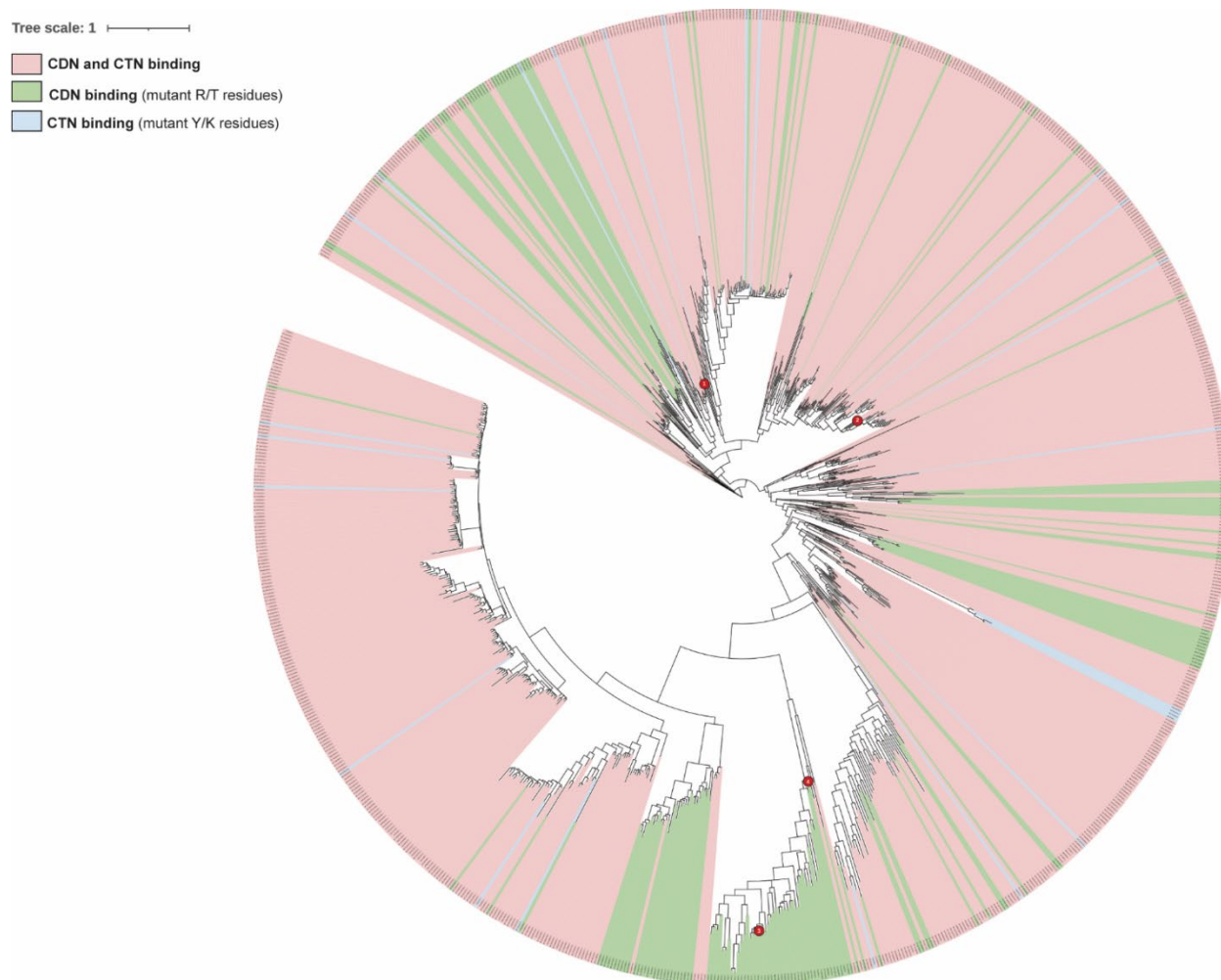


Figure 3.11: Phylogenetic analysis of unique Acb2 homologs across the genomes of prokaryotes and prokaryotic viruses

Phylogenetic tree of all 878 unique Acb2 protein sequences and classified based on the ability of Acb2 to accommodate CDN and CTN sequences. Branches denoted with the red circles were studied in vitro and/or in vivo: (1) *P. aeruginosa* phage PaMx33, (2) *P. aeruginosa* phage JBD67, (3) *E. coli* phage T4, (4) *Serratia* phage CHI14. Related to Figure 3.4 and 3.5.

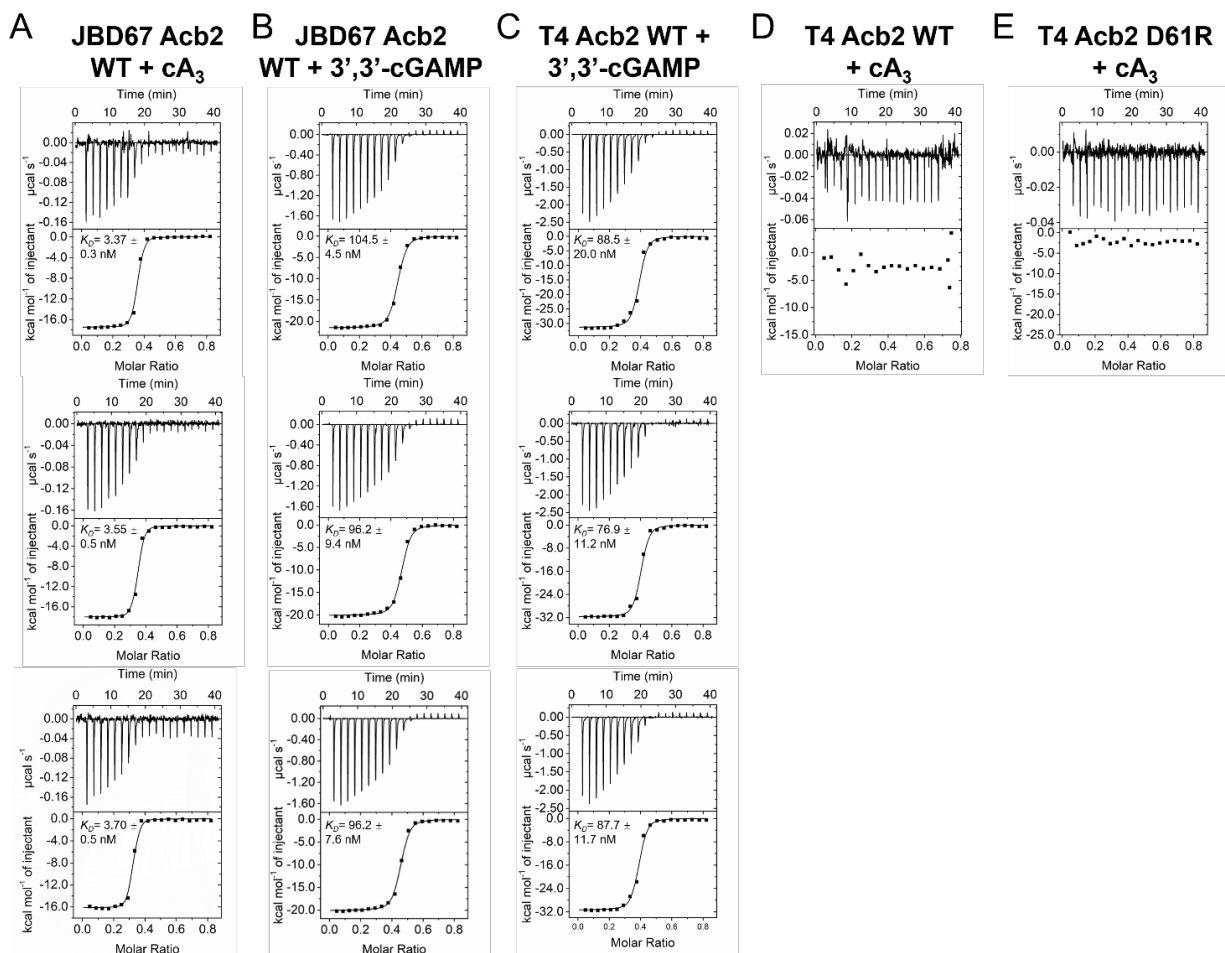


Figure 3.12: The binding spectrums of JBD67-Acb2 and T4-Acb2 studied by ITC assays (A-B) ITC assays to test binding of cyclic oligonucleotides to JBD67-Acb2. (C-D) ITC assays to test binding of 3',3'-cGAMP to T4-Acb2. (E) ITC assays to test binding of cA₃ to T4-Acb2 D61R. Related to Figure 3.4.

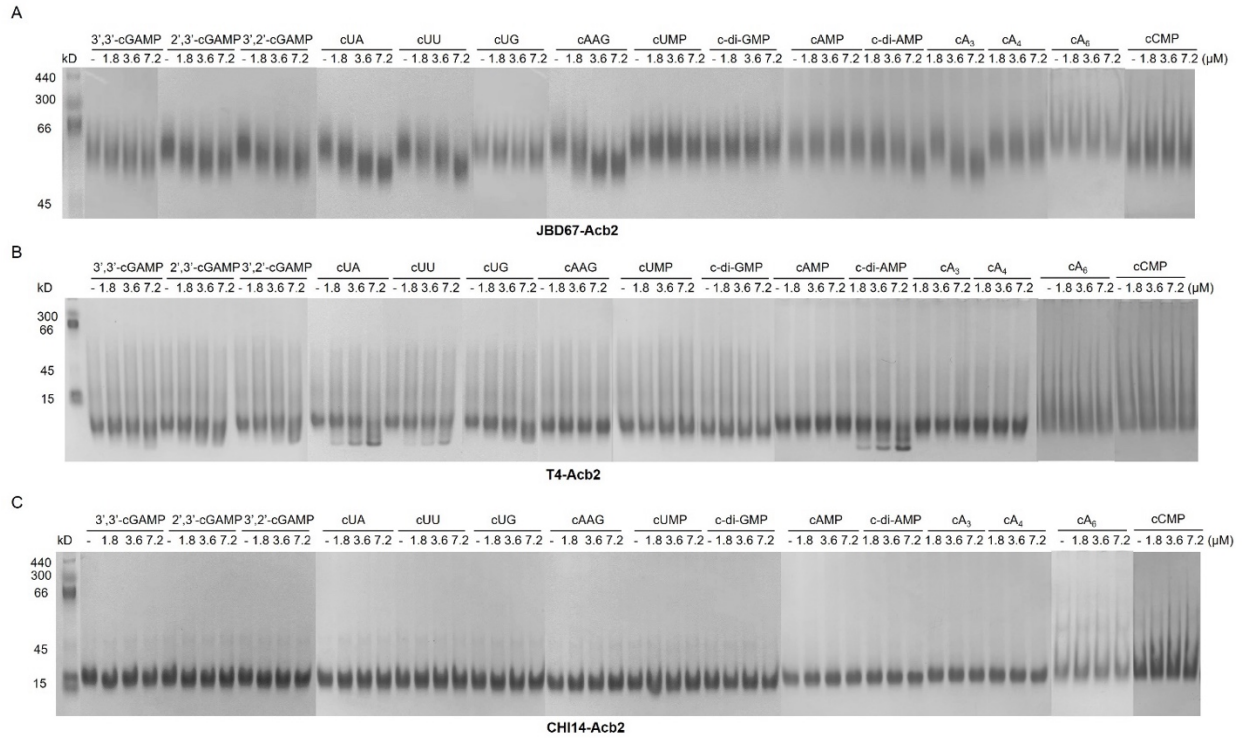


Figure 3.13: The binding spectrums of Acb2 homologs studied by native PAGE
(A-C) Native PAGE assay showed the binding of cyclic nucleotides to JBD67-Acb2, T4-Acb2 and CHI14-Acb2. The proteins were incubated with small molecules at indicated concentrations. Then the samples were subjected to native PAGE. Related to Figure 3.4.

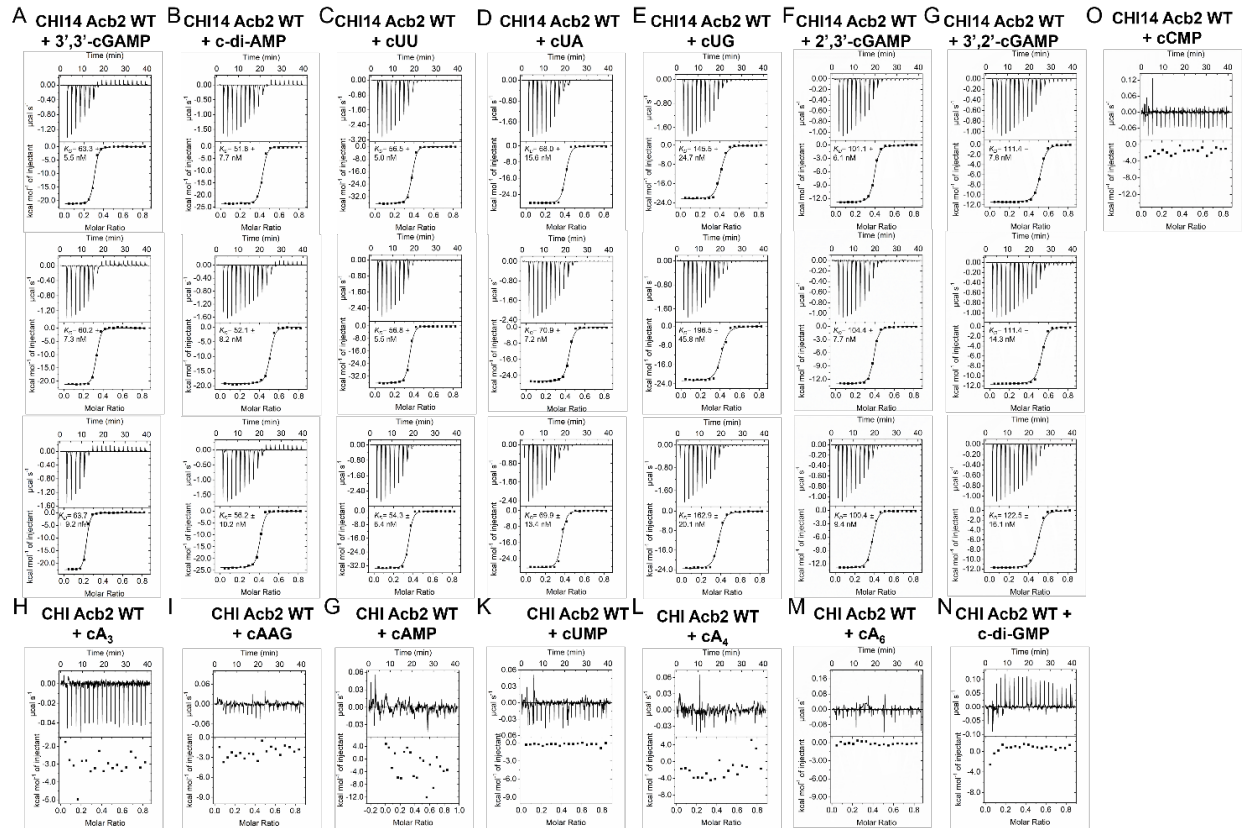


Figure 3.14: The binding spectrum of CHI14-Acb2 studied by ITC assays (A-O) ITC assays to test binding of cyclic nucleotides to CHI14-Acb2. Related to Figure 3.4.

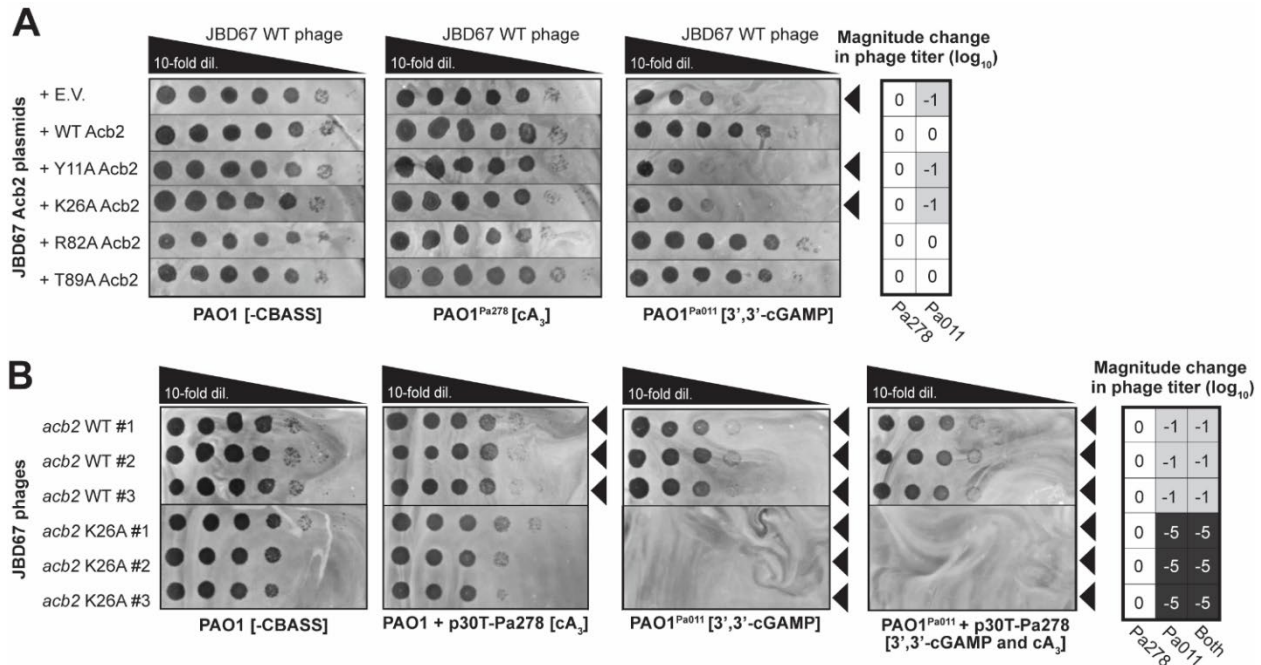


Figure 3.15: Mutations in Acb2 binding residues differentially impacts phage titer

(A) Plaque assays with JBD67 WT phage spotted in 10-fold serial dilutions on PAO1 strains harboring an empty vector (E.V.) plasmid or JBD67 Acb2 variants. The PAO1 strains either contain no CBASS operon (-CBASS), a chromosomally integrated Pa011 CBASS operon (PAO1^{Pa011}), or a chromosomally integrated Pa278 CBASS operon (PAO1^{Pa278}). These plaque assays were used to quantify the order of magnitude change in phage titer by comparing the number of spots (with plaques, or clearings if plaques were not visible) on the PAO1^{Pa011} or PAO1^{Pa278} CBASS-expressing strains divided by the PAO1 (-CBASS) strain (n=3). Basal expression of the Pa011 CBASS operon and 0.3mM IPTG-inducible expression of the Pa278 CBASS operon is sufficient for phage targeting. Black arrowheads highlight significant CBASS-dependent reductions in phage titer. **(B)** Plaque assays with JBD67 phages spotted in 10-fold serial dilutions on PAO1 strains with and without CBASS: PAO1 + p30T-E.V. (-CBASS), PAO1 + p30T-Pa278, PAO1^{Pa011} + p30T-E.V., PAO1^{Pa011} + p30T-278. These plaque assays were used to quantify the order of magnitude change in phage titer (n=3). Basal expression of the Pa278 CBASS operon is sufficient for phage targeting. Black arrowheads highlight significant CBASS-dependent reductions in phage titer. Related to Figure 3.5.

3.9. Tables

Table 3.1: Data collection and refinement statistics

	Acb2-2',3'- cGAMP	Acb2-3',2'- cGAMP	Acb2-cA₃	Acb2- cAAG	Acb2-3',3'- cGAMP- cA₃
PDB code	8J8O	8IXZ	8IY0	8IY1	8IY2
Data collection					
Space group	P321	P321	P321	P321	P321
Cell dimensions					
a, b, c (Å)	106.0 106.0 101.6	104.0 104.0 101.1	103.9 103.9 101.9	103.6 103.6 101.4	103.4 103.4 101.5
α, β, γ (°)	90 90 120	90 90 120	90 90 120	90 90 120	90 90 120
Resolution (Å)	50-2.24 (2.28-2.24)	50-2.32 (2.36-2.32)	50-2.26 (2.30-2.26)	50-2.10 (2.14-2.10)	50-2.76 (2.81-2.76)
Unique reflections	31815 (1484)	27614 (1352)	29547 (1474)	36272 (1648)	16565 (824)
Completeness (%)	99.5 (94.3)	100.0 (100.0)	98.7 (99.1)	98.1 (92.8)	99.7 (100.0)
Rmeas (%)	10.6 (96.7)	8.4 (60.8)	12.3 (103.7)	9.9 (87.9)	13.3 (101.2)
Redundancy	4.8 (3.9)	17.6 (13.1)	4.8 (4.8)	17.6 (13.6)	9.8 (8.9)
//σ(<i>I</i>)	18.2 (1.4)	50.0 (4.8)	18.3 (2.2)	47.9 (4.1)	20.8 (2.5)
Statistics for Refinement					
Rwork (%)	23.8 (32.4)	23.0 (27.3)	21.5 (25.2)	22.1 (24.6)	24.0 (34.8)
Rfree (%)	27.3 (34.6)	27.4 (32.6)	25.8 (35.0)	24.9 (28.8)	28.9 (40.1)
No. atoms	4915	4741	5019	5072	5051
Protein	4416	4396	4440	4440	4396
Ligand/ion	270	270	396	402	628
Solvent	229	75	183	230	27
B factors	51.90	55.65	48.17	45.56	57.43
Protein	52.14	56.07	49.77	47.10	58.87
Ligand/ion	50.60	51.32	33.26	31.55	47.68
Solvent	47.16	47.03	41.65	40.42	49.83
R.m.s.d.					
Bond angles (°)	1.49	2.49	2.37	2.90	2.42
Bond length (Å)	0.013	0.016	0.014	0.029	0.016
Ramachandran Plot (%)					
Favored region	99.07	96.26	97.59	96.67	97.01
Allowed region	0.93	3.74	2.41	3.33	2.99
Outliers	0.00	0.00	0.00	0.00	0.00

Table 3.2: Acb2 homolog protein sequences

Full table online ([doi: 10.1016/j.molcel.2023.11.026](https://doi.org/10.1016/j.molcel.2023.11.026)).

Chapter 4: CBASS protects cells from phage-induced lysis in *Pseudomonas aeruginosa*

4.1. Summary

CBASS immunity can be effectively inhibited or evaded by phage, such phage proteins that disrupt cyclic oligonucleotide signaling or phages that acquire mutations in structural proteins. In response, bacterial hosts may increase cyclase activity to amplify its signals and overcome resistant phage. Here, using an established native model system of Type II-A CBASS in *Pseudomonas aeruginosa*, we demonstrate that overexpressing the synthase (cGAS-like enzyme, CdnA) significantly improves CBASS targeting of sensitive and resistant phage due to >500-fold increases in 3',3'-cGAMP signal production. Furthermore, counter to the established dogma that increasing CBASS manifests as a cell death response, we observe that bacterial hosts harboring endogenous or hyperactive CBASS enables cells to grow better in the presence of phage infection (MOI >1) compared to cells lacking CBASS immunity. This outcome extends to heterologously expressed Type II-A CBASS on a plasmid or in the chromosome of *P. aeruginosa* strain that naturally lacks the system, alongside the addition of exogenous 3',3'-cGAMP signals to bacteria with endogenously expressed CBASS. We also observed that CBASS resistant phages with mutations in their major capsid protein (MCP) can be complemented with expression of the capsid prohead, but not the MCP alone, and enables host cells to re-target phage and grow similarly to those with hyperactive CBASS. While the role of the capsid prohead in CBASS immune activation is still being elucidated, our collective findings demonstrate that increasing CBASS immunity in our native *P. aeruginosa* host enables effective and potent targeting of phages and manifests in a cell survival response.

4.2. Introduction

The diversity of innate immune mechanisms that use synthases and signaling cascades to induce an anti-viral immune response has substantially grown across eukaryotes^{70,124,125} and prokaryotes^{20-22,126,127} over the past decade. Cyclic GMP-AMP synthase (cGAS) is evolutionarily conserved enzyme that can produce one or more unique cyclic oligonucleotides, in which thousands of cGAS-like

homologs have been identified in animals^{70,71,119} and bacteria^{31,88,111,113,128} to produce at least 16 signals. Bacterial cGAS/DncV-like nucleotidyltransferases (CD-NTases) produce signals that activate distinct effector proteins, all of which are proposed to induce a cell death response to limit viral (phage) replication and protect the surrounding community of bacterial cells^{21,24,68,83–85}, collectively referred to as cyclic-oligonucleotide-based anti-phage signaling system (CBASS). Despite the bacteria's effective and potent immune response, phages have evolved an expanding repertoire of anti-immune mechanisms to overcome CBASS. Phages may harbor proteins that degrade cyclic di- or trinucleotides (Acb1)⁴⁸, sequester cyclic di- or trinucleotides (Acb2^{50,51}; Tad1 and Tad2⁵²), produce competing cyclic dinucleotides¹²⁹, or reconstitute host metabolites⁵⁴. Phages may alternatively harbor mutations in their major capsid protein (MCP)^{50,67}, capsid packaging proteins^{67,68}, or tail fiber proteins⁶⁷ to evade CBASS targeting, but the mechanism of evasion has yet to be understood. However, given the rapid pace of the bacteria-phage arms race, we anticipate that bacteria may overcome resistant phage through tuning or increasing CD-NTase activity.

Studying the co-evolution between bacteria and phage within in their native system has already led to critical insights into CD-NTases function. Notably, the study of a native *Vibrio cholerae* strain led to the discovery of the first CD-NTase, known as DncV, that produces 3',3'-cGAMP signaling molecules³². This native model system further revealed that increasing DncV expression impacts cell growth^{32,130} and that DncV and CBASS-dependent changes in cell growth can be modulated with host metabolites^{131–133}. These observations were all shown in the absence of phage infection and may not be directly implicated in CBASS immunity. In our previous study, however, we established a native model system of Type II-A CBASS in *Pseudomonas aeruginosa* that is homologous to the *V. cholerae* system, including a CD-NTase producing 3',3'-cGAMP (CdnA) that signals to and activates a phospholipase effector protein (CapV), and potentially targets the dsDNA lytic phage PaMx41 >10,000-fold⁵⁰. This led us to discover phages that evolved to overcome CBASS through the acquisition of a potent inhibitor (Acb2)^{50,51} or the acquisition of mutations in the major capsid protein (MCP)⁵⁰.

Here, we continue using our native Type II-A CBASS model system and observed that the bacterial host can overcome phage-encoded *acb2*, as well as mutant *mcp*, upon increasing CdnA expression and resultant 3',3'-cGAMP signals by >500-fold. Surprisingly, counter to the established dogma the CBASS results in a cell death response, bacteria expressing endogenous and overexpressed CdnA enables cells to grow substantially better in the presence of phage infection (MOI >1) compared to cells lacking functional CBASS. These observations extend to heterologous expressed Type II-A CBASS, in which the full operon is expressed on a plasmid or integrated within the chromosome of another *P. aeruginosa* strain that naturally lacks the system. We also observed that the addition of exogenous 3',3'-cGAMP to the media of our bacteria with endogenous expression of CBASS rescued anti-phage activity and cell growth. Furthermore, returning to our resistant phage with *mcp* mutations, we observed that overexpressing the entire capsid prohead increased anti-phage activity and cell growth akin to our observations with increased expression of CdnA or the full CBASS operon. Although we are still elucidating the role of the phage capsid prohead in CBASS activation, our native model system in *P. aeruginosa* demonstrates that increasing CBASS immunity enables the host to overcome resistant phages and manifests as cell survival, presenting a significant shift in the field's current understanding of CBASS.

4.3. Results

4.3.1. Increasing CdnA activity overcomes CBASS resistant phage

Our previously established native model system of Type II-A CBASS in the *Pseudomonas aeruginosa* strain BWHPA011 (Pa011) targeted a single dsDNA lytic phage, PaMx41, that acquired both an inhibitor (*Acb2*) or major capsid protein (MCP) mutations to effectively evade CBASS targeting⁵⁰. To determine whether bacterial hosts harboring CBASS can overcome these resistant phages, we used the native Pa011 host and initially overexpressed the most upstream step in the system – the CdnA synthase that produces 3',3'-cGAMP signaling molecules (Figure 4.1A-B). Upon overexpression of CdnA in the Pa011 WT strain, both sensitive ($\Delta*acb2*$) and resistant PaMx41 phages (*+acb2* or *+mcp* mutant) were targeted over two orders of magnitude (Figure 4.1C, 4.6B). In the Pa011 strain with a

catalytically dead CdnA or Cap3, overexpressing CdnA rescued CBASS anti-phage activity and PaMx41 phage titer was reduced by two to five orders of magnitude (Figure 4.1C, 4.6B). We previously demonstrated that Cap3, a JAB-like protease, is not required for CBASS⁵⁰, but is involved in regulating CdnA activity^{53,87}. By comparison, in the Pa011 strain with catalytically dead Cap2, overexpressing CdnA partially rescued CBASS anti-phage activity (Figure 4.1C, 4.6B). This data aligns with recent studies demonstrating that Cap2, a E1/E2-like ligase, conjugates host factors onto CdnA (or CdnA onto itself) to 'prime' or enhance CdnA activation and then Cap3 can remove these conjugates to reduce CdnA activity^{53,87,134}. Lastly, in the Pa011 strain without the CBASS operon or a catalytically dead CapV effector, PaMx41 phages replicated normally in the presence of CdnA, demonstrating that increasing CdnA activity is specific to CBASS and CapV effector activity.

To validate whether the Pa011 strains overexpressing CdnA harbored an active enzyme, intracellular 3',3'-cGAMP levels were measured in cells following PaMx41 Δ acb2 phage infection. In the cells overexpressing CdnA, ~6.5 μ M of 3',3'-cGAMP was detected compared to ~0.013 μ M of 3',3'-cGAMP in cells with endogenous levels of CdnA (Figure 4.1D). These data demonstrate that overexpressing CdnA results in over 500-fold increase in 3',3'-cGAMP levels in the presence and absence of phage, suggesting that CdnA can be constitutively active at high levels and more effectively overcome resistant phage. Furthermore, based on these 3',3'-cGAMP concentrations, we can estimate the total number of 3',3'-cGAMP molecules per *P. aeruginosa* cell as well as the total number of Acb2 proteins necessary to sequester all intracellular 3',3'-cGAMP and enable phage survival.

$$\text{Equation 1: Volume of rod-shaped bacterial cell (cylinder)} = \pi * \text{radius}^2 * \text{length}$$

$$\text{Equation 2: Total number of cGAMP molecules} = \text{Concentration of cGAMP (mol/L)} * \text{Volume of cell (L)} * N_A$$

$$N_A = \text{Avogadro's number, } 6.022 * 10^{23} \text{ molecules/mol}$$

Given the average size of a *P. aeruginosa* cell (0.5-0.8 μ m wide and 1.5-3.0 μ m long¹³⁵; Equation 1), a hyperactive Pa011 cell may produce ~571 to 4,675 total 3',3'-cGAMP molecules whereas an

endogenously active Pa011 cell may produce ~1 to 9 total 3',3'-cGAMP molecules per cell (Equation 2). In turn, based on the stoichiometry of two Acb2 proteins binding one 3',3'-cGAMP molecule⁵⁰, phage need to produce ~1,141 to 9,350 Acb2 proteins to survive in a hyperactive Pa011 cell, but only need to produce ~2 to 18 Acb2 proteins to survive in an endogenously active Pa011 cell. While the total amount of intracellular 3',3'-ccGAMP and Acb2 is likely underestimated compared to the actual quantities inside a *P. aeruginosa* cell, they highlight the vastly different requirements phages must meet to resist CBASS immunity in each Pa011 host.

Lastly, to further demonstrate CdnA hyperactivity, immunoblotting was performed to analyze the presence of conjugated proteins, which again primes or enhances CdnA enzymatic activity^{53,87}. In Pa011 WT strain overexpressing CdnA, a strong band representing CdnA (42 kDa) was observed alongside 'laddering' of additional proteins representing CdnA conjugates (Figure 4.1E). Of the three unique bands found in CdnA overexpression strain, they may represent CdnA multimers, but co-IP/MS will be required to test this model. However, in cells with endogenous CdnA levels or lacking CdnA altogether, no band the size of CdnA was observed and further demonstrates the low levels of CdnA and 3',3'-cGAMP in the native Pa011 host. Altogether, these results show that increasing CdnA activity can effectively overcome CBASS resistant phage.

4.3.2. Increasing CBASS improves cell growth upon phage infection

The current model of CBASS immunity depends on a cell death response to stop phage infection and protect surrounding bacterial cells. To date, all studies heterologously express diverse CBASS operons on a plasmid within well-characterized *Escherichia coli* strains that naturally lack CBASS^{21,24,67,83,85,113}. Therefore, to determine whether cell death occurs in the context of a native bacteria-phage interactions, we studied the bacterial cell response in the endogenously active and hyperactive Type II-A CBASS in *P. aeruginosa* over the course of PaMx41 Δ acb2 phage infection. Surprisingly, in the hyperactive Pa011 WT strain overexpressing CdnA, cells grow remarkably well in the presence of low to high multiplicities of infection (MOIs 0.2-20) similarly to uninfected cells (Figure

4.2A). This improvement in cell growth was also observed in the Pa011 strains with catalytically dead CdnA, Cap2, and Cap3 (Figure 4.7), indicating that increasing CdnA expression can overcome deficits in CdnA activation and improve cell growth. By comparison, in the endogenously active Pa011 WT strain, cells grow more slowly and eventually plateaued (Figure 4.2A) whereas the Pa011 strains without the CBASS operon or a catalytically dead CapV effector exhibited MOI-dependent cell death (Figure 4.2A, 4.7).

To further investigate whether overexpressing CdnA may reach a point that is toxic to cells, arabinose was titrated into the media then cells were infected with PaMx41 Δ *acb2* phage. Cells grown in 0.05% arabinose, which is predicted to increase gene expression ~50-fold⁹⁸, results in improved cell growth and anti-phage activity (Figure 4.8). In cells grown in 0.1% arabinose, which is predicted to increase gene expression ~250-fold⁹⁸, results in a slight growth defect compared to cells with lower arabinose induction or cells without overexpressing CdnA, but potent anti-phage activity remains (Figure 4.8). However, cell growth in 0.3% arabinose resulted in a significant growth defect albeit a potent anti-phage response (Figure 4.8). Based on these results, we continued to study the Type II-A CBASS response with low arabinose induction because it provides strong anti-phage defense without incurring cellular toxicity and is therefore a useful model system to assess the cellular outcome of CBASS activity.

To determine whether increased cell growth is due to viable cells effectively stopping phage infection, we initially measured bacterial cell viability and phage titer over several hours using an intermediate MOI of 2 to ensure that all bacterial cells would be infected with one or more phage. In both the endogenously active and hyperactive Pa011 CBASS strains, the bacterial cell count remained stable at $\sim 10^8$ CFU/ml and then slowly increased to $\sim 10^9$ CFU/ml or $\sim 10^{10}$ at eight hours post infection for the endogenously active or hyperactive strains, respectively (Figure 4.2B). While the starting bacterial cell count was the same for Pa011 Δ CBASS strain, the cell counts eventually crashed to $\sim 10^5$ CFU/ml (Figure 4.2B), demonstrating the PaMx41 phage can slowly albeit effectively lyse these cells over

three orders of magnitude in the absence of CBASS. Furthermore, the endogenously active Pa011 strain reduced PaMx41 Δ *acb2* phage titer over two orders of magnitude whereas the hyperactive strain reduced PaMx41 Δ *acb2* phage titer over three orders of magnitude compared to the Pa011 Δ CBASS strain (Figure 4.2.C), validating the CBASS immunity is active and effectively targeting phage.

To further study the viability of single bacterial cells, we used flow cytometric analysis to measure propidium iodide fluorescence over the course of PaMx41 Δ *acb2* phage infection. Propidium iodide (PI) is a membrane impermeable dye that enters cells with porous or damaged cells and then binds to DNA and release red fluorescence, and therefore selectively dyes dead cells. In contrast, intact cells do not uptake PI dye and metabolically active cells with minor membrane damage are predicted to pump out the dye and retain low levels of PI/red fluorescence. In both the endogenously active and hyperactive Pa011 strains, <6% of PI/red fluorescence was detected over the course of phage infection compared to heat-killed control cells that effectively uptake and retain the PI dye (Figure 4.2E). Taken together, these collective results demonstrate that Type II-A CBASS can effectively stop PaMx41 phage infection while protecting cells from phage-induced lysis in a manner that does not compromise the overall cell viability.

4.3.3. Distinct CBASS model systems improve cell growth

To determine whether heterologous expression of CBASS operons that are naturally found in *P. aeruginosa* clinical isolates function similarly to a native model system, we established chromosomal and plasmid-based expression systems of Pa011 Type II-A and Pa278 Type III-C CBASS operons in the well-studied *P. aeruginosa* strain PAO1 that naturally lacks both systems (Figure 4.3A). Given the broader phage sensitivity of PAO1, we were able to test additional phages with and without known CBASS inhibitors, such as the dsDNA temperate phage JBD67 with and without *acb2*^{50,51}, the dsDNA lytic jumbophage PhiKZ with *tad1*⁵², and the dsDNA temperate phage D3 without any known CBASS inhibitors. In agreement with our previous studies, the PAO1^{Pa011} and PAO1^{Pa278} chromosomal strains differentially target JBD67 and D3 phages, but cannot target the highly resistant jumbophage PhiKZ,

compared to the PAO1^{EV} control strain (Figure 4.3B). In the strains expressing Pa011 and Pa278 on a plasmid, the titer of JBD67 and D3 phages is reduced an additional one to three orders of magnitude (Figure 4.3B). D3 phage continues to remain resistant to Pa278 Type III-C CBASS, suggesting it harbors a potent inhibitor of the system or lacks the activating cue. In these same strains, however, the titer of PhiKZ is effectively reduced by five orders of magnitude (Figure 4.3B). This data demonstrates that CBASS may overcome and potentially target PhiKZ upon overexpression of the full CBASS operon. Similar data was also reported in study that systematically expressed diverse *P. aeruginosa* anti-phage systems on a plasmid within a PAO1 host¹³⁶, whereby their Type III-C CBASS host reduced the titer of a PhiKZ-like phage by five orders of magnitude similarly to our observations (98-100% a.a. identity, 100% coverage with our operon). However, their Type II-A CBASS host (78-89% a.a. identity, 97-100% coverage with our operon) did not reduce the titer of their PhiKZ-like phage, highlighting the nuances of bacteria-phage interactions in heterologous expression systems.

We next chose to examine cell growth in the Pa011 Type II-A and Pa278 Type III-C CBASS heterologous systems over the course of JBD67 Δ *acb2* phage infection. In both strains, cells grew remarkably well in the presence of low to high multiplicities of infection (MOIs 0.2-20) similarly to the uninfected cells (Figure 4.3C). However, there was a slight growth defect in the chromosomally integrated Pa011 strain (PAO1^{Pa011}) at the highest MOI, which is likely due to the lower levels of CBASS operon expression relative to expressing the full operon on a plasmid. By contrast, the strain lacking the Pa011 Type II-A CBASS operon eventually crashed at all MOIs (Figure 4.3C). These results further validate that increasing Type II-A CBASS immunity protects cells rather than result in cell death²¹. In comparison to the Pa278 strains, cells grew well at low to intermediate MOIs (0.2-2), but a growth defect was observed at the highest MOI of 20, likely due to phage replication (Figure 4.3C). These collective findings demonstrate that both native and heterologous CBASS model systems infected by either lytic or temperate phages have the potential to elicit a cell growth phenotype, thereby protecting cells from phage-induced lysis.

4.3.4. Exogenous cGAMP improves CBASS-dependent cell growth

As a final measure to demonstrate that increasing CBASS immunity can improve cell growth in the presence of phage infection, we recapitulated the hyperactive Pa011 Type II-A CBASS strain with the addition of exogenous 3',3'-cGAMP signals comparable to increasing intracellular CdnA and 3',3'-cGAMP levels (Figure 4.4A). To do so, 3',3'-cGAMP was titrated into the media and then cells were infected with an intermediate MOI of PaMx41 Δ acb2 phage. Addition of <10 μ g/ml of exogenous 3',3'-cGAMP did not change cell growth during phage infection (Figure 4.4B). Excitingly, addition of 20 to 100 μ g/ml of exogenous 3',3'-cGAMP rescued cell growth in the catalytically dead CdnA, Cap2, and Cap3 strains during phage infection (Figure 4.9C), which was also observed in these cells when overexpressing the active CdnA enzyme (Figure 4.7). Addition of 50 to 100 μ g/ml of exogenous 3',3'-cGAMP slightly improved cell growth in the Pa011 WT strain during phage infection (Figure 4.9C). By contrast, addition of any amount of exogenous 3',3'-cGAMP to the Pa011 strains without the CBASS operon or a catalytically dead CapV effector did not improve cell growth (Figure 4.9C), indicating that exogenous 3',3'-cGAMP specifically improves CBASS activity and dependent on the CapV effector. Importantly, despite the significant activity of exogenous 3',3'-cGAMP, the addition of this molecule to uninfected cells did not result in a growth defect and demonstrates that high 3',3'-cGAMP levels are safe for cells. This is the second instance demonstrating that a bacterial CBASS host can respond to exogenous cGAMP signals in a manner dependent on its effector protein, specifically \sim 72 μ g/ml of 3',2'-cGAMP molecules activates a Cap5 endonuclease effector¹³⁷. However, to put these cGAMP levels into context, the Pa011 strain overexpressing CdnA contains \sim 4 μ g/ml of intracellular 3',3'-cGAMP whereas the Pa011 strain with endogenous levels of CdnA contains \sim 1*10⁻³ μ g/ml of intracellular 3',3'-cGAMP (Figure 4.1D). Although the native Pa011 host harbors exceedingly low levels of 3',3'-cGAMP, it is still possible that the 3',3'-cGAMP molecules signal to adjacent cells and 'prime' or enhance CBASS immunity in a way that is not observable with OD₆₀₀ measurements and therefore requires additional experiments to critically examine CBASS-dependent activity. That withstanding, the critical observation here is that high levels of 3',3'-cGAMP – whether they are

obtained through overexpression of CdnA or addition of exogenous molecules – improves cell growth and anti-phage activity.

In eukaryotes, the cGAS-STING signaling system harbors several proteins known to transport cGAMP between cells and degrade extracellular cGAMP molecules¹³⁸. Given the evolutionary conservation between eukaryotic and bacterial cGAS-based immune systems, the presence of these cGAMP transporters or degraders may suggest that the bacterial system may participate in intercellular cGAMP signaling. Performing a structural-based homology search with known eukaryotic cGAMP transporters – SLC191A, SCL46A, LRRC8, and P2X7R – revealed over 700 SLC191A and SCL46A candidates in bacteria and over 80 of those hits in *P. aeruginosa*. By contrast, there were seven poor candidates for LRRC8 and P2X7R transporters. Upon closer examination of the top candidates of *P. aeruginosa* cGAMP transporters, we found that they belong to the Major Facilitator Superfamily (MFS) (Figure 4.4C), which is conserved across all domains of life and belongs to one of the largest families of membrane transport proteins¹³⁹. Additionally, performing a structural-based homology search with the eukaryotic extracellular cGAMP hydrolase – ENPP1 – revealed over 100 candidates in bacteria and over 12 candidates in *P. aeruginosa* that are all described as uncharacterized protein. That withstanding, a previous study examining eukaryotic ENPP1 tested the function of a bacterial version encoded in *Xanthomonas axonopodis* pv. *cititri* and found that it retains the catalytic active site and enzymatic function¹⁴⁰. The *P. aeruginosa* candidate also retains the active site residue (Figure 4.4C), providing additional evidence that it may be an active enzyme. These data collectively suggest that 3',3'-cGAMP molecules may signal to nearby cells to amplify CBASS immunity.

4.3.5. Phage capsid proheads are induce CBASS activity

To further investigate the evasion mechanism of phages harboring mutations in their major capsid protein (MCP), we systemically expressed combinations of the PaMx41 phage structural proteins within the native Pa011 Type II-A CBASS host. To start, we examined the known PaMx41 morphogenesis and structural gene locus⁹³ and further identified a putative scaffold protein (personal

communication with Alan Davidson; Figure 4.5). Based on the well-studied mechanism of T4 capsid assembly¹⁴¹, we could propose a model for PaMx41 capsid assembly (Figure 4.5B). Furthermore, in our previous study⁵⁰, we identified that the CBASS escape mutations aligned to the protein-protein interface of the MCP capsomer (Figure 4.5C) – the basic hexameric unit of MCPs that come together to form the capsid prohead¹⁴¹. We subsequently constructed plasmids with different combinations of proteins involved in PaMx41 capsid assembly (Figure 4.5D).

In the presence of our minimal capsid prohead construct (portal, scaffold, and major capsid protein), but not the MCP alone⁵⁰, resulted in a significant increase in CBASS-dependent anti-phage activity against the WT and MCP mutant escape phages by four orders of magnitude (Figure 4.5E). However, expressing a prohead with a MCP mutation largely abolishes this complementation activity (Figure 4.10A). Expressing the MCP or prohead construct results in comparable levels of MCP proteins, as revealed by immunoblotting (Figure 4.10B), suggesting that the WT prohead assembly complements the mutant phage and potentially simulates CBASS activity (Figure 4.10A). In the Pa011 Δ CBASS strain, overexpressing the WT capsid prohead does not induce cell toxicity nor impact phage replication (Figure 4.10A). In the Pa011 strains with catalytically dead CdnA, CapV, and Cap2, this effect is partially abolished and phage titer improves by one order of magnitude (Figure 4.10C), suggesting that CBASS enzymatic activities are not essential for this phenotype and requires additional follow-up experiments to mutate or delete other domains of the CBASS genes. Interestingly, when the MCP mutations are combined (e.g. I121T capsid prohead construct and S330P MCP phage and vice versa), we observed a 10-fold decrease in phage titer in a CBASS-independent manner, suggesting that these MCP mutations within the same capsid are not fit. In all Pa011 prohead overexpression strains, however, the PaMx41 phage encoding *acb2* remained highly resistant to CBASS (Figure 4.5E, 4.10A and C), further highlighting the strong inhibitory function of Acb2.

To determine whether the capsid prohead is involved in CBASS activation or CBASS targeting, we initially attempted to measure intracellular 3',3'-cGAMP levels in our Pa011 Type II-A CBASS model

systems infected with WT and mutant MCP phages. However, a recent study reported that mutations in phage structural proteins can drastically alter phage infection kinetics within the presence of CBASS⁶⁷. In turn, any measurements of intracellular 3',3'-cGAMP must take into consideration the different lengths of time for WT and mutant MCP phage to complete their replication cycle. Therefore, to characterize phages infection kinetics, we performed a single-step growth curve experiment and our preliminary results suggest that mutant MCP slows down phage replication compared to the WT MCP (Figure 4.10D). That withstanding, the final number of mutant MCP phage particles collected from Pa011 WT and Δ CBASS cells were similar, whereas the final number of WT MCP phage particles from Pa011 WT cells was reduced by one order of magnitude compared to the Pa011 Δ CBASS cells (Figure 4.10D). Future experiments are needed to validate these results and then apply this information to quantify 3',3'-cGAMP.

In parallel, given that hyperactive Pa011 CBASS increases cell growth, we measured cell growth during phage infection, we measured cell growth in the native Pa011 strain overexpressing the WT capsid prohead over the course of PaMx41 Δ acb2 phage infection. Our preliminary results show that the Pa011 WT strain overexpressing WT capsid prohead grows significantly better in the presence of low to high MOIs compared to the Pa011 WT and Δ CBASS control strains (Figure 4.5F). By comparison, in the Pa011 catalytically dead CdnA and CapV strains, overexpressing the WT capsid prohead still appears to improve cell growth albeit less significantly than the fully functional Pa011 WT strain (Figure 4.11). While there is evidence that the capsid prohead is involved in CBASS activity, we are still exploring whether the capsid prohead interacts with or enhances CBASS function in a way that is not dependent on enzymatic activity.

4.4. Discussion

Establishing a native model system of Type II-A CBASS in *P. aeruginosa* has uncovered critical insights into how CBASS co-evolves and responds to phage infection. This type of CBASS type depends on a CdnA synthase to produce 3',3'-cGAMP signaling molecules that activate a

phospholipase CapV effector and stops phage infection^{21,50}. We initially discovered that phages overcome CBASS through acquisition of Acb2, a potent inhibitor of CBASS that sequesters a broad spectrum of cyclic di- and trinucleotide signaling molecules^{50,51}, and then further evade CBASS immunity through acquisition of mutations in their major capsid protein⁵⁰. Using this native Pa011 Type II-A CBASS host, we found that overexpressing CdnA vastly increases the production of 3',3'-cGAMP molecules >500-fold compared to endogenously active CdnA (~6.5 and 0.013 μM). These data align with previous studies overexpressing the DncV synthase or the full Type II-A CBASS operon, measuring ~1.2 and 1.6 μM of intracellular 3',3'-cGAMP^{21,130}, respectively. Moreover, the hyperactive Pa011 host also increases CBASS anti-phage activity, reducing the titer of CBASS resistant phages by over three orders of magnitude. For the resistant phages naturally expressing Acb2, these findings demonstrate that CBASS can effectively overwhelm Acb2 and that its inhibitory 'sponging' mechanism can fail. This failure is likely due to the limited stoichiometry of Acb2, wherein the excess 3',3'-cGAMP molecules bind to and activate CapV. A previous study of Type II-A CBASS in *Vibrio cholerae* host discovered that the activated CapV protein degrades phosphatidylethanolamine (PE) and phosphatidylglycerol (PG), the major phospholipids in the *V. cholerae* cell membrane, and then releases free fatty acids¹³⁰, suggesting that CapV remodels the cell membrane to adapt towards different environmental stresses.

To date, all studies conclude that CBASS functions through an abortive infection mechanism, in which the effector proteins target host^{21,24,83,113} and/or phage^{85,88} components to induce cell death upon phage infection and subsequently protect the surrounding cells from phage¹⁴². For Type II-A CBASS, studying the system in its native *V. cholerae* host demonstrated that overexpressing the DncV synthase reduces cell growth and leads to abnormal cell morphology and small colony formation^{32,130}. Heterologous expression of the full Type II-A CBASS operon in an *E. coli* host demonstrated that cell growth is rapidly reduced upon phage infection at high MOI (2) relative to cells lacking CBASS²¹. Furthermore, the study used the dsDNA temperate P1 phage, which typically completes its lytic replication cycle in 60 minutes, and observed CapV-dependent cell membrane abnormalities as early

as 40 minutes post-infection and then cell lysis²¹. Surprisingly, the hyperactive and endogenously active Type II-A CBASS in *P. aeruginosa* demonstrated CapV-dependent cell survival following phage infection at increasingly high MOIs (2-20). We also observed this cell growth phenotype upon heterologous expression of the full Type II-A CBASS operon in *P. aeruginosa*, and excitingly, upon the addition of exogenous 3',3'-cGAMP molecules cells grew in a CapV-dependent manner. These collective Pa011 Type II-A CBASS model systems demonstrate that CBASS can protect cells from phage-induced lysis. As such, our leading model of Type II-A CBASS in *P. aeruginosa* is that the CapV effector remodels the cell membrane to prevent late-stage phage maturation and lysis and therefore enables cells to continue growing in the presence of phage infection (Figure 4.1B). Altogether, these finding presents a significant shift in the field's current understanding of CBASS, indicating that CBASS anti-phage activity induces cell death or cell growth responses.

Phages have co-evolved to evade CBASS immunity through acquisition of inhibitors alongside mutating structural proteins involved in capsid assembly^{50,67,68}, suggesting that the capsid plays a critical role in CBASS activity. Using the native and heterologous Pa011 Type II-A CBASS hosts, we observed that distinct phages gain mutations in the major capsid protein (MCP) that localize the protein-protein interface of maturing capsids. Based on previous studies¹⁴¹, it is known that the phage scaffold, portal, and major capsid proteins assemble into a prohead and then recruit additional structural proteins to build the mature capsid. We found that overexpressing the phage capsid prohead, but not the MCP alone, increases CBASS anti-phage activity and cell growth following phage infection. Further, our preliminary results demonstrate that phage harboring the MCP mutations replicate more slowly compared to phage with WT MCP. Studies of heterologously expressed Type I-A and Type I-B CBASS in *E. coli* also identified CBASS escape phage with mutations in their MCP and observed that these mutant MCP phage lysed cultures ~60 minutes slower compared to the WT MCP phage⁶⁷, demonstrating a delay in phage infection kinetics. Despite these collective findings, it remains unclear whether the phage capsid activates CBASS or evades the CBASS effector. In future work, we will test two models of Type II-A CBASS activation include: (i) CBASS directly detects the

capsid prohead structure or assembly, and/or (ii) CBASS detects the changes in host metabolism that is a byproduct of structural protein production or DNA replication. It is possible that two distinct activators are needed to turn on CBASS because no single phage activator has been sufficient to activate CBASS *in vivo*. However, we cannot rule out that Type II-A CBASS may target the phage capsid prohead or assembly because the CapV effector functions at the cell membrane and late-stage phage maturation and lysis also occur at the membrane. Taken together, this study establishes an entirely new CBASS immune response depends on cell survival and highlights importance of studying bacteria-phage interactions in native model systems.

4.5. Author Contributions

Erin Huiting (EH) and Joseph Bondy-Denomy conceived the project and designed experiments. EH performed all *in vivo* experiments and wrote the manuscript. Ying Yang assisted with western blot experiments, and Wearn-Xin Yee assisted with flow cytometry experiments.

4.6. Materials and Methods

Bacterial strains and phages

The *P. aeruginosa* strains (BWHPSA011 and PAO1) and *E. coli* strains (DH5 α and SM10) were grown in Lysogeny broth (LB) medium at 37°C both with aeration at 175 r.p.m. Plating was performed on LB solid agar with 10 mM MgSO₄ when performing phage infections, and when indicated, gentamicin (50 μ g/ml or *P. aeruginosa* and 15 μ g/ml for *E. coli*) was used to maintain the pHERD30T plasmid. Gene expression of pHERD30T constructs was induced by the addition of L-arabinose, and gene expression of chromosomal insertions was induced by isopropyl- β -D-thiogalactopyranoside (IPTG). Final concentrations are indicated in methods and figure legends.

Episomal gene expression

The shuttle vector that replicates in *P. aeruginosa* and *E. coli*, pHERD30T⁹⁸ was used for cloning and episomal expression of genes in *P. aeruginosa* BWHPSA011 (Pa011) or ATCC 27853 (Pa278). Pa011

CdnA (NCBI ID: Q024_03601), Pa011 Type II-A CBASS operon (CapV, CdnA, Cap2, Cap3), and Pa278 Type III-C CBASS operon (TRIP13, CdnD, NucC, HORMA3, HORMA2) were cloned with ~50bp upstream. The PaMx41 capsid constructs were cloned directly downstream of the promoter. A final arabinose concentration of 0.05% or 0.1% was used to induce expression of each construct. This vector has an arabinose-inducible promoter and a selectable gentamicin marker. Vector was digested with SacI and PstI restriction enzymes unless stated otherwise and then purified. Inserts were amplified by PCR using bacterial overnight culture or phage lysate as the DNA template, and joined into the pHERD30T vector at the SacI-PstI restriction enzyme cut sites by Hi-Fi DNA Gibson Assembly (NEB) following the manufacturer's protocol. The resulting plasmids were transformed into *E. coli* DH5 α . All plasmid constructs were verified by sequencing using primers that annealed to sites outside the multiple cloning site. *P. aeruginosa* cells were transformed with the pHERD30T constructs using electroporation or conjugation via SM10 *E. coli* cells.

Chromosomal CBASS integration

For chromosomal insertion of the Pa011 CBASS operon, the integrating vector pUC18-mini-Tn7T-LAC⁹⁹ and the transposase expressing helper plasmid pTNS3¹⁰⁰ were used to insert the Pa011 Type II-A CBASS operon or Pa278 Type III-C CBASS operon at the Tn7 locus in *P. aeruginosa* PAO1 strain (PAO1^{Pa011} or PAO1^{Pa278}). The Pa011 operon was cloned with ~250bp upstream and the Pa278 operon was cloned with ~50bp upstream, and 0 mM IPTG and 0.3 mM IPTG was necessary to induce expression of each respective operon. The pUC18-mini-Tn7T-LAC empty vector (E.V.) served as the control strain (Pa^{EV}). The vector was linearized using around-the-world PCR, treated with DpnI, and then purified. Two overlapping inserts encompassing the CBASS operon were amplified by PCR using Pa011 overnight culture as the DNA template, and joined into the pUC18-mini-Tn7T-LAC vector at the SacI-PstI restriction enzyme cut sites by Hi-Fi DNA Gibson Assembly (NEB) following the manufacturer's protocol. The resulting plasmids were used to transform *E. coli* DH5 α . All plasmid constructs were verified by sequencing using primers that annealed to sites outside the multiple cloning site. *P. aeruginosa* PAO1 cells were electroporated with pUC18-mini-Tn7T-LAC and pTNS3

and selected for on gentamicin. Potential integrants were screened by colony PCR with primers PTn7R and PglmS-down, and then verified by sequencing using primers that anneal to sites outside the attTn7 site. Electrocompetent cell preparations, transformations, integrations, selections, plasmid curing, and FLP-recombinase-mediated marker excision with pFLP were performed as described previously⁹⁹.

Phage growth

All phages were grown at 37°C with solid LB agar plates containing 20 ml of bottom agar containing 10 mM MgSO₄ and antibiotics or inducers, as appropriate. Phages were grown on a permissible *P. aeruginosa* host, such as Pa011 ΔCBASS or PAO1 WT, which lack CBASS. Whole plate infections were performed with 150 μl of overnight cultures infected with 10 μl of low titer phage lysate (>10⁴⁻⁷ pfu/ml), and then mixed with 3 ml of 0.7% top agar 10 mM MgSO₄ for plating on the LB solid agar. After incubating 37°C overnight, SM buffer was added until the solid agar lawn was completely covered and then incubated for 5-10 minutes at room temperature. The whole cell lysate was collected and a 1% volume of chloroform was added, and then left to shake gently on an orbital shaker at room temperature for 15 min followed by centrifugation at maximum g for 1 min to remove cell debris. The supernatant phage lysate was stored at 4°C for downstream assays.

Plaque assays

Plaque assays were conducted at 37°C with solid LB agar plates. 150 μl of overnight bacterial culture was mixed with top agar and plated. Phage lysates were diluted 10-fold in SM buffer and then 1.5 μl spots were applied to the top agar after it had been poured and solidified.

Intracellular 3',3'-cGAMP measurements

Cell lysates were prepared similarly to previous methods^{21,50}, in which *P. aeruginosa* BWHPA011 (Pa011) cells harboring a catalytically dead *capV* gene (CapV^{S48A}) were used and then transformed with a pHERD30T vector expressing Pa011 CdnA or an empty vector (EV) control. Cells were taken

from overnight culture, diluted 1:100 in 150ml LB medium with 10 mM MgSO₄ added, Gentamycin (50 µg/ml), and Arabinose (0.1%) in a 500ml flask, and then grown at 37°C (175 r.p.m.) until reaching an OD_{600nm} of ~0.3. From the culture, 50ml of cells were kept uninfected and 50ml of cells were then infected with PaMx41Δ*acb2* to obtain an MOI of ~5 and ensure at least one or more phages were infecting each bacterial cell. After 60 minutes following infection, the culture was centrifuged at 7,500 g for 10 mins at 4°C. Following centrifugation, supernatant was removed and pellets were kept on ice until resuspended in 600 µl of phosphate buffer (50 mM sodium phosphate (pH 7.4), 300 mM NaCl, 10% (v/v) glycerol). The resuspended pellet was supplemented with 1 µl hen-lysozyme (Sigma-Aldrich), vortexed briefly, and incubated at 25°C for 10 min. The resuspended cells were then mixed with Lysing Matrix B (MP) beads and cells were disrupted mechanically using Mini-Beadbeater 16 Biospec Products (1 cycle of 2:30, 3,450 oscillations/m, at 4 °C). Cell lysates were then centrifuged at 16,000 g for 10 min at 4°C. For each condition, the supernatant was loaded onto a 3kDa filter (Amicon Ultra-0.5 centrifugal filter unit; Merk) and then centrifuged at 16,000 g for 45 min at 4 °C. The flow-through (containing small molecules less than 3kDa) was used as the sample for 3',3'-cGAMP measurements, and each sample was run in technical triplicate on a 3',3'-cGAMP ELISA Kit (Arbor Assays) and standards were prepared in the same phosphate buffer. 3',3'-cGAMP concentrations were calculated using a sigmoidal standard curve via GraphPad Prism (v 9.4.1).

Western blot

For protein expression, 10 mL cultures of cells were grown in LB with Gentamycin (50 µg/ml) and Arabinose (0.1%) at 37 °C shaking at 175 r.p.m. When the cultures reached OD₆₀₀ of ~0.6, cells were centrifuged at 9,000 g and resuspended in 500 µl lysis buffer (25 mM Tris-HCl pH 8.0, 150 mM NaCl, 10 mM imidazole, 0.5 mM TCEP, protease inhibitor). Lysis was performed by sonication at 20% amplitude for 10 s, four times. Insoluble material was removed from the lysate by centrifugation at 21,000 g for 30 min. The soluble fraction was collected and mixed 3:1 with 4x Laemmli buffer supplemented with β-mercaptoethanol and boiled for 10 minutes. These samples were run on precast SDS-PAGE gels (Bio-Rad) and transferred to PVDF membranes. The membranes were blocked with

TBS-T buffer (1x TBS, 0.1% Tween-20) supplemented with 5% skim milk. Custom primary antibodies for Pa011 CdnA or PaMx41 orf11 (α -CdnA and α -orf11, Genscript) were then added to the skim milk buffer at a titer of 1:1000 and left to incubate at room temperature for one hour. The membranes were washed 3x with 10 mL of TBS-T, then incubated with α -Rabbit (Cell Signaling, cat# 7074S) secondary antibody at a titer of 1:1000 for 45 minutes at room temperature. The membrane was washed 3x with 10 mL of TBS-T and developed with Clarity Max ECL substrate (Bio-Rad). Western blot images were taken with an Azure Biosystems C400 imager.

OD₆₀₀ cell growth curve experiments

Overnight cultures were diluted 1:100 in 25 ml LB medium with 10 mM MgSO₄, antibiotics and inducers, as appropriate (150ml flask), and then grown at 37°C (175 r.p.m.) until reaching an OD₆₀₀ of ~0.3. From the culture, 140 μ l was aliquoted in a 96-well plate and infected with <10 μ l of phage to reach a final MOI of 20, 2, and 0.2. Each infection was performed in technical triplicate, and cultured with maximum double orbital rotation at 37 °C for 12h with OD₆₀₀ measurements taken every 5 minutes using a BioTek Synergy H1 microplate reader (Gen5 software).

CFU and PFU measurements

Overnight cultures were diluted 1:100 in 25 ml LB medium with 10 mM MgSO₄, antibiotics and inducers, as appropriate (150ml flask), and then grown at 37 °C (175 r.p.m.) until reaching an OD₆₀₀ of ~0.3. From the culture, 3 ml aliquots were prepared in 6 ml glass culture tubes. One aliquot was kept uninfected and another infected with < 20 μ l of phage to reach a final MOI of 2. Cultures were incubated at 37 °C (90 r.p.m.) using a Fisherbrand Isotemp shaking water bath. Pre-infection (0h) and then 2-, 4-, 6-, and 8-hours post-infection aliquots were taken to measure colony forming units (CFU), plaque forming units (PFU), and single-cell flow cytometry measurements (described below). For CFU counts, 1 or 10 μ l of culture was diluted in SM buffer to prevent further growth and then plated on solid agar with antibiotics and inducers, as appropriate. For PFU counts, 50 μ l of culture was collected with 5 μ l of chloroform, centrifuged at maximum g for 1 min, and then stored at 4°C. Whole plate infections

were performed as described above. After incubating 37°C overnight, individual colonies or plaques were counted and CFU/ml or PFU/ml calculated, respectively.

Single-step growth curve experiments

Overnight cultures were diluted 1:100 in 25 ml LB medium with 10 mM MgSO₄ (150ml flask), and then grown at 37°C (175 r.p.m.) until reaching an OD₆₀₀ of ~0.3. From the culture, 2ml aliquots of cells were centrifuged at 9,000 g for 3 minutes and supernatant removed. Cells were resuspended in 200 µl LB medium with 10 mM MgSO₄. One aliquot was kept uninfected and another infected with phage to reach a final MOI of 0.2. Cells were kept on ice for 20 minutes to effectively absorb phage. Cells were centrifuged at 9,000 g for 3 minutes, supernatant carefully removed to eliminate unabsorbed phage, and resuspended in 1 ml of fresh LB medium with 10 mM MgSO₄. An aliquot of phage was taken here as the first time point (T:0). The remaining culture was transferred to a 3 ml glass culture tube and incubated at 37 °C (90 r.p.m.) using a Fisherbrand Isotemp shaking water bath. At 0, 20-, 40-, 60-, 80-, and 120-minutes post-infection 50 µl aliquots were taken and added to 5 µl of chloroform, spun down at maximum g for 1 min, and then stored at 4 °C. Whole plate infections were performed as described above. After incubating 37°C overnight, individual colonies or plaques were counted and CFU/ml or PFU/ml calculated, respectively. Frequency of surviving phage was calculated using the PFU/ml of output phage normalized to PFU/ml input phage.

Flow cytometry

Cultures were prepared as described above. Pre-infection, 1 ml of culture was collected and served as the first time point (T:0h) and another 1 ml served as the heat-killed positive control (95°C for 10 min). At 2-, 4-, 6-, and 8-hours post-infection, 200 µl of culture was collected. For each sample, an equal volume of diluted Propidium Iodide (PI) was added (1:1000 in 1x PBS, Thermo Fisher, LIVE/DEAD Fixable Red Dead Cell Stain Kit, L34971), briefly vortexed, and then incubated for 30 min at room temperature, shaking, and covered from light. Cells were centrifuged at 9,000 g for 3 mins, supernatant removed, and resuspended in 200 µl of 3% PFA. Cells were briefly vortexed, incubated

for 15 min at room temperature and covered from light. Cells were centrifuged at 9,000 g for 3 mins, supernatant removed, and resuspended in 1 ml 1x PBS (twice). Cells resuspended in 200 µl of PBS and stored overnight at 4°C and covered from light. Cells were then analyzed on a BD LSRFortessa X-20 (BD Biosciences) using BD FACSDiva software version 9.0.0 with >20,000 post-gating single cell events recorded for each sample. PI+ cells was calculated using the frequency of events (cells) in the PI-expressing population out of the single-cell population. The data was analyzed with FlowJo v10.10.0 and gating strategy is shown in Figure 4.12.

Exogenous 3',3'-cGAMP experiments

Cells were prepared and measured as described for the OD₆₀₀ experiments. However, from the culture, 140 µl was aliquoted in a 96-well plate and then 5 to 15 µl of diluted 3',3'-cGAMP (Sigma Aldrich, SML1232) was added to reach a final concentration of 1 to 100 µg/ml of cGAMP. Cells were incubated at room temperature for 1 minute. Afterwards <10 µl of phage to reach a final MOI of 2. Each infection was performed in biological replicate.

Structural homology search

Structural homologs of *Homo sapiens* SLC191A (AF: Q9BY10), SCL46A (AF: Q9BY10), and ENPP1 (PDB: 6WET) were identified using Foldseek¹¹⁸. Specifically, these proteins were queried against all computationally predicted proteins in the AlphaFold database^{107,143} and experimentally solved proteins in the RCSB Protein Data Bank (PDB) within the taxonomic filter bacteria and 3Di/AA alignment mode. The resulting proteins were considered positive hits with a 3Di E-value of <1e-3 and amino acid coverage of >80%.

Computational modeling of phage capsid

Models of *P. aeruginosa* PaMx41 (orf11) phage capsid proteins were generated using AlphaFold2¹⁰⁷ and aligned using the PyMol “super” function to the different chains of the *E. coli* T4 phage capsid structure (PDB: 6UZC), which was previously shown⁵⁰.

Quantification and Statistical analyses

Statistical details for each experiment can be found in the figure legends and outlined in the corresponding methods details section. Data are plotted with error bars representing standard deviation (s.d.) or standard error mean (s.e.m.) as indicated in the legends.

4.7. Figures

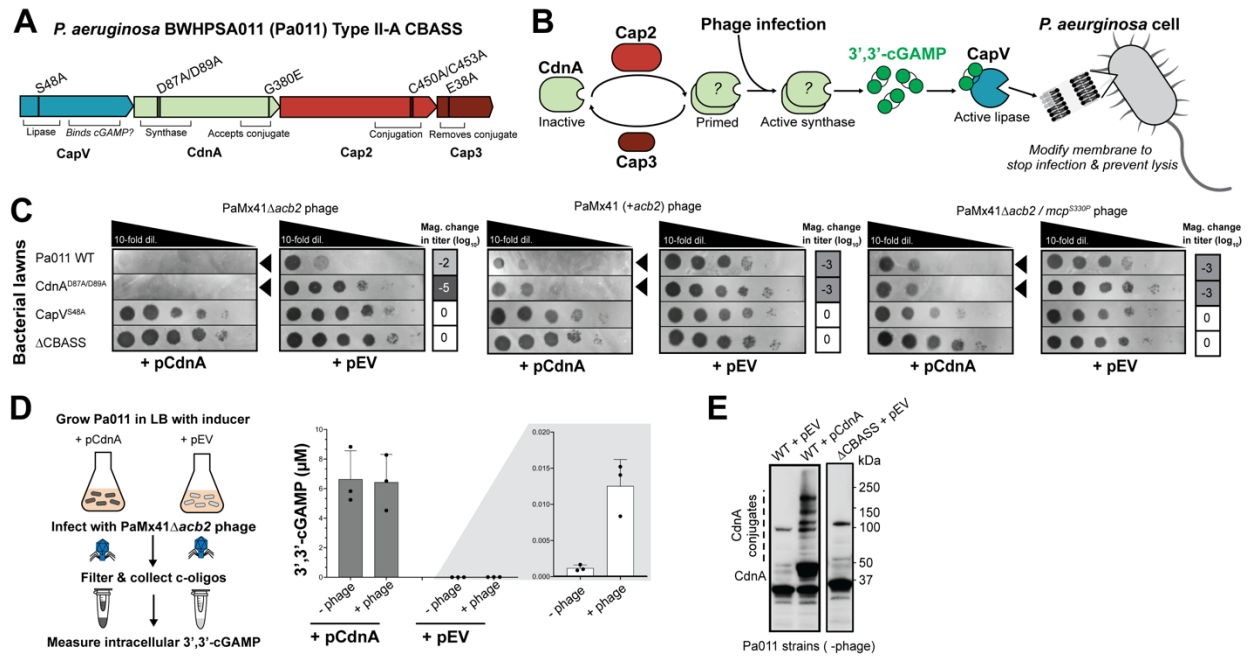


Figure 4.1: Increasing CdnA activity overcomes CBASS resistant phage

(A) *Pseudomonas aeruginosa* strain BWHPA011 (Pa011) Type II-A CBASS operon with domains and functional mutants indicated. (B) Working model of Pa011 Type II-CBASS immunity, wherein CdnA produces a 3',3'-cGAMP signals to activate the CapV effector and then modifies the cell membrane to stop the infection and prevent phage-induced cell lysis. (C) PaMx41 phage that is CBASS sensitive (Δ *acb2*) or CBASS resistant (+*acb2* or +*mcp*) mutant) spotted across lawns of Pa011 WT, CdnA or CapV catalytically dead, Δ CBASS strains expressing CdnA or empty vector (EV) plasmids (0.1% Arabinose, n=3). These plaque assays were used to quantify the order of magnitude change in phage titer by comparing the number of spots (with plaques, or clearings if plaques were not visible) on the CdnA overexpressing strain divided by the EV strain. Black arrowheads highlight significant reductions in phage titer. (D) Preparation of bacterial cells and quantification of intracellular 3',3'-cGAMP produced in Pa011 CapV^{S48A} cells expressing CdnA or EV plasmids in the absence or presence of PaMx41 Δ *acb2* phage over 60 minutes (MOI:5, 0.1% Arabinose; n=3). (E) Immunoblotting CdnA protein in Pa011 WT or Δ CBASS cells expressing CdnA or EV plasmids in the absence of phage using a custom anti-CdnA antibody (a.a. 393-353).

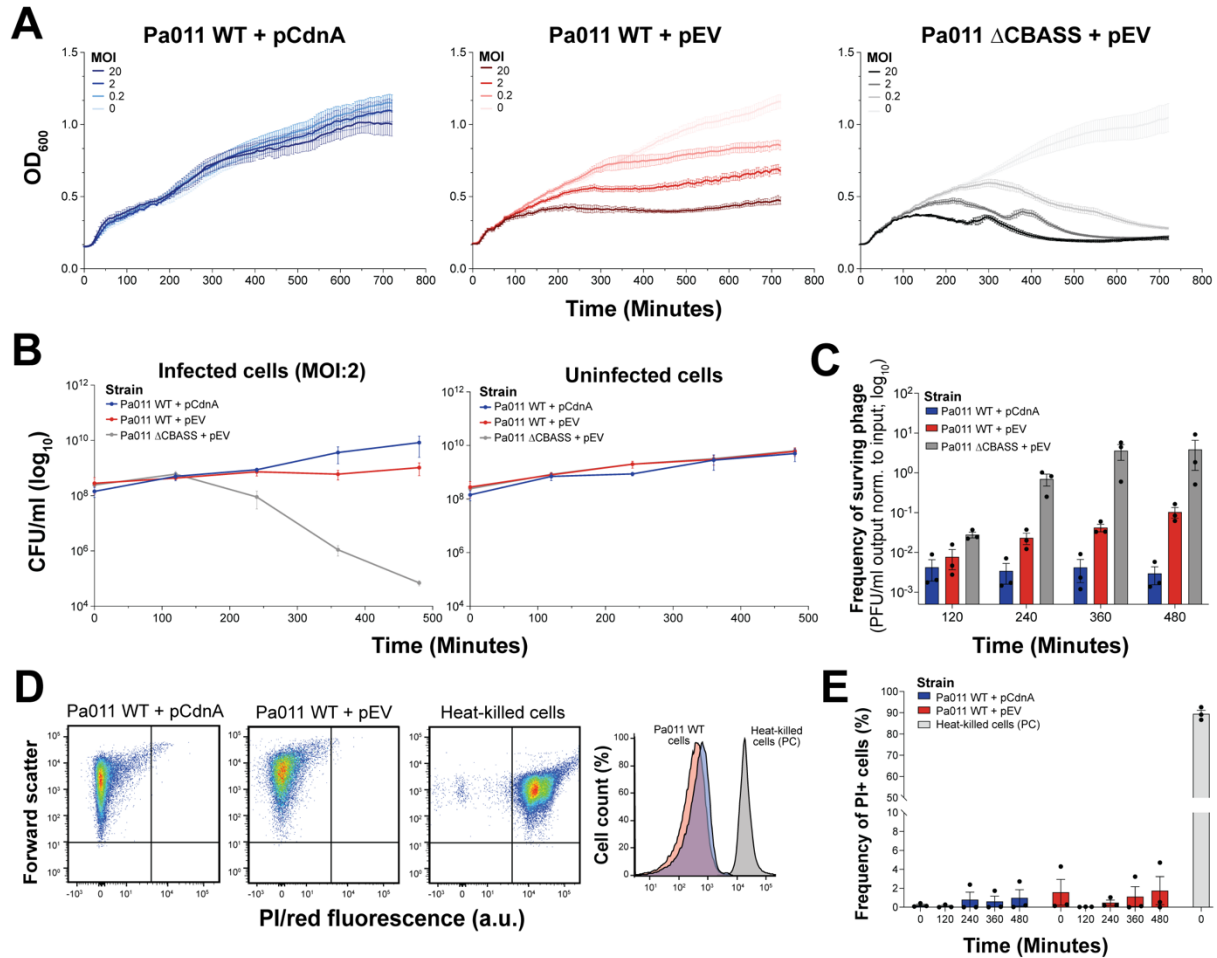


Figure 4.2: Increasing CBASS immunity improves cell growth upon phage infection

(A) OD₆₀₀ measurements of Pa011 strains expressing CdnA or EV plasmids infected with an increasing multiplicity of infection (MOI) of PaMx41 Δ acb2 phage over 720 minutes (0.5% Arabinose, n=3 +/- s.d.). (B) Colony forming units (CFU/ml) and (C) frequency of surviving phage (PFU/ml of output normalized to input; log₁₀) of infected and uninfected Pa011 strains. (D) Flow cytometry dot plot or histogram representation of Propidium iodide (PI) negative (live) and positive (porous or dead) cells at 480 minutes post-infection. The histogram cell count is scaled as the percentage of the maximum cell count. Heat-killed cells as used as a positive control (PC). (E) Frequency of PI+ cells (from single bacterial cells) of infected Pa011 strain. Assays performed in B-E used PaMx41 Δ acb2 phage over 480 minutes (MOI:2, 0.05% Arabinose; n=3 +/- s.e.m).

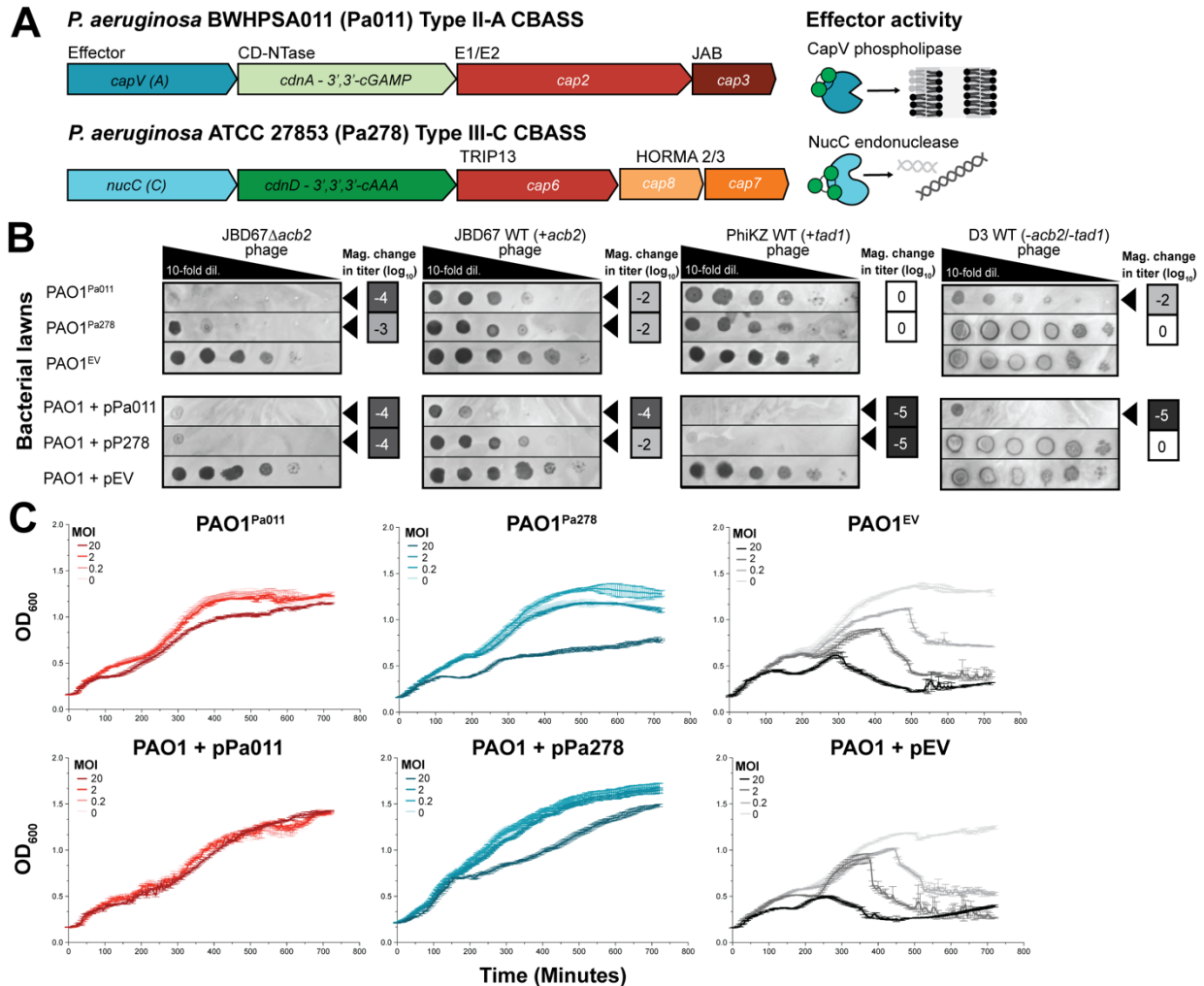


Figure 4.3: Heterologously expressed Type II-A and Type III-C CBASS improves anti-phage activity and cell growth

(A) *Pseudomonas aeruginosa* strains BWHP5A011 (Pa011) Type II-A or ATCC 27853 (Pa278) Type III-C CBASS operons. (B) Phage that is CBASS sensitive (Δ *acb2* or -*acb2*) or CBASS resistant (+*acb2* or +*tad1*) spotted across lawns of *P. aeruginosa* PAO1 strains harboring Pa011 Type II-A CBASS or Pa278 Type III-C CBASS operons. Chromosomally integrated CBASS operons PAO1^{Pa011} (0 mM IPTG), PAO1^{Pa278} (0.3 mM IPTG), or miniTn7 empty vector (EV, 0.3 mM IPTG). Plasmid expressing CBASS operons + pPa011, + pPa278, or pHERD30T EV (all 0.1% Arabinose) (n=3). These plaque assays were used to quantify the order of magnitude change in phage titer by comparing the number of spots (with plaques, or clearings if plaques were not visible) on the CBASS expressing strain divided by the EV strain. Black arrowheads highlight significant reductions in phage titer. (C) OD₆₀₀ measurements of strains described in (B) are infected with an increasing MOI of JBD67Δ*acb2* phage over 720 minutes (n=3 +/- s.d.).

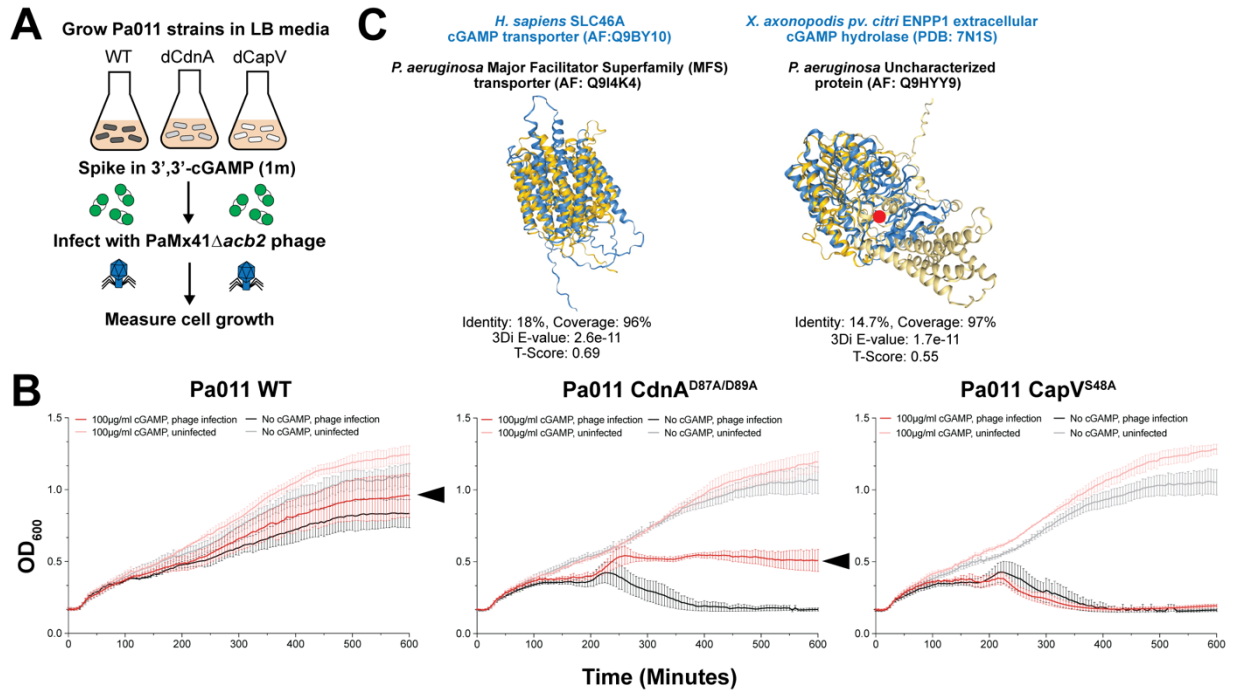


Figure 4.4: Exogenous 3',3'-cGAMP induce CBASS-dependent cell growth

(A) Preparation of bacterial cells. (B) OD₆₀₀ measurements of Pa011 WT, CapA^{D87A/D89A} (dCdnA), CapV^{S48A} (dCapV) strains infected with or without PaMx41Δ*acb2* phage (MOI:2) and with or without 3',3'-cGAMP (100µg/ml) over 10 hours (n=3 +/- s.d). Arrow highlights significant changes in cell density. (C) Predicted *Pseudomonas aeruginosa* cGAMP transporter or hydrolase (yellow) aligned with predicted *Homo sapiens* SLC46A transporter or *Xanthomonas axonopodis* pv. *citri* ENPP1 hydrolase (blue), respectively. Red circle represents the known active site of ENPP1¹⁴⁰. Structural alignments performed with Foldseek¹¹⁸ and output 3Di E-values, T-Score (>0.5 highly similar protein topology), a.a. sequence identity, and a.a. coverage data provided below each respective alignment.

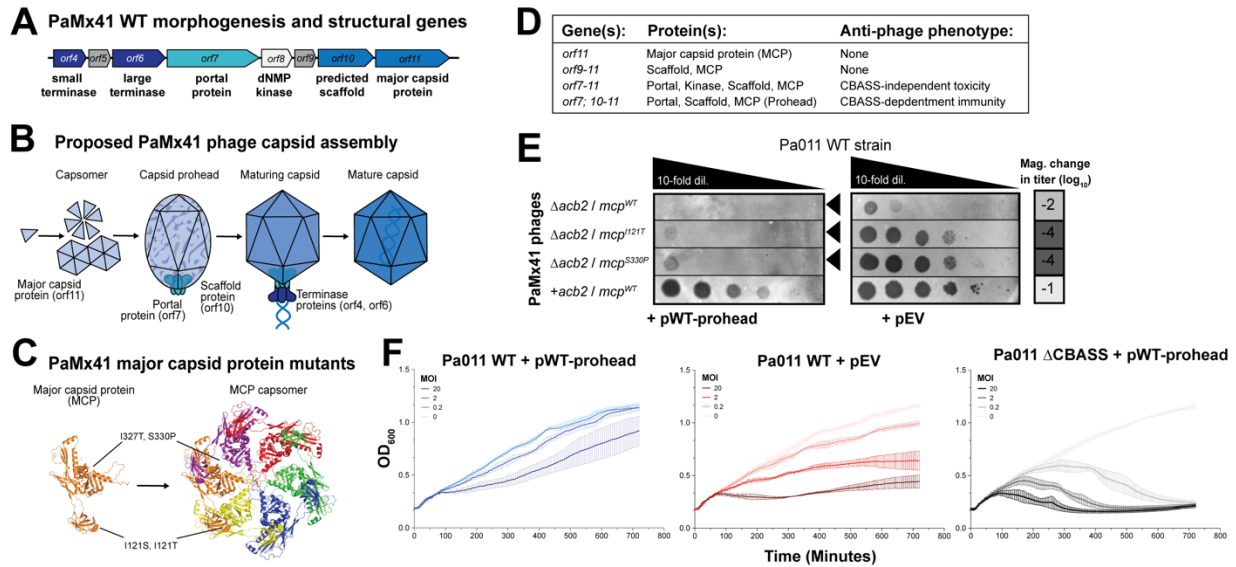


Figure 4.5: Phage capsid prohead induces CBASS immunity

(A) PaMx41 phage locus for morphogenesis genes (white), structural capsid genes (blues), and hypothetical/unknown genes (gray). (B) Schematic of proposed PaMx41 capsid assembly process based on the well-studied T4 phage capsid¹⁴¹. (C) Predicted PaMx41 phage major capsid protein (MCP) and the MCP capsomer with indicated CBASS escape mutations at the protein-protein interface. (D) Summary of gene constructs tested for anti-phage activity in the native Pa011 host and their outcomes in lower panel. (E) PaMx41 phage that is CBASS sensitive ($\Delta acb2$) or CBASS resistant ($+acb2$ or $+mcp$ mutant) spotted across lawns of Pa011 WT expressing the WT capsid prohead or EV plasmids. These plaque assays were used to quantify the order of magnitude change in phage titer by comparing the number of spots (with plaques, or clearings if plaques were not visible) on the WT prohead overexpressing strain divided by the EV strain (0.1% Arabinose, $n=3$). Black arrowheads highlight notable reductions in phage titer. (F) OD₆₀₀ measurements of Pa011 WT or $\Delta CBASS$ strains overexpressing WT capsid prohead or EV plasmids infected with PaMx41 $\Delta acb2$ phage over 12 hours ($n=3$ +/- s.d.).

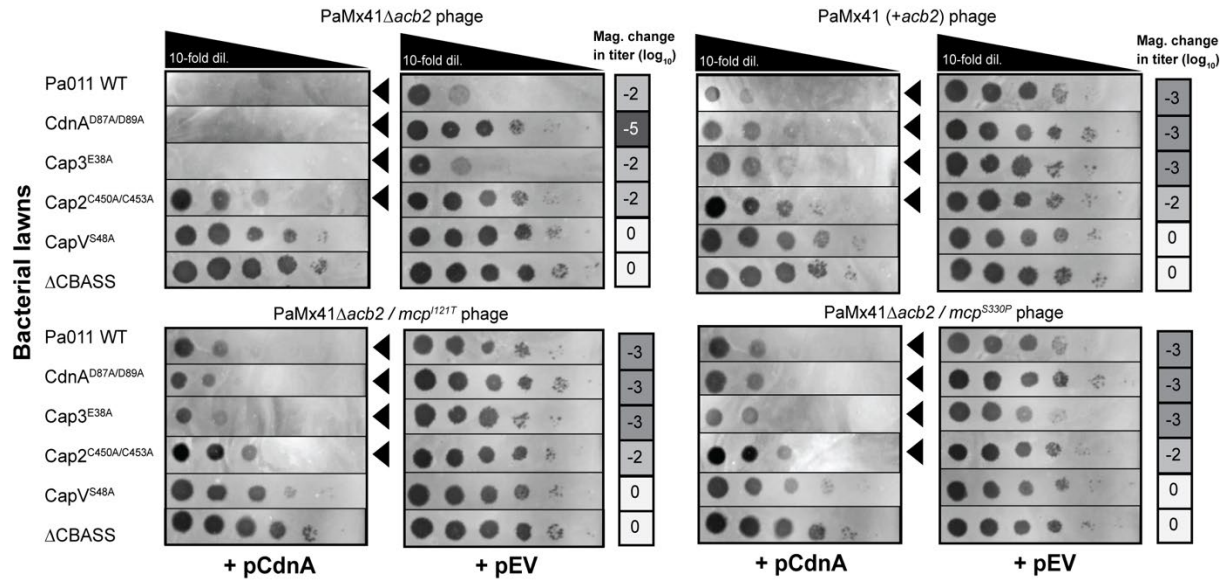


Figure 4.6: Increasing CdnA activity overcomes phage with Acb2 and MCP mutations

PaMx41 phage that is CBASS sensitive (Δ acb2) or CBASS resistant (+acb2 or +mcp mutants) spotted across lawns of Pa011 WT, Δ CBASS, or CBASS gene mutant cells expressing CdnA or empty vector (EV) plasmids. These plaque assays were used to quantify the order of magnitude change in phage titer by comparing the number of spots (with plaques, or clearings if plaques were not visible) on the CdnA overexpression strain divided by the EV strain (0.01% Arabinose; n=3). Black arrowheads highlight notable reductions in phage titer. Related to Figure 4.1.

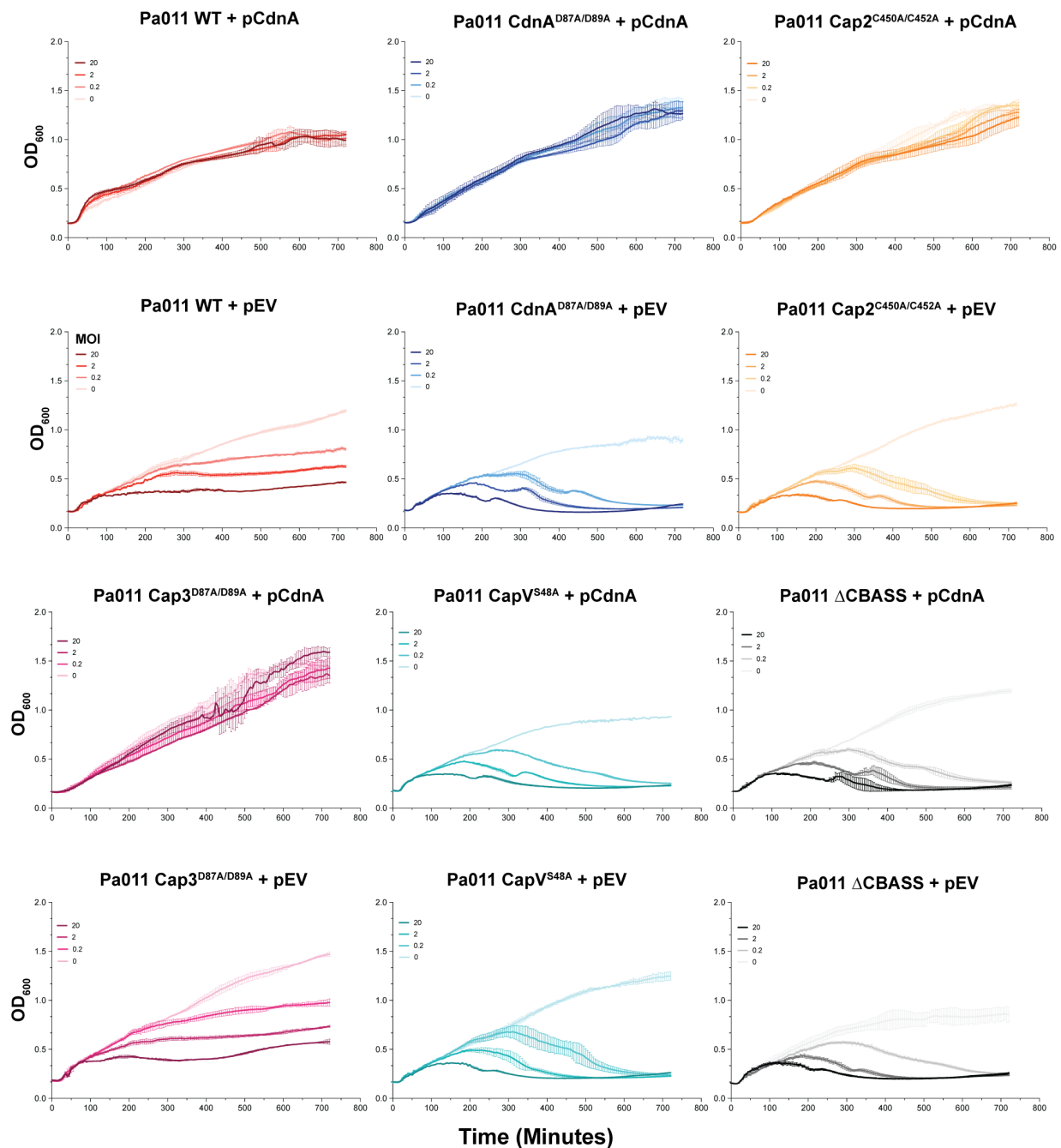


Figure 4.7: Improved cell growth is dependent on CapV effector activity

OD₆₀₀ measurements of Pa011 strains overexpressing CdnA or EV plasmids infected with an increasing multiplicity of infection (MOI) of PaMx41Δ*acb2* phage over 720 minutes (0.05% Arabinose, n=3 +/- s.d.). Related to Figure 4.2.

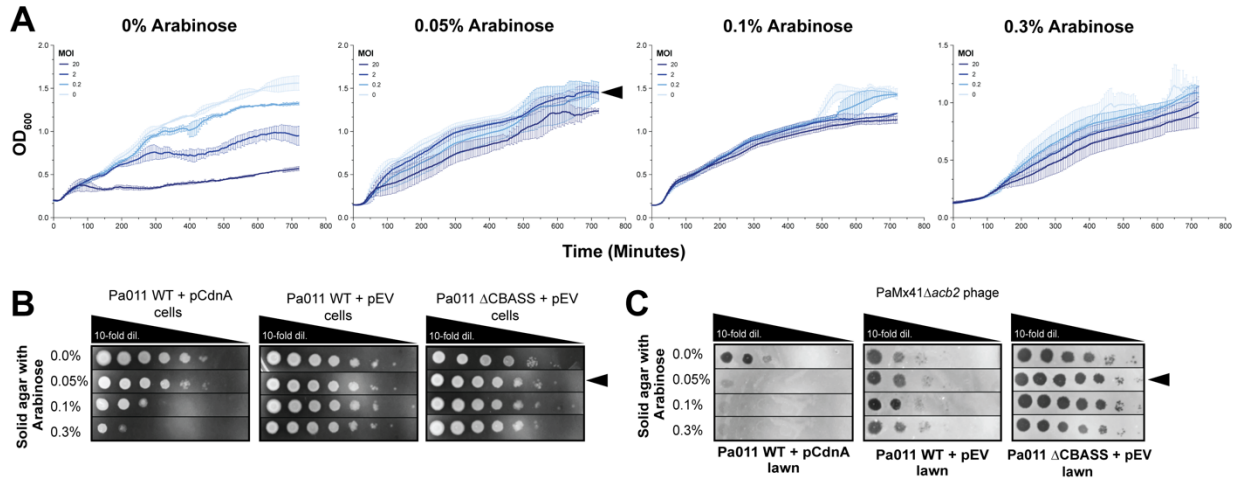


Figure 4.8: CBASS-dependent cell growth is tunable and can become toxic

(A) OD₆₀₀ measurements of Pa011 WT overexpressing CdnA induced with increasing percentages of Arabinose inducer and then infected with PaMx41Δ*acb2* phage (MOI:2) over 720 minutes (n=1 +/- s.d.). (B) Pa011 WT strains from (A) spotted across solid agar with increasing percentages of arabinose inducer (n=1). (C) PaMx41Δ*acb2* phage spotted across lawns of Pa011 WT or ΔCBASS strains expressing CdnA or empty vector (EV) (n=1). Black arrows highlight the conditions used in Figure 4.2 that balance cell viability or toxicity with anti-phage activity.

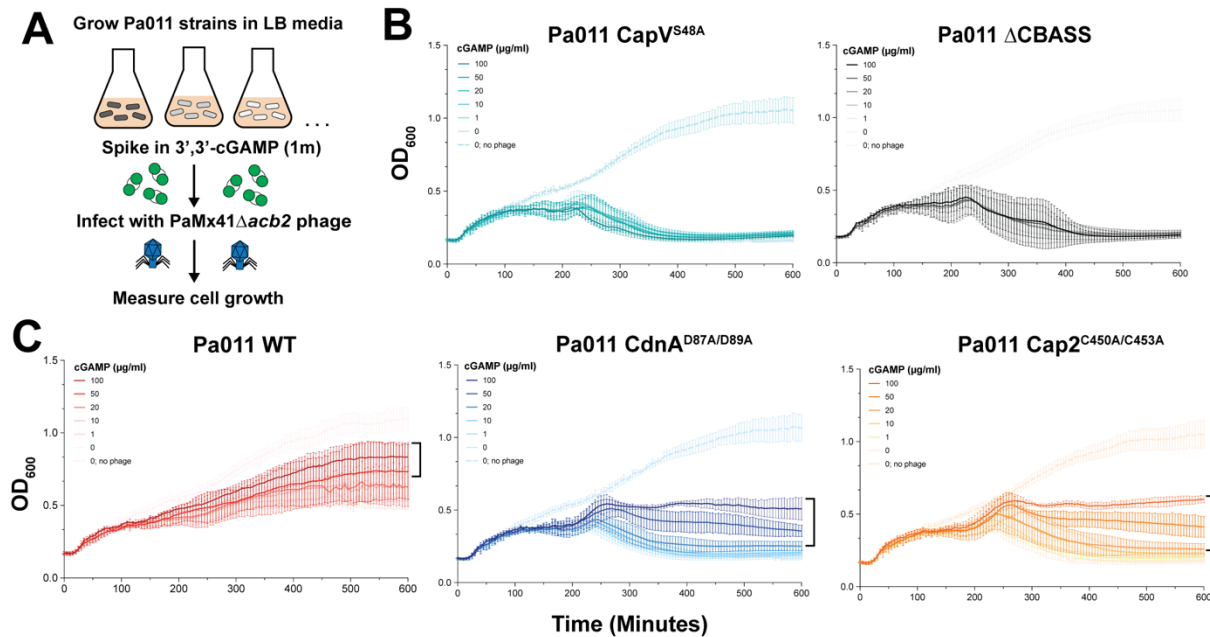


Figure 4.9: High levels of exogenous 3',3'-cGAMP is necessary to induce CBASS-dependent cell growth

(A) Preparation of bacterial cells. (B-C) OD₆₀₀ measurements of Pa011WT, ΔCBASS, or CBASS mutant strains infected with or without PaMx41Δ*acb2* phage (MOI:2) and increasing concentrations of 3',3'-cGAMP over 10 hours (n=3 +/- s.d.). (B) Includes Pa011 strains that do not change cell density in response to exogenous 3',3'-cGAMP compared to (C) Pa011 strains that are rescued with exogenous 3',3'-cGAMP. Black brackets highlight increases in cell density relative to untreated cells. Related to Figure 4.4.

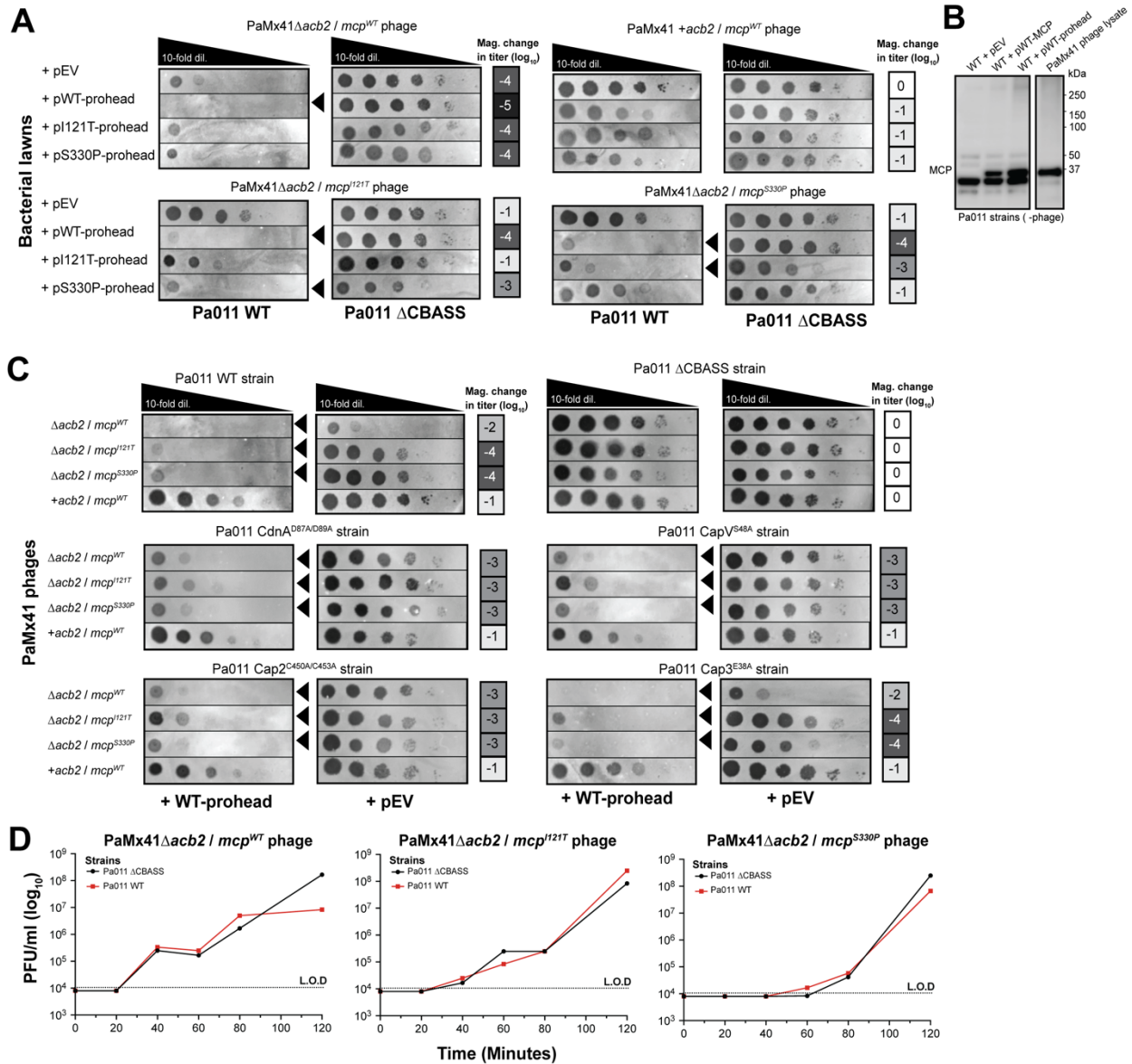


Figure 4.10: WT and mutant capsid proheads impact CBASS anti-phage activity

(A) PaMx41 phage that is CBASS sensitive ($\Delta*acb2*$) or CBASS resistant (+*acb* or +*mcp* mutants) spotted across lawns of Pa011 WT or Δ CBASS strains overexpressing WT capsid prohead, mutant capsid prohead, or empty vector (EV) plasmids. (B) Immunoblotting PaMx41 MCP in Pa011 WT cells expressing the WT MCP, wildtype prohead, or empty vector (EV) plasmids in the absence of phage using a custom anti-MCP antibody (a.a. 139-152). PaMx41 cell lysate served as a positive control. (C) PaMx41 phage spotted across lawns of Pa011 WT, Δ CBASS, or CBASS gene mutant strains expressing WT prohead or EV plasmids. Plaque assays in (A) and (D) were used to quantify the order of magnitude change in phage titer by comparing the number of spots (with plaques, or clearings if plaques were not visible) on the prohead overexpressing strain divided by the EV strain (0.1% Arabinose, n=3). Black arrowheads highlight notable reductions in phage titer. (D) Single-step growth curve of PaMx41 $\Delta*acb2*$ phages with WT and mutant MCP grown in the presence of Pa011 WT or Δ CBASS cells (MOI:0.2, n=1). Related to Figure 4.5.

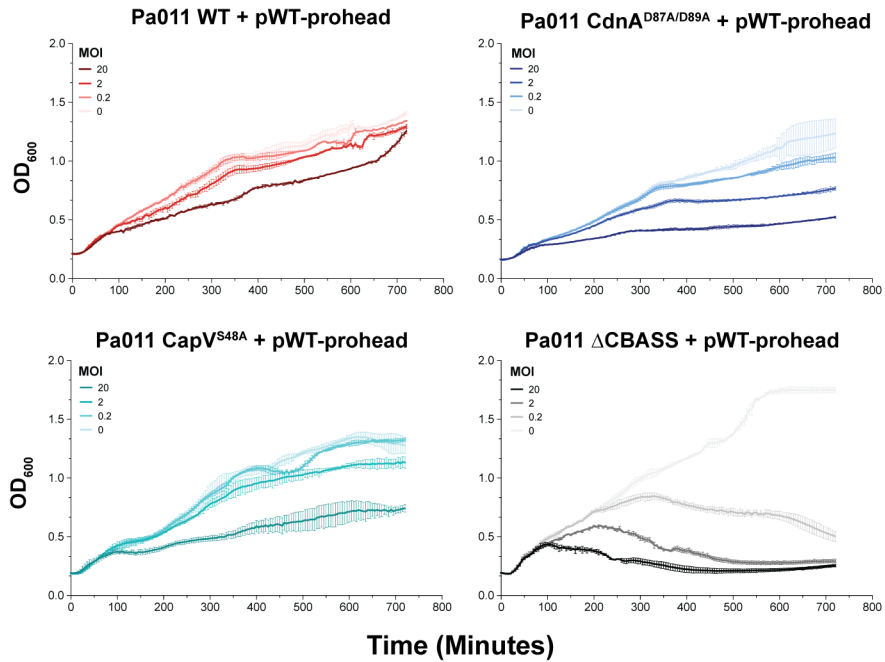


Figure 4.11: WT capsid proheads induce cell growth in CBASS-dependent manner
 OD₆₀₀ measurements of Pa011 strains overexpressing wildtype capsid prohead and infected with an increasing multiplicity of infection (MOI) of PaMx41Δ*acb2* phage over 720 minutes (0.1% Arabinose, n=1). Related to Figure 4.5.

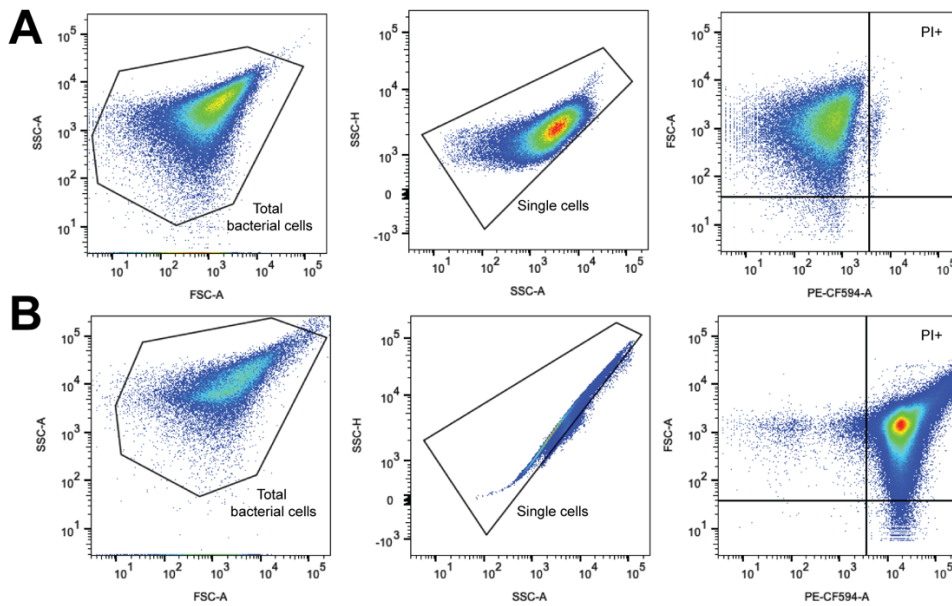


Figure 4.12: Flow cytometry gating strategy for propidium iodide expressing cells
 (A) Gating strategy schematic for Propidium iodide (PI)-expressing bacterial cells and (B) heat-killed positive control (dead) cells. Note that cell shape (SSC-H v SSC-A) differs significantly between healthy (A) and dead (B) cells in *P. aeruginosa*. This was observed with over three biological replicates.

References

1. Tesson, F. *et al.* A Comprehensive Resource for Exploring Antiphage Defense: DefenseFinder Webservice, Wiki and Databases. *bioRxiv* (2024).
2. Tock, M. R. & Dryden, D. T. F. The biology of restriction and anti-restriction. *Curr Opin Microbiol* **8**, 466–472 (2005).
3. Hille, F. *et al.* The Biology of CRISPR-Cas: Backward and Forward. *Cell* **172**, 1239–1259 (2018).
4. Johnson, M. C. *et al.* Core defense hotspots within *Pseudomonas aeruginosa* are a consistent and rich source of anti-phage defense systems. *Nucleic Acids Res* **51**, 4995–5005 (2023).
5. Cheng, R. *et al.* A nucleotide-sensing endonuclease from the Gabija bacterial defense system. *Nucleic Acids Res.* **49**, 5216–5229 (2021).
6. Gao, L. A. *et al.* Prokaryotic innate immunity through pattern recognition of conserved viral proteins. *Science (1979)* **377**, eabm4096 (2022).
7. Bari, S. M. N. *et al.* A unique mode of nucleic acid immunity performed by a multifunctional bacterial enzyme. *Cell Host Microbe* **30**, 570–582.e7 (2022).
8. Tal, N. *et al.* Bacteria deplete deoxynucleotides to defend against bacteriophage infection. *Nat Microbiol* **7**, 1200–1209 (2022).
9. Antine, S. P. *et al.* Structural basis of Gabija anti-phage defence and viral immune evasion. *Nature* **625**, 360–365 (2024).
10. Tuck, O. T. *et al.* Hachiman is a genome integrity sensor. *bioRxiv* (2024).
11. Bobonis, J. *et al.* Bacterial retrons encode phage-defending tripartite toxin-antitoxin systems. *Nature* **609**, 144–150 (2022).
12. Hsueh, B. Y. *et al.* Phage defence by deaminase-mediated depletion of deoxynucleotides in bacteria. *Nat Microbiol* **7**, 1210–1220 (2022).

13. Ka, D., Oh, H., Park, E. & Kim Jeong-Han and Bae, E. Structural and functional evidence of bacterial antiphage protection by Thoeis defense system via NAD⁺ degradation. *Nat. Commun.* **11**, 2816 (2020).
14. Garb, J. *et al.* Multiple phage resistance systems inhibit infection via SIR2-dependent NAD⁺ depletion. *Nat Microbiol* **7**, 1849–1856 (2022).
15. Duncan-Lowey, B. *et al.* Cryo-EM structure of the RADAR supramolecular anti-phage defense complex. *Cell* **186**, 987–998.e15 (2023).
16. Gao, Y. *et al.* Molecular basis of RADAR anti-phage supramolecular assemblies. *Cell* **186**, 999–1012.e20 (2023).
17. Rousset, F. *et al.* A conserved family of immune effectors cleaves cellular ATP upon viral infection. *Cell* **186**, 3619–3631.e13 (2023).
18. Shen, Z., Lin, Q., Yang, X.-Y., Fosuah, E. & Fu, T.-M. Assembly-mediated activation of the SIR2-HerA supramolecular complex for anti-phage defense. *Mol. Cell* **83**, 4586–4599.e5 (2023).
19. Tang, D. *et al.* Multiple enzymatic activities of a Sir2-HerA system cooperate for anti-phage defense. *Mol. Cell* **83**, 4600–4613.e6 (2023).
20. Tal, N. *et al.* Cyclic CMP and cyclic UMP mediate bacterial immunity against phages. *Cell* **184**, 5728–5739.e16 (2021).
21. Cohen, D. *et al.* Cyclic GMP-AMP signalling protects bacteria against viral infection. *Nature* **574**, 691–695 (2019).
22. Ofir, G. *et al.* Antiviral activity of bacterial TIR domains via immune signalling molecules. *Nature* **600**, 116–120 (2021).
23. Millman, A. *et al.* Bacterial Retrons Function In Anti-Phage Defense. *Cell* **183**, 1551–1561.e12 (2020).
24. Duncan-Lowey, B., McNamara-Bordewick, N. K., Tal, N., Sorek, R. & Kranzusch, P. J. Effector-mediated membrane disruption controls cell death in CBASS antiphage defense. *Mol Cell* **81**, 5039–5051.e5 (2021).

25. Johnson, A. G. *et al.* Bacterial gasdermins reveal an ancient mechanism of cell death. *Science (1979)* **375**, 221–225 (2022).
26. Sabonis, D. *et al.* TIR domains produce histidine-ADPR conjugates as immune signaling molecules in bacteria. *bioRxiv* (2024).
27. Bernheim, A. *et al.* Prokaryotic viperins produce diverse antiviral molecules. *Nature* **589**, 120–124 (2021).
28. Zhang, T. *et al.* Direct activation of a bacterial innate immune system by a viral capsid protein. *Nature* 1–9 (2022).
29. LeRoux, M. *et al.* The DarTG toxin-antitoxin system provides phage defence by ADP-ribosylating viral DNA. *Nat Microbiol* **7**, 1028–1040 (2022).
30. Doron, S. *et al.* Systematic discovery of antiphage defense systems in the microbial pangenome. *Science (1979)* **359**, (2018).
31. Whiteley, A. T. *et al.* Bacterial cGAS-like enzymes synthesize diverse nucleotide signals. *Nature* **567**, 194–199 (2019).
32. Davies, B. W., Bogard, R. W., Young, T. S. & Mekalanos, J. J. Coordinated regulation of accessory genetic elements produces cyclic di-nucleotides for *V. cholerae* virulence. *Cell* **149**, 358–370 (2012).
33. Kranzusch, P. J. *et al.* Structure-Guided Reprogramming of Human cGAS Dinucleotide Linkage Specificity. *Cell* **158**, 1011–1021 (2014).
34. Burroughs, A. M., Zhang, D., Schäffer, D. E., Iyer, L. M. & Aravind, L. Comparative genomic analyses reveal a vast, novel network of nucleotide-centric systems in biological conflicts, immunity and signaling. *Nucleic Acids Res* **43**, 10633–10654 (2015).
35. Millman, A., Melamed, S., Amitai, G. & Sorek, R. Diversity and classification of cyclic-oligonucleotide-based anti-phage signalling systems. *Nat Microbiol* **5**, 1608–1615 (2020).
36. Fitzgerald, K. A. & Kagan, J. C. Toll-like Receptors and the Control of Immunity. *Cell* **180**, 1044–1066 (2020).

37. Burch-Smith, T. M. & Dinesh-Kumar, S. P. The Functions of Plant TIR Domains. *Science's STKE* **2007**, (2007).
38. Hanoune, J. & Defer, N. Regulation and Role of Adenylyl Cyclase Isoforms. *Annu Rev Pharmacol Toxicol* **41**, 145–174 (2001).
39. Bondy-Denomy, J., Pawluk, A., Maxwell, K. L. & Davidson, A. R. Bacteriophage genes that inactivate the CRISPR/Cas bacterial immune system. *Nature* **493**, 429–432 (2013).
40. Pinilla-Redondo, R. *et al.* Discovery of multiple anti-CRISPRs highlights anti-defense gene clustering in mobile genetic elements. *Nat. Commun.* **11**, 5652 (2020).
41. Samuel, B. & Burstein, D. *A Diverse Repertoire of Anti-Defense Systems Is Encoded in the leading Region of Plasmids.* *bioRxiv* (2023).
42. Athukoralage, J. S., Rouillon, C., Graham, S., Grüşchow, S. & White, M. F. Ring nucleases deactivate type III CRISPR ribonucleases by degrading cyclic oligoadenylate. *Nature* **562**, 277–280 (2018).
43. Athukoralage, J. S. *et al.* An anti-CRISPR viral ring nuclease subverts type III CRISPR immunity. *Nature* **577**, 572–575 (2020).
44. Athukoralage, J. S. & White, M. F. Cyclic oligoadenylate signalling and regulation by ring nucleases during type III CRISPR defence. *RNA* **27**, 855–867 (2021).
45. Yirmiya, E. *et al.* Phages overcome bacterial immunity via diverse anti-defence proteins. *Nature* **625**, 352–359 (2024).
46. Wilkinson, M., Wilkinson, O. J., Feyerherm Connie and Fletcher, E. E., Wigley, D. B. & Dillingham, M. S. Structures of RecBCD in complex with phage-encoded inhibitor proteins reveal distinctive strategies for evasion of a bacterial immunity hub. *Elife* **11**, (2022).
47. Azam, A. H. *et al.* *Viruses Encode tRNA and Anti-Retron to Evade Bacterial Immunity.* *bioRxiv* (2023).
48. Hobbs, S. J. *et al.* Phage anti-CBASS and anti-Pycsar nucleases subvert bacterial immunity. *Nature* **605**, 522–526 (2022).

49. Leavitt, A. *et al.* Viruses inhibit TIR gcADPR signaling to overcome bacterial defense. *Nature* (2022).
50. Huiting, E. *et al.* Bacteriophages inhibit and evade cGAS-like immune function in bacteria. *Cell* **186**, 864–876.e21 (2023).
51. Cao, X. *et al.* Phage anti-CBASS protein simultaneously sequesters cyclic trinucleotides and dinucleotides. *Mol. Cell* **84**, 375–385.e7 (2024).
52. Li, D. *et al.* Single phage proteins sequester TIR- and cGAS-generated signaling molecules. *bioRxiv* (2023).
53. Jenson, J. M., Li, T., Du, F., Ea, C.-K. & Chen, Z. J. Ubiquitin-like conjugation by bacterial cGAS enhances anti-phage defence. *Nature* **616**, 326–331 (2023).
54. Osterman, I. *et al.* Phages Reconstitute NAD⁺ to Counter Bacterial Immunity. *bioRxiv* (2024).
55. Eaglesham, J. B., Pan, Y., Kupper, T. S. & Kranzusch, P. J. Viral and metazoan poxins are cGAMP-specific nucleases that restrict cGAS-STING signalling. *Nature* **566**, 259–263 (2019).
56. Nomburg, J., Price, N. & Doudna, J. A. Birth of new protein folds and functions in the virome. *bioRxiv* (2024).
57. Millman, A. *et al.* An expanded arsenal of immune systems that protect bacteria from phages. *Cell Host Microbe* **30**, 1556–1569.e5 (2022).
58. Maffei, E. *et al.* Systematic exploration of Escherichia coli phage–host interactions with the BASEL phage collection. *PLoS Biol* **19**, e3001424 (2021).
59. Georjon, H. & Bernheim, A. The highly diverse antiphage defence systems of bacteria. *Nat. Rev. Microbiol.* **21**, 686–700 (2023).
60. Iwasaki, A. A virological view of innate immune recognition. *Annual Review Microbiology* **66**, 177–196 (2012).
61. Remick, B. C., Gaidt, M. M. & Vance, R. E. Effector-Triggered Immunity. *Annual Reviews Immunology* (2023).

62. Vance, R. E., Isberg, R. R. & Portnoy, D. A. Patterns of pathogenesis: discrimination of pathogenic and nonpathogenic microbes by the innate immune system. *Cell Host Microbe* **6**, 10–21 (2009).
63. Depardieu, F. *et al.* A Eukaryotic-like Serine/Threonine Kinase Protects Staphylococci against Phages. *Cell Host Microbe* **20**, 471–481 (2016).
64. Cooley, W., Sirotkin, K., Green, R. & Snyder, L. A new gene of Escherichia coli K-12 whose product participates in T4 bacteriophage late gene expression: interaction of lit with the T4-induced polynucleotide 5'-kinase 3'-phosphatase. *J Bacteriol* **140**, 83–91 (1979).
65. Bingham, R., Ekunwe, S. I., Falk, S., Snyder, L. & Kleanthous, C. The major head protein of bacteriophage T4 binds specifically to elongation factor Tu. *Journal of Biological Chemistry* **275**, 23219–23226 (2000).
66. Stokar-Avihail, A. *et al.* Discovery of phage determinants that confer sensitivity to bacterial immune systems. *Cell* (2023).
67. Richmond-Buccola, D. *et al.* Convergent mutations in phage virion assembly proteins enable evasion of Type I CBASS immunity. *bioRxiv* (2023).
68. Banh, D. V. *et al.* Bacterial cGAS senses a viral RNA to initiate immunity. *Nature* **623**, 1001–1008 (2023).
69. Sun, L., Wu, J., Du, F., Chen, X. & Chen, Z. J. Cyclic GMP-AMP synthase is a cytosolic DNA sensor that activates the type I interferon pathway. *Science* (1979) **339**, 786–791 (2013).
70. Li, Y. *et al.* cGLRs are a diverse family of pattern recognition receptors in innate immunity. *Cell* (2023).
71. Slavik, K. M. *et al.* cGAS-like receptors sense RNA and control 3'2'-cGAMP signalling in *Drosophila*. *Nature* **597**, 109–113 (2021).
72. Tesson, F. *et al.* Systematic and quantitative view of the antiviral arsenal of prokaryotes. *Nat. Commun.* **13**, 2561 (2022).
73. Abby, S. S., Denise, R. & Rocha, E. P. C. Identification of Protein Secretion Systems in Bacterial Genomes Using MacSyFinder Version 2. *Methods Mol. Biol.* **2715**, 1–25 (2024).

74. Marino, N. D. *et al.* Discovery of widespread type I and type V CRISPR-Cas inhibitors. *Science* (1979) **362**, 240–242 (2018).
75. Silas, S. *et al.* Activation of programmed cell death and counter-defense functions of phage accessory genes. *bioRxiv* (2023).
76. Li, Y. *et al.* A Family of Novel Immune Systems Targets Early Infection Of-Forming Jumbo Phages. *bioRxiv* (2022).
77. Barbalat, R., Ewald, S. E., Mouchess, M. L. & Barton, G. M. Nucleic Acid Recognition by the Innate Immune System. *Annu Rev Immunol* **29**, 185–214 (2011).
78. Margolis, S. R., Wilson, S. C. & Vance, R. E. Evolutionary Origins of cGAS-STING Signaling. *Trends in Immunology* vol. 38 733–743 Preprint at <https://doi.org/10.1016/j.it.2017.03.004> (2017).
79. Li, X.-D. *et al.* Pivotal roles of cGAS-cGAMP signaling in antiviral defense and immune adjuvant effects. *Science* (1979) **341**, 1390–1394 (2013).
80. Wu, J. *et al.* Cyclic GMP-AMP is an endogenous second messenger in innate immune signaling by cytosolic DNA. *Science* (1979) **339**, 826–830 (2013).
81. Ishikawa, H. & Barber, G. N. STING is an endoplasmic reticulum adaptor that facilitates innate immune signalling. *Nature* **455**, 674–678 (2008).
82. Burdette, D. L. *et al.* STING is a direct innate immune sensor of cyclic di-GMP. *Nature* **478**, 515–518 (2011).
83. Lowey, B. *et al.* CBASS Immunity Uses CARF-Related Effectors to Sense 3′–5′- and 2′–5′-Linked Cyclic Oligonucleotide Signals and Protect Bacteria from Phage Infection. *Cell* **182**, 38–49.e17 (2020).
84. Morehouse, B. R. *et al.* Cryo-EM structure of an active bacterial TIR-STING filament complex. *Nature* **608**, 803–807 (2022).
85. Lau, R. K. *et al.* Structure and mechanism of a cyclic trinucleotide-activated bacterial endonuclease mediating bacteriophage immunity. *Mol Cell* **77**, 723–733 (2020).

86. Ye, Q. *et al.* HORMA Domain Proteins and a Trip13-like ATPase Regulate Bacterial cGAS-like Enzymes to Mediate Bacteriophage Immunity. *Mol. Cell* **77**, 709–722.e7 (2020).
87. Ledvina, H. E. *et al.* An E1–E2 fusion protein primes antiviral immune signalling in bacteria. *Nature* **616**, 319–325 (2023).
88. Ye, Q. *et al.* HORMA Domain Proteins and a Trip13-like ATPase Regulate Bacterial cGAS-like Enzymes to Mediate Bacteriophage Immunity. *Mol Cell* **77**, 709–722 (2020).
89. Csörgő, B. *et al.* A compact Cascade–Cas3 system for targeted genome engineering. *Nat Methods* **17**, (2020).
90. Ha, A. D. & Denver, D. R. Comparative genomic analysis of 130 bacteriophages infecting bacteria in the genus *Pseudomonas*. *Front Immunol* **9**, 1–13 (2018).
91. Guan, J. *et al.* Bacteriophage genome engineering with CRISPR–Cas13a. *Nat Microbiol* **7**, 1956–1966 (2022).
92. Holm, L., Laiho, A., Törönen, P. & Salgado, M. DALI shines a light on remote homologs: One hundred discoveries. *Protein Science* **32**, e4519 (2023).
93. Cruz-Plancarte, I., Cazares, A. & Guarneros, G. Genomic and transcriptional mapping of PaMx41, archetype of a new lineage of bacteriophages infecting *Pseudomonas aeruginosa*. *Appl Environ Microbiol* **82**, 6541–6547 (2016).
94. Li, L. *et al.* Hydrolysis of 2'3'-cGAMP by ENPP1 and design of nonhydrolyzable analogs. *Nat Chem Biol* **10**, 1043–1048 (2014).
95. Eaglesham, J. B. & Kranzusch, P. J. Conserved strategies for pathogen evasion of cGAS-STING immunity. *Curr. Opin. Immunol.* **66**, 27–34 (2020).
96. Yu, Y. T. & Snyder, L. Translation elongation factor Tu cleaved by a phage-exclusion system. *PNAS* **91**, 802–806 (1994).
97. Abby, S. S., Néron, B., Ménager Hervé and Touchon, M. & Rocha, E. P. C. MacSyFinder: a program to mine genomes for molecular systems with an application to CRISPR-Cas systems. *PLoS One* **9**, e110726 (2014).

98. Qiu, D., Damron, F. H., Mima, T., Schweizer, H. P. & Yu, H. D. pBAD-based shuttle vectors for functional analysis of toxic and highly regulated genes in *Pseudomonas* and *Burkholderia* spp. and other bacteria. *Applications in Environmental Microbiology* **74**, 7422–7426 (2008).
99. Choi, K.-H. & Schweizer, H. P. mini-Tn7 insertion in bacteria with single attTn7 sites: example *Pseudomonas aeruginosa*. *Nat Protoc* **1**, 153–161 (2006).
100. Choi, K. H. *et al.* Genetic tools for select-agent-compliant manipulation of *Burkholderia pseudomallei*. *Appl Environ Microbiol* **74**, 1064–1075 (2008).
101. Shanks, R. M. Q., Caiazza, N. C., Hinsa, S. M., Toutain, C. M. & O'Toole, G. A. *Saccharomyces cerevisiae*-based molecular tool kit for manipulation of genes from gram-negative bacteria. *Appl Environ Microbiol* **72**, 5027–5036 (2006).
102. Hmelo, L. R. *et al.* Precision-engineering the *Pseudomonas aeruginosa* genome with two-step allelic exchange. *Nat Protoc* (2015) doi:10.1038/nprot.2015.115.
103. Meeske, A. J. *et al.* A phage-encoded anti-CRISPR enables complete evasion of type VI-A CRISPR-Cas immunity. *Science* (1979) **369**, 54–59 (2020).
104. Rouillon, C., Athukoralage, J. S., Graham, S., Gruschow, S. & White, M. F. Investigation of the cyclic oligoadenylate signaling pathway of type III CRISPR systems. in *Methods in Enzymology* vol. 616 191–218 (Academic Press Inc., 2019).
105. Desper, R. & Gascuel, O. Theoretical Foundation of the Balanced Minimum Evolution Method of Phylogenetic Inference and Its Relationship to Weighted Least-Squares Tree Fitting. *Mol Biol Evol* **21**, 587–598 (2004).
106. Letunic, I. & Bork, P. Interactive tree of life (iTOL) v5: An online tool for phylogenetic tree display and annotation. *Nucleic Acids Res* **49**, W293–W296 (2021).
107. Jumper, J. *et al.* Highly accurate protein structure prediction with AlphaFold. *Nature* **596**, 583–589 (2021).
108. Otwinowski, Z. & Minor, W. Processing of X-ray diffraction data collected in oscillation mode. in *Methods in Enzymology* vol. 276 307–326 (Academic Press, 1997).

109. Emsley, P., Lohkamp, B., Scott, W. G. & Cowtan, K. Features and development of Coot. *Acta Crystallogr D Biol Crystallogr* **66**, 486–501 (2010).
110. Adams, P. D. *et al.* PHENIX: building new software for automated crystallographic structure determination. *Acta Crystallogr D Biol Crystallogr* **58**, 1948–1954 (2002).
111. Fatma, S., Chakravarti, A., Zeng, X. & Huang, R. H. Molecular mechanisms of the CdnG-Cap5 antiphage defense system employing 3',2'-cGAMP as the second messenger. *Nat Commun* **12**, (2021).
112. Ko, T. P. *et al.* Crystal structure and functional implication of bacterial STING. *Nat Commun* **13**, (2022).
113. Morehouse, B. R. *et al.* STING Cyclic Dinucleotide Sensing Originated in Bacteria. *Nature* vol. 586 (2020).
114. Molina, R., Sofos, N. & Montoya, G. Structural basis of CRISPR-Cas Type III prokaryotic defence systems. *Current Opinion in Structural Biology* vol. 65 119–129 Preprint at <https://doi.org/10.1016/j.sbi.2020.06.010> (2020).
115. van Beljouw, S. P. B., Sanders, J., Rodríguez-Molina, A. & Brouns, S. J. J. RNA-targeting CRISPR–Cas systems. *Nature Reviews Microbiology* vol. 21 21–34 Preprint at <https://doi.org/10.1038/s41579-022-00793-y> (2023).
116. Mayo-Muñoz, D. *et al.* Type III CRISPR-Cas provides resistance against nucleus-forming jumbo phages via abortive infection. *Mol Cell* **82**, 4471–4486.e9 (2022).
117. Athukoralage, J. S. & White, M. F. Cyclic Nucleotide Signaling in Phage Defense and Counter-Defense. *Annu Rev Virol* (2022) doi:10.1146/annurev-virology-100120.
118. van Kempen, M. *et al.* Fast and accurate protein structure search with Foldseek. *Nat Biotechnol* **42**, 243–246 (2024).
119. Cai, H. *et al.* A Novel Virus-Induced Cyclic Dinucleotide, 2'3'-c-Di-GMP, Mediates STING-Dependent Antiviral Immunity in *Drosophila*. *bioRxiv* (2023).
120. Woodward, J. J. I. A. P. DA. c-di-AMP Secreted by Intracellular *Listeria monocytogenes* Activates a Host Type I Interferon Response. *Science* (1979) **328**, 1703–5 (2010).

121. Katoh, K., Rozewicki, J. & Yamada, K. D. MAFFT online service: multiple sequence alignment, interactive sequence choice and visualization. *Brief Bioinform* **20**, 1160–1166 (2019).
122. Steinegger, M. & Söding, J. MMseqs2 enables sensitive protein sequence searching for the analysis of massive data sets. *Nat Biotechnol* **35**, 1026–1028 (2017).
123. Price, M. N., Dehal, P. S. & Arkin, A. P. FastTree 2—approximately maximum-likelihood trees for large alignments. *PLoS One* **5**, e9490 (2010).
124. Kristiansen, H., Gad, H. H., Eskildsen-Larsen, S., Despres, P. & Hartmann, R. The Oligoadenylate Synthetase Family: An Ancient Protein Family with Multiple Antiviral Activities. *Journal of Interferon & Cytokine Research* **31**, 41–47 (2011).
125. Culbertson, E. M. & Levin, T. C. Eukaryotic CD-NTase, STING, and viperin proteins evolved via domain shuffling, horizontal transfer, and ancient inheritance from prokaryotes. *PLoS Biol* **21**, (2023).
126. Kazlauskienė, M., Kostiuk, G., Venclovas, Č., Tamulaitis, G. & Siksnys, V. A cyclic oligonucleotide signaling pathway in type III CRISPR-Cas systems. *Science (1979)* **357**, 605–609 (2017).
127. Niewoehner, O. *et al.* Type III CRISPR-Cas systems produce cyclic oligoadenylate second messengers. *Nature* **548**, 543–548 (2017).
128. Chakravarti, A. Elucidating the molecular mechanisms of antiviral defense systems. (University of Illinois at Urbana-Champaign, Champaign, 2022).
129. Ho, P., Chen, Y., Biswas, S., Canfield Ethan and Abdolvahabi, A. & Feldman, D. E. Bacteriophage antidefense genes that neutralize TIR and STING immune responses. *Cell Rep* **42**, 112305 (2023).
130. Severin, G. B. *et al.* Direct activation of a phospholipase by cyclic GMP-AMP in El Tor *Vibrio cholerae*. *Proc Natl Acad Sci U S A* **115**, E6048–E6055 (2018).
131. Severin, G. B. *et al.* Activation of a *Vibrio cholerae* CBASS anti-phage system by quorum sensing and folate depletion. *mBio* **14**, (2023).

132. Brenzinger, S. *et al.* The *Vibrio cholerae* CBASS phage defence system modulates resistance and killing by antifolate antibiotics. *Nat Microbiol* **9**, 251–262 (2024).
133. Zhu, D. *et al.* Structural Biochemistry of a *Vibrio cholerae* Dinucleotide Cyclase Reveals Cyclase Activity Regulation by Folates. *Mol Cell* **55**, 931–937 (2014).
134. Krüger, L. *et al.* Reversible conjugation of a CBASS nucleotide cyclase regulates bacterial immune response to phage infection. *Nat Microbiol* (2024) doi:10.1038/s41564-024-01670-5.
135. Iglewski, B. H. *Pseudomonas*. in *Medical Microbiology* (ed. Barson, S.) (The University of Texas Medical Branch at Galvestone, Galveston, 1996).
136. Costa, A. R. *et al.* Accumulation of defense systems in phage-resistant strains of *Pseudomonas aeruginosa*. *Sci Adv* **10**, (2024).
137. Rechkoblit, O. *et al.* Activation of CBASS Cap5 endonuclease immune effector by cyclic nucleotides. *Nat Struct Mol Biol* (2024) doi:10.1038/s41594-024-01220-x.
138. Ritchie, C., Carozza, J. A. & Li, L. Biochemistry, Cell Biology, and Pathophysiology of the Innate Immune cGAS–cGAMP–STING Pathway. *Annu Rev Biochem* **91**, 599–628 (2022).
139. Pao, S. S., Paulsen, I. T. & Saier, M. H. Major Facilitator Superfamily. *Microbiology and Molecular Biology Reviews* **62**, 1–34 (1998).
140. Carozza, J. A. *et al.* ENPP1’s regulation of extracellular cGAMP is a ubiquitous mechanism of attenuating STING signaling. *Proceedings of the National Academy of Sciences* **119**, (2022).
141. Yap, M. L. & Rossmann, M. G. Structure and function of bacteriophage T4. *Future Microbiol* **9**, 1319–1327 (2014).
142. Aframian, N. & Eldar, A. Abortive infection antiphage defense systems: separating mechanism and phenotype. *Trends Microbiol* **31**, 1003–1012 (2023).
143. Varadi, M. *et al.* AlphaFold Protein Structure Database: massively expanding the structural coverage of protein-sequence space with high-accuracy models. *Nucleic Acids Res* **50**, D439–D444 (2022).

Publishing Agreement

It is the policy of the University to encourage open access and broad distribution of all theses, dissertations, and manuscripts. The Graduate Division will facilitate the distribution of UCSF theses, dissertations, and manuscripts to the UCSF Library for open access and distribution. UCSF will make such theses, dissertations, and manuscripts accessible to the public and will take reasonable steps to preserve these works in perpetuity.

I hereby grant the non-exclusive, perpetual right to The Regents of the University of California to reproduce, publicly display, distribute, preserve, and publish copies of my thesis, dissertation, or manuscript in any form or media, now existing or later derived, including access online for teaching, research, and public service purposes.

DocuSigned by:

C5705EF2046A40F... Author Signature

5/20/2024
Date